ISBN: 978-81-994425-3-5

Materials Science Frontiers:

From Chemical Principles to Physical Applications

Editors:

Mr. Digambar D. Kulkarni

Dr. Sachin P. Patil

Dr. Pratibha Sharma

Dr. Kailash A. Gedekar



Bhumi Publishing, India

First Edition: October 2025

Materials Science Frontiers:

From Chemical Principles to Physical Applications

(ISBN: 978-81-994425-3-5)

DOI: https://doi.org/10.5281/zenodo.17504991

Editors

Mr. Digambar D. Kulkarni

Department of Physics,

Dapoli Urban Bank Senior Science College,

Dapoli, Dist. Ratnagiri, M.S.

Dr. Sachin P. Patil

Department of Chemistry,
S.T.E.S. & Co-Op. Edu. Society Ltd.
Science Senior College, Shahada, M.S.

Dr. Pratibha Sharma

Department of Chemistry,

Lingaya's Vidyapeeth,

Faridabad, Haryana

Dr. Kailash A. Gedekar

Department of Physics,

KDK College of Engineering,

Nagpur, M.S.



October 2025

Copyright © Editors

Title: Materials Science Frontiers: From Chemical Principles to Physical Applications

Editors: Mr. Digambar D. Kulkarni, Dr. Sachin P. Patil,

Dr. Pratibha Sharma, Dr. Kailash A. Gedekar

First Edition: October 2025

ISBN: 978-81-994425-3-5



DOI: https://doi.org/10.5281/zenodo.17504991

All rights reserved. No part of this publication may be reproduced or transmitted, in any form or by any means, without permission. Any person who does any unauthorized act in relation to this publication may be liable to criminal prosecution and civil claims for damages.

Published by Bhumi Publishing,

a publishing unit of Bhumi Gramin Vikas Sanstha



Nigave Khalasa, Tal – Karveer, Dist – Kolhapur, Maharashtra, INDIA 416 207

E-mail: <u>bhumipublishing@gmail.com</u>



Disclaimer: The views expressed in the book are of the authors and not necessarily of the publisher and editors. Authors themselves are responsible for any kind of plagiarism found in their chapters and any related issues found with the book.

PREFACE

The field of materials science stands at the crossroads of chemistry, physics, and engineering, driving technological progress and innovation across diverse disciplines. The book *Materials Science Frontiers: From Chemical Principles to Physical Applications* has been conceived to present a comprehensive overview of the foundational principles, emerging trends, and real-world applications that define the dynamic landscape of modern materials research. It aims to serve as a bridge between fundamental concepts and advanced applications, highlighting how the understanding of atomic and molecular interactions enables the design and development of new functional materials.

This volume brings together contributions from researchers and academicians working in interdisciplinary domains of materials chemistry, condensed matter physics, nanotechnology, and applied engineering. The chapters cover a broad range of topics, including synthesis, characterization, structural analysis, and the functional properties of materials used in electronics, photonics, catalysis, energy storage, and biomedical applications. Special emphasis has been placed on the interrelation between chemical composition, structural organization, and physical behavior, which governs the performance and sustainability of modern materials.

In an era marked by rapid technological advancement and environmental consciousness, the study of materials science plays a pivotal role in addressing global challenges such as renewable energy generation, resource conservation, and green manufacturing. This book seeks to inspire readers—students, educators, and researchers alike—to explore innovative approaches that merge scientific insight with practical utility.

The editors express sincere gratitude to all contributing authors for their scholarly input and commitment, and to the reviewers for their valuable suggestions that enhanced the quality of this compilation. We also extend our appreciation to the publishers for their support in bringing this work to fruition. It is our hope that *Materials Science Frontiers: From Chemical Principles to Physical Applications* will serve as a valuable reference and inspiration for future explorations in this everevolving field.

TABLE OF CONTENT

Sr. No.	Book Chapter and Author(s)	Page No.
1.	INNOVATIVE ZERO LIQUID DISCHARGE STRATEGY FOR	1 – 14
	OPTIMIZED AND SUSTAINABLE RO DESALINATION	
	Islam Safia Abdelli, Salima Attouti and Ibrahim Bettaher	
2.	EXPERIMENTAL INVESTIGATION OF 4-[(FURAN-2-	15 – 39
	YLMETHYLIDENE)AMINO]-5-METHYL-4H-1,2,4-TRIAZOLE-	
	3-THIOL AS AN EFFICIENT CORROSION INHIBITOR	
	ON MARAGING STEEL IN 1M HCL	
	Rachael N. Mary, Ronald Nazareth,	
	Deepa Urs Mysore Veeraraje Urs and Suchetan P. Adimule	
3.	SYNTHESIS OF TETRAPHENYLETHYLENE-	40 - 46
	AND OLIGOPHENYLENEVINYLENE-CORED DENDRIMERS	
	Priyabrata Roy	
4.	NONLINEAR OPTICAL PROPAGATION: SELF-FOCUSING,	47 – 53
	BEAM COLLAPSE, AND FILAMENTATION IN KERR MEDIA	
	Swagatam Deva Nath and Chiranjit Hazarika	
5.	FOUNDATIONS OF MOLECULAR THERMODYNAMICS	54 – 60
	THROUGH STATISTICAL PARTITION FUNCTIONS	
	Naveen Awasthi	
6.	THE FUTURE OF MATERIALS SCIENCE: CONVERGENCE OF	61 – 89
	CHEMISTRY, PHYSICS, AND ARTIFICIAL INTELLIGENCE	
	Rajesh Kumar Mishra, Divyansh Mishra and Rekha Agarwal	
7.	MATRICES IN VIDEO GAMES	90 – 96
	R. Muthamizh Selvi	
8.	APPLICATION OF NANOMATERIALS IN THE FOOD	97 – 108
	PACKAGING INDUSTRY: ASSESSMENT OF AWARENESS	
	LEVEL AMONG MANUFACTURERS IN BENGALURU CITY	
	Mahalakshmi Arumugam and B Avinash Sathyalingeshwar	
9.	RECENT PROGRESS AND CHALLENGES IN BIOMASS-DERIVED	109 – 122
	POROUS ACTIVATED CARBON FOR	
	ENERGY STORAGE DEVICES	
	T. Rajesh Kumar, M. Paramasivam, Nivedha Lincy. C,	
	S. Dorothy, P. Santharaman and A. Maheshwaran	

10.	ELECTRICAL PROPERTIES OF KAOLINITE MINERALS	123 - 129
	Rajanish Saikia and Swagatam Deva Nath	
1.	MATERIALS SCIENCE AND RENEWABLE ENERGY	130 - 135
	Swagatam Deva Nath	
2.	SYNTHESIS AND PROPERTIES OF DERIVATIVES OF NOVEL	136 - 145
	THIOSEMICARBAZONES INCLUDING 3-CHLOROPHENYL	
	THIAZOLE HETEROCYCLES	
	Kisan K. Gadge	
3.	GREEN SYNTHESIS OF 2D MATERIALS USING	146 - 152
	BIO-INSPIRED CHEMICAL PATHWAYS	
	Simerpreet	
L4.	NANOTECHNOLOGY: FROM CHEMICAL PRINCIPLES TO	153 - 167
	PHYSICAL APPLICATIONS	
	Priya Paneru and Veena Pal	

(ISBN: 978-81-994425-3-5)

INNOVATIVE ZERO LIQUID DISCHARGE STRATEGY FOR OPTIMIZED AND SUSTAINABLE RO DESALINATION

Islam Safia Abdelli*1, Salima Attouti and Ibrahim Bettaher

Faculty of Science and Technology,

Abdelhamid Ibn Badis University, Mostaganem, Algeria, 27000

*Corresponding author E-mail: <u>safia.abdelli@univ-mosta.dz</u>

Abstract:

This study presents a Zero Liquid Discharge (ZLD) scheme for Reverse Osmosis (RO) desalination, incorporating ultrafiltration pretreatment and Electrodialysis (ED) for brine concentration. The proposed system strategically splits the RO brine reject, directing specific fractions to an electrolyser and an evaporator—both powered by renewable energy sources.

Key findings highlight the treatment plant's capacity to produce 792 cubic meters of freshwater per day, reducing the feedwater salt concentration from 4,660 ppm to just 30 ppm—demonstrating highly efficient desalination. The recycling of brine fractions to various subsystems within the ZLD loop further enhances resource utilization and minimizes waste.

A significant outcome of the model is the daily co-production of 2,269.27 kg of hydrogen, achieved with a relatively low energy input of 74,885.91 kWh. The integration of solar energy into the system reduces dependence on fossil fuels, thereby promoting sustainability and lowering the carbon footprint of the desalination process.

With a brine salt concentration of 13,648 ppm and a ZLD index of 2.7%, the system also provides valuable insights into environmental performance and long-term water security. Notably, the proposed ZLD scheme reduces brackish water intake from 1,200 to 871.52 cubic meters per day—a 27% reduction—underscoring its potential to conserve freshwater resources.

Overall, these results demonstrate the effectiveness of the conceptual ZLD configuration in improving brackish water treatment efficiency, supporting sustainable desalination, and advancing integrated water-energy recovery strategies.

Keywords: Zero Liquid Discharge (ZLD), Reverse Osmosis (RO) desalination, Renewable energy, Brine reject, Fresh water production, Water security.

Introduction:

Addressing freshwater scarcity is crucial for global economic development and environmental sustainability. Brackish Water Reverse Osmosis (BWRO) and Seawater Reverse Osmosis (SWRO) have become reliable desalination technologies, contributing to a global freshwater

production capacity that now exceeds 120 million cubic meters per day (Panagopoulos, 2023). Despite this progress, conventional brine disposal methods from desalination processes pose serious environmental risks. It is estimated that industries discharge approximately 380 billion cubic meters of wastewater annually, with nearly half released into the environment without treatment (Jones *et al.*, 2021).

Zero Liquid Discharge (ZLD) offers a sustainable alternative, aiming to maximize water recovery while converting waste into solid salt residues, thereby eliminating the need for liquid discharge. The adoption of ZLD is increasingly driven by stringent environmental regulations, mounting freshwater scarcity, and the high costs associated with conventional wastewater treatment (Amutha, 2017). Traditionally, ZLD systems relied on energy-intensive thermal processes (Roberts *et al.*, 2010), but more recent configurations integrate membrane technologies—including Reverse Osmosis (RO)—to pre-concentrate brine, significantly reducing overall energy consumption (Petersen *et al.*, 2018).

Numerous studies have demonstrated that integrating RO into ZLD systems yields notable energy and cost savings, although operational challenges remain, such as membrane fouling and scaling (Tong *et al.*, 2016). Pilot projects have shown the feasibility of combining RO with ultrafiltration pretreatment to achieve high recovery ratios, despite these limitations. For instance, Bond and Veerapaneni (Bond *et al.*, 2007) developed a pilot ZLD system incorporating ultrafiltration followed by multiple RO stages to enhance system performance.

Furthermore, Electrodialysis (ED) has been explored as an effective method for brine concentration. This technique uses electric potential and ion-exchange membranes to selectively transport ions, producing separate low- and high-salinity streams (Bond *et al.*, 2008). Wu *et al.* (2019) addressed key challenges in the electrolysis of high-salinity wastewater, while Loganathan *et al.* (2016) introduced Electrodialysis Reversal (EDR) to mitigate membrane fouling and scaling. Notably, EDR has shown the ability to concentrate brine up to 100,000 ppm with Specific Energy Consumption (SEC) ranging from 7 to 15 kWh/m³. Korngold *et al.* (2009) piloted an integrated RO-EDR system that achieved water recovery rates between 79% and 98% for brackish water desalination.

Panagopoulos (2021) proposed a comprehensive ZLD system that integrates RO with a brine concentrator and crystallizer, applicable to both BWRO and SWRO scenarios. Building on this body of work, the present study proposes a novel application designed to retrofit existing RO desalination units into ZLD systems. The proposed scheme introduces an electrolyser powered by an evaporator utilizing solar and thermal energy sources.

This approach represents an applied extension of the research conducted by Gadalla *et al.* (2023), translating theoretical insights into a practical, sustainable desalination framework. The system is modeled using mass and energy balance equations to evaluate its feasibility and performance, with the ultimate goal of advancing energy-efficient and environmentally responsible desalination practices.

Methodology:

The proposed method outlined in this study aims to address the environmental concerns associated with the disposal of brine reject from RO desalination units, which can be quite problematic. This approach, termed Zero Liquid Discharge (ZLD), suggests dividing the brine reject into multiple fractions, typically three splits. Figure 1 illustrates a Process Flow Diagram (PFD) depicting the ZLD approach.

Conceptual Model Description

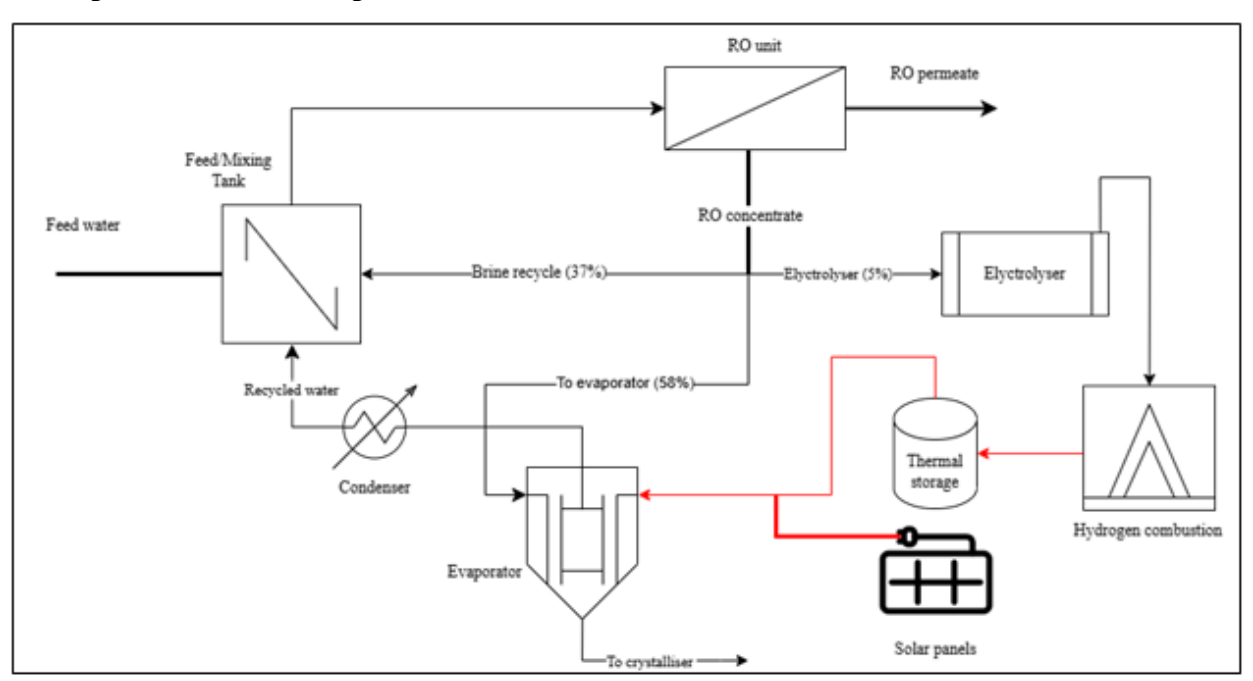


Figure 1: Conceptual model process flow diagram for a BWRO system implementing a ZLD approach (Source: Gadalla *et al.*, 2023)

This study proposes modifying BWRO desalination units to implement ZLD. The brine reject is divided into three fractions. One fraction is used in an electrolyser powered by renewable energy to produce hydrogen, which can be utilized for various applications, including providing heat to thermal storage. The second fraction enters an evaporation system powered by solar energy and hydrogen heat to produce fresh water and concentrate the brine further. The fresh water is recycled to the RO module, reducing the salinity of the brine feed and minimizing the volume of water drawn from wells. The third fraction is recycled with the saline source water before

entering the RO unit. The concentrated brine can be disposed of by reinjection into surface water or deep wells, depending on environmental costs. The conceptual process results in fresh water, hydrogen, and salts, achieving zero liquid discharge.

Conceptual Model Equations:

RO Membrane Unit

The conceptual model involves equations for mass and energy balance, as well as salt concentration balances around individual units shown in Figure 1. Apart from these balance equations, the model also incorporates the characteristic performance of each piece of equipment. An essential component in the model is the Reverse Osmosis (RO) module, which is responsible for producing a fresh water stream from the brackish water feed stream at a recovery rate (R) based on the volume of the brine/saline source water. The salt concentration of the brine reject is calculated using a salt balance around the RO unit, assuming that the salinities of the brackish water and the fresh water are provided. The equation (1) representing this balance is:

$$Xbr \times Vbr \times \rho br = Xbw \times Vbw \times \rho bw - Xfw \times Vfw \times \rho fw \dots (1)$$

Where V_{br} is the volumetric flow rate (in liters per day, L/d) of the brine reject from the RO unit, V_{bw} is the volumetric flow rate (in liters per day, L/d) of the saline brackish water source feed, V_{fw} is the volumetric flow rate (in liters per day, L/d) of the fresh water, ρ_{bw} is the density of brackish water (1015 kg/m³), ρ_{fw} is the density of fresh water, X_{bw} , X_{br} , and X_{fw} are the salt concentrations (in parts per million, ppm) in the brackish water feed, brine reject stream, and fresh water stream produced, respectively.

The mass balance and salt balance calculations around the RO unit are determined according to the equation (2):

$$Vsc \times \rho bw = Vbr \times \rho bw + Vfw \times \rho fw \dots (2)$$

Where V_{sc} represents the volumetric flow rate (in liters per day, L/d) of the saline combined feed to the RO unit.

The volumetric flow rate (V_{sc}) and salt concentration of the combined stream, utilized in reverse osmosis (RO), are determined by the mixing tank equilibrium, represented by the equations (3) and (4):

$$Vsc \times \rho bw = Vbr \times \rho bw + Vfw \times (1 - rel - re)\rho bw + Vbr \times rev \times Rev \times \rho fw \dots (3)$$

$$Xsc \times Vsc \times \rho bw = Vbr \times \rho bw + Vfw \times \rho fw + Xbr \times Vbr \times (1 - rel - rev) \times \rho bw \dots (4)$$

Here, R_{ev} denotes the evaporation rate fraction achieved in the evaporator, resulting in pure water vapor. It's important to note that the salt concentration of the water vapor leaving the evaporator is zero.

Electrolyser

Electrolysis stands as a vital method for hydrogen generation from saline water sources like seawater or brackish water. However, challenges arise due to chlorine and oxygen evolution at the anode. Brine water's diverse ions, such as Na⁺, Cl⁻, Mg²⁺, Ca²⁺, complicate seawater electrolysis, with high Cl⁻ concentrations leading to chloride evolution. Additionally, Ca²⁺ and Mg²⁺ may precipitate, forming Ca(OH)₂ and Mg(OH)₂ at the cathode. Hydrogen evolution diminishes with rising OH⁻ concentration, while oxygen evolution is bolstered by Cl⁻ presence. The chlorine produced can be sold or utilized for various purposes, including bromine ion oxidation. Unlike desalination processes, electrolysis directly splits water into hydrogen and oxygen. Electricity for this technology can be sourced from renewables like photovoltaic cells or wind, or from the conventional grid. The fundamental electrolysis equation is:

$$H_2O + Electricity = H_2 + \frac{1}{2}O_2....(5)$$

This suggests that for every mole of water electrolyzed, 1 mole of hydrogen is produced while a half mole of oxygen is released. Consequently, a mass balance on the electrolyser yields the equations (6) and (7):

mH2 =
$$\frac{mH20}{MH2}$$
 × MH2(6)
 $mH20 = (1 - Xbr) \times Vbr \times rel \times \rho bw$ (7)

Here, $m_{\rm H2O}$ represents the mass flow rate of brackish water fraction from brine reject of RO, $m_{\rm H2}$ represents the mass flow rate of hydrogen produced, $M_{\rm H2O}$ and $M_{\rm H2}$ are the molecular masses of water and hydrogen respectively. The typical energy demand ($\Delta E_{\rm el}$) for electrolysis ranges from 33 to 56 kWh/kg of hydrogen produced. As of 2022, commercial electrolysis requires around 53 kWh of electricity to produce one kg of hydrogen, which holds 39.4 kWh (HHV) of energy. Therefore, the total energy required ($\Delta E_{\rm tot}$) for procuring hydrogen with a mass flow rate $m_{\rm H2}$ can be determined by equation (8):

$$\Delta \text{Etot} = mH2 + \Delta \text{Eel} \dots (8)$$

If this energy is provided by solar photovoltaic cells, the number of cells (n_{cell}) is calculated using the power produced from each PV cell (P_{cell}) and the sunny hours per day (θ_{sun}), according to the equation (9):

$$ncell = 1Pcell + 1\theta sun + \Delta Etot \dots (9)$$

It's important to note that the electrolyser is used to provide hydrogen necessary as a heat source for evaporation. In cases where a large fraction of brine reject is directed to the electrolyser, the hydrogen produced may exceed the necessity of evaporation. Consequently, the surplus hydrogen can be sold or utilized in fuel cells for other purposes.

Evaporator

Evaporation equipment can function either as a single effect or multiple effects. Heat is applied to convert a brine solution or salty water into water vapor. In a single-effect evaporator, supplying a pound of steam can generate approximately 0.9 Kg of water vapor or steam from a kilogram of water (as noted by Kern). The remaining 0.1 Kg of water retains the majority of the salt. The produced water vapor is condensed and recycled back to the RO unit to diminish the salt content of the brackish water source, while the concentrated brine is directed to crystallizers or evaporation ponds. The evaporator model is delineated by the equations below:

$$mev = Vbr \times rev \times \rho bw \dots (10)$$

$$mwv = mev \times Rev \dots (11)$$

$$mbrc = mev - mwv \dots (12)$$

$$Xsl = mev \times \frac{Xbr}{mbrc}$$
....(13)

In these equations, m_{ev} represents the mass flow rate of brine feed to the evaporator, m_{wv} represents the mass flow rate of water vapor produced in the evaporator, m_{brc} represents the mass flow rate of brine concentrate from the evaporator, and X_{sl} represents the salt concentration in the brine concentrate leaving the evaporator.

ZLD Performance

The proposed ZLD flowsheet introduces a new parameter called pZLD, which is defined as the ratio of the brine reject from the entire plant to the fresh brackish water drawn from the wells. This parameter, calculated using the formula (14):

$$pZLD = \frac{mbrc}{(Vbw \times \rho bw)} \dots (14)$$

Serves as a measure of the modified unit's performance in achieving zero liquid discharge (ZLD). While an absolute value of zero for pZLD indicates ideal performance, it's important to note that this value may not always represent the optimal condition. Assessing the effectiveness of the modified RO desalination unit involves analyzing its cost implications and the resulting profit from the modifications.

Study Area

The theoretical model is put to the test by simulating the desalination process of brackish water containing 4660 ppm TDS, withdrawn from a nearby well at chemicals factory located in Algeria.

This factory relies on reverse osmosis for water treatment purposes. RO systems are used to purify process water, boiler feedwater, cooling water and other water sources required in manufacturing processes. By removing impurities such as minerals, chemicals, and dissolved

solids, reverse osmosis ensures that water used in industrial operations meets the required quality standards. This helps prevent equipment corrosion, scaling, and fouling, ensuring efficient and reliable manufacturing processes.

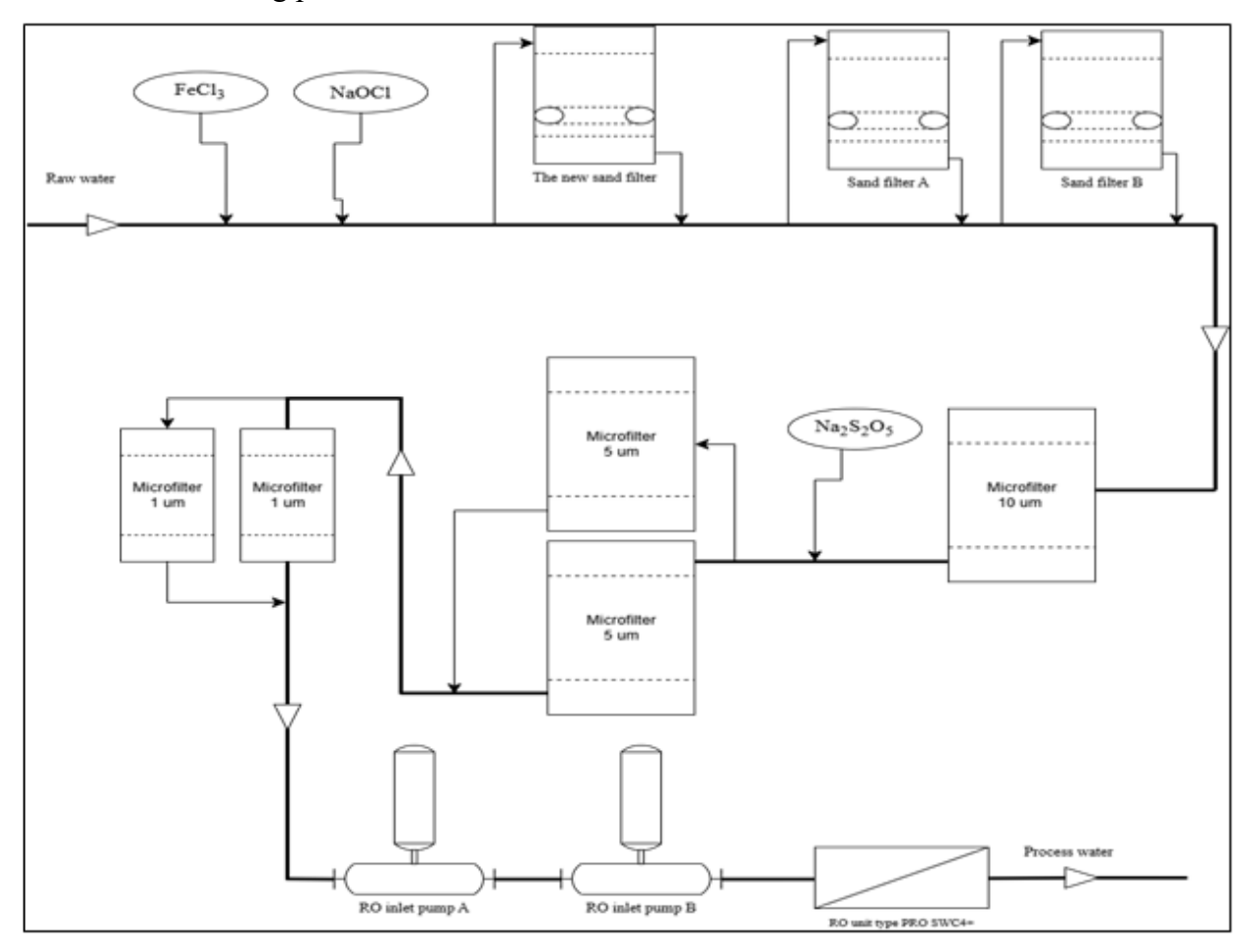


Figure 2: Flow scheme of water treatment plant

The RO unit at the factory studied is part of a larger water treatment plant, that ensures the production of process water with less than 30 ppm TDS. To achieve this, the brackish water drawn from a well goes through several treatment steps, which can be divided into two types of treatment, chemical treatment and physical treatment.

In the full treatment process, the initial step involves dosing flocculant (FeCl₃) to facilitate the aggregation of suspended particles, enabling their efficient removal through filtration. Concurrently, a carefully measured amount of disinfectant (NaOCl) is introduced to the system to preemptively counteract bacterial proliferation. Subsequently, the water undergoes filtration over a sand layer, effectively eliminating physical impurities. Following this, a reducing chemical (Na₂S₂O₅) is administered to neutralize any residual free chlorine, ensuring the water's safety for consumption. To prevent the precipitation of sparingly soluble salts on reverse osmosis membranes, a scaling inhibitor (PermaTreat NALCO) is introduced. The core of the treatment

lies in the reverse osmosis unit, where feed water is subjected to desalination, rendering it purified and suitable for use. Lastly, another dose of disinfectant is administered to maintain prophylactic safety against bacterial growth throughout the system, guaranteeing the delivery of clean and potable water (Lakshmanan and Murugesan, 2014).

From Raw Water to Process Water

Flocculant

The first step in this water treatment plant is the addition of a flocculant to the raw water, aimed at coagulating colloidal matter. The particles in a colloidal suspension are primarily negatively charged. The flocculant helps to reduce the repulsion forces and to link the particles together. This process, known as coagulation, produces filterable particles during a certain exposure time. These particles can reach sizes up to $100~\mu m$, allowing them to be removed in a subsequent filtration step.

A typical flocculant used is a solution of iron (III) chloride (FeCl₃). The dosage amount is related to the treated flow rate and the content of colloidal matter in the raw water. The impact on the removal of colloidal matter should be determined through laboratory research.

As a general guideline for dosing, a concentration of 5 - 20 mg/l of FeCl₃ in the raw water can be adjusted.

Chlorination

The purpose of dosing disinfectant into the raw water is to prevent bacterial growth in the downstream equipment. A typical disinfectant used is a diluted solution of sodium hypochlorite (NaOCl). The dosing amount depends on the treated flow rate and the type and number of bacteria present in the permeate water. The impact on the bacteria should be determined through laboratory research. Typical values for disinfection by sodium hypochlorite are as follows:

- Active component: 12% (weight) of chlorine = 150 mg/ml chlorine
- Dosing amount: 0.5 mg/l (content in the raw water)

Sand Filter

The sand filter plays a pivotal role in physical water treatment, particularly as a pre-treatment for systems like reverse osmosis, aiming to reduce the maximum amount of solid matter to 50 ppm, while colloidal matter will not be treated. Structurally, it comprises two layers of gravel: a supportive bottom layer with grain sizes ranging from 1 to 2 mm, and an upper layer with grain sizes between 0.7 and 1.2 mm (Lakshmanan and Murugesan, 2014).

As water flows from top to bottom during filtration, particles adhere to the gravel. Over time, this accumulation increases the pressure drop across the filter layer, necessitating a backwash

process typically at a pressure threshold of 0.5 bar. During backwashing, the flow direction reverses from bottom to top, expelling trapped particles, with the flow rate boosted to approximately 1.5 to 2 times that of filtration, ensuring thorough cleaning.

Originally, there was only one sand filtration step composed of two filters that worked alternately. A new sand filter was added before the original ones to help filter out the maximum amount of particles, providing better protection for the microfilters and the reverse osmosis membranes.

De-chlorination

De-chlorination of raw water aims to eliminate residual free chlorine, typically injected during disinfection to combat bacteria and oxidize inorganic compounds. Maintaining a controlled level of free chlorine post-treatment is essential for preventing contamination. However, free chlorine can harm reverse osmosis membranes due to their sensitivity to oxidizing agents. Therefore, it is necessary to remove free residual chlorine by injecting a chemical deoxidizing agent. A typical reducing agent used for this purpose is a diluted solution of sodium metabisulfite (Na₂S₂O₅).

Scaling Inhibitor

The purpose of dosing scaling inhibitor into raw water is to prevent the precipitation of sparingly soluble salts, such as carbonates of alkaloids of soil (e.g. CaCO₃, MgCO₃), and oxides of iron, manganese, and alumina. This inhibition is important to maintain membrane integrity within the RO unit, ensuring consistent permeate flow and applied pressure according to design specifications.

Microfiltration

Originally, the water would go through filters of 5 microns and 1 micro meter before entering the reverse osmosis unit, with each filter having a secondary unit in case of maintenance or a malfunction. A 10 microns filter was added to protect the RO membranes after the ground team discovered an increase in pressure and the membranes regenerative periods decreased.

Reverse Osmosis Unit

The reverse osmosis (RO) unit, as illustrated in Figure 1, is the main component of the water treatment plant. This unit consists of 35 polyamide membranes housed within 7 pressure vessels, with each vessel containing 5 membranes. A high-pressure pump is used to increase the pressure on the salt side of the RO unit to above 32 bar, which forces the water to flow across the semi-permeable membrane. This process leaves behind most of the dissolved salts (approximately 95%-99%).

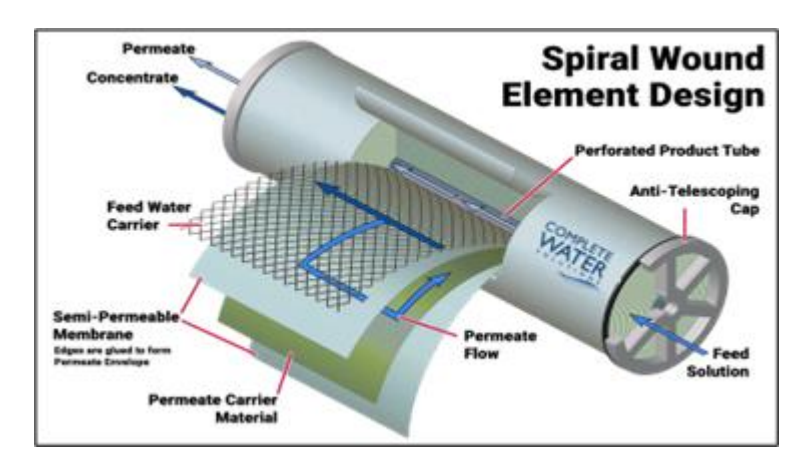


Figure 3: Schematic of the Reverse Osmosis (RO) Membrane System (Source: complete-water.com)

Within the membrane system, the feed water is separated into a low-saline product, known as permeate, and a high-saline solution, referred to as concentrate, brine or reject stream. Initially, the permeate exited the RO unit at a rate of 35 m³/h, and the concentrate at 15 m³/h. However, due to various factors such as time and the effects of scaling and fouling on the membranes, these values have decreased to 33 m³/h for permeate and 17 m³/h for concentrate.

The processed water is stored in a 1000 cubic meter underground storage tank and is subsequently utilized in various processes throughout the factory. The brine, which does not pose environmental risks, is typically disposed of in remote, uninhabited areas.

Problematic Aspects of Reverse Osmosis in Water Treatment

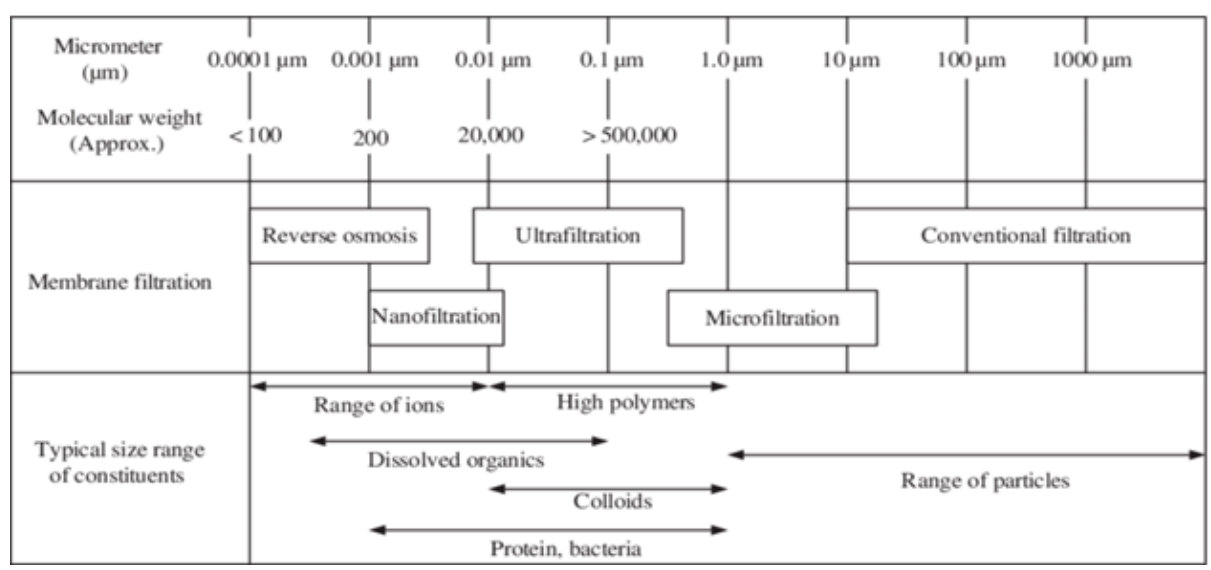


Figure 4: Different types of filters and their respective membranes properties Source: Chiam and Sarbatly, 2014

Reverse osmosis is one of the most effective forms of water filtration because unlike chemical or carbon filtration systems, which use certain materials to attract or directly target the contaminants in the water, reverse osmosis works by pushing water through a semi-permeable

membrane with pores around 0.0001 microns, allowing only water molecules to pass while trapping contaminants, organic materials, and salts. Initially developed for seawater desalination and reducing heavy metals, reverse osmosis is now widely used in government, commercial, military, and residential applications (see

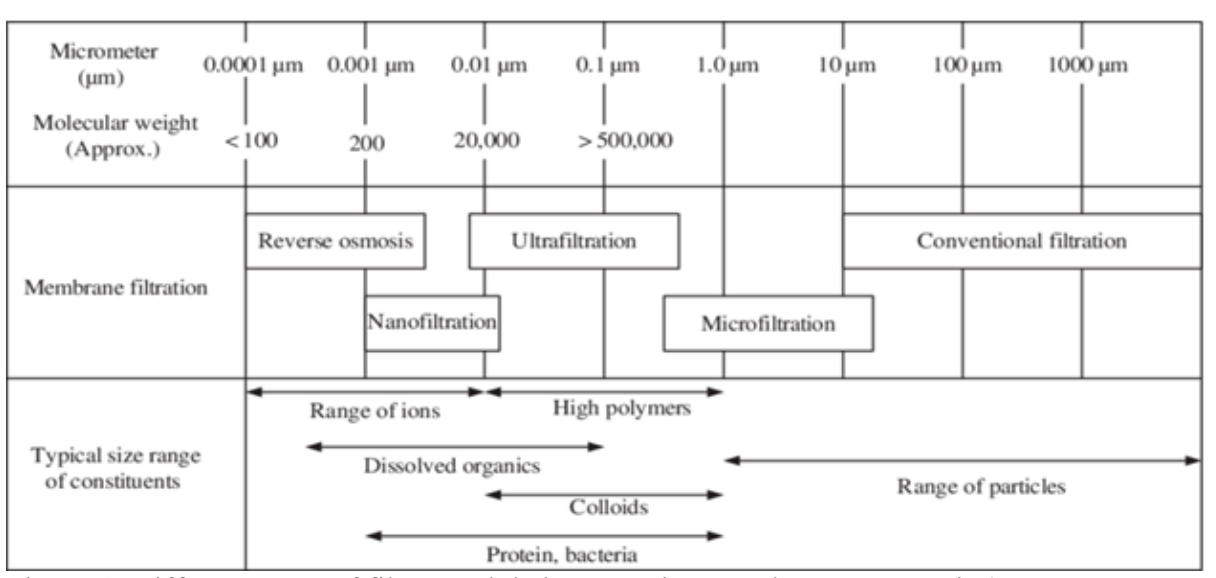


Figure 4: Different types of filters and their respective membranes properties).

One of the biggest disadvantages to reverse osmosis water systems is wasted water. Studies show various reverse osmosis systems can waste between 3 and 20 times as much water as they produce (Panagopoulos, 2023). There are numerous ongoing efforts such as ZLD systems to address this issue in the near future, driven by concerns over water scarcity and climate change.

Application and Calculations

To evaluate the practicality of our conceptual model, we will use operational data from the water treatment plant of a chemicals manufacturing facility. Additionally, we will employ the latest version of IMSDesign (Integrated Membrane Solutions Design), an open-access membrane projection software developed by Hydranautics. This advanced tool is specifically designed for the efficient and accurate design and analysis of membrane-based systems, such as Reverse Osmosis (RO) and Nanofiltration (NF) units.

Our objective is to compare the results generated by our conceptual model with those obtained from IMSDesign, in order to validate and refine our calculations. Particular attention will be given to the salt concentration in the brine reject stream (X_{br}), as this parameter is critical for several model computations and for assessing the overall performance of the proposed ZLD system.

Case Study and Results

In this study, a theoretical model was developed and applied to evaluate a Zero Liquid Discharge (ZLD) desalination scheme for the treatment of brackish water with a Total Dissolved Solids

(TDS) concentration of 4,660 ppm. The proposed system integrates a Reverse Osmosis (RO) membrane unit with downstream components—an electrolyser and an evaporator—to manage and recycle the RO brine reject. This configuration aims to reduce the overall salt concentration in the recycle streams, enhance water recovery, and minimize liquid waste discharge.

The model was tested using a simulated water treatment plant capable of producing 792 cubic meters per day of fresh water with a final salt concentration of 30 ppm. The RO unit operated at a recovery rate of 66%. In the baseline scenario—prior to the integration of the ZLD concept—the plant required an intake of 1,200 cubic meters per day of brackish water from a well to maintain full production capacity. After applying the ZLD model, the intake was reduced to 871.52 cubic meters per day, representing a 27% reduction in raw water usage.

Key outcomes from the model are as follows:

- Water intake from the well: 871.52 m³/day
- Distribution of RO brine reject:
 - o To electrolyser: 5%
 - o To evaporator: 58%
- o Recycled to feed/mixing tank: 37%
- Recycled brine salt concentration: 4,660 ppm
- Mixed RO feed flow rate: 1,200 m³/day
- Hydrogen production: 2,269.27 kg/day
- Minimum electricity requirement: 74,885.91 kWh
- Solar energy input: 4 kW per cell (with an average solar exposure of 8.18 hours/day)
- Salt concentration of RO brine: 13,648 ppm
- ZLD index: 2.7%

These results confirm the model's effectiveness in optimizing brackish water desalination, reducing freshwater extraction, and improving resource efficiency. The integration of waste recycling—distributing the RO brine reject among the electrolyser, evaporator, and feed tank—demonstrates a practical approach to minimize environmental discharge while maximizing reuse within the system.

Additionally, the co-production of hydrogen at a rate of over 2,200 kg/day introduces an energy recovery dimension to the desalination process. When coupled with solar energy, this approach contributes to a more sustainable and energy-efficient water treatment solution.

The values for brine stream separation (to the electrolyser and evaporator) were adopted based on findings from Gadalla *et al.* (2023), which reported a 2–14% variation in brine salt concentration and feed flow rates under different operating conditions. Although this study is theoretical and does not include experimental validation, the incorporation of literature-based parameters allows for a realistic assessment of system feasibility and performance in comparable operational contexts.

Overall, the proposed ZLD scheme demonstrates strong potential for sustainable water resource management, high-efficiency desalination, and integrated energy recovery—making it a promising approach for addressing water scarcity and environmental concerns in arid and semi-arid regions.

Conclusion:

In this study, a conceptual Zero Liquid Discharge (ZLD) scheme is proposed for treating brackish water using a Reverse Osmosis (RO) membrane unit. The model introduces a novel approach by splitting the brine reject from the RO system between an electrolyser and an evaporator, thereby lowering the salt concentration in the recycle streams fed back to the RO unit. Mathematical models have been developed to represent the performance of each component within the ZLD system, enabling sensitivity analyses with respect to various operational parameters.

The model was tested on an RO system designed to produce 792 cubic meters of freshwater per day from brackish water containing 4,660 ppm of salt. At an RO recovery rate of 66%, the proposed scheme reduced brackish water intake from 1,200 to 871.52 cubic meters per day—a 27% reduction. These results demonstrate the potential of the proposed ZLD configuration to significantly improve the efficiency and sustainability of brackish water treatment.

Acknowledgements:

This research did not receive any specific grant from funding agencies in the public, commercial, or not-for-profit sectors. This work was supported by the Directorate General for Scientific

Research and Technological Development (DG-SRTD), Ministry of Higher Education and Scientific Research of Algeria.

References:

- 1. Amutha, K. (2017). Sustainable chemical management and zero discharges. In *Sustainable fibres and textiles* (pp. 347–366). The Textile Institute Book Series.
- 2. Bond, R., Veerapaneni, S., Warner, J., & Roggensack, P. (2007). Zero liquid discharge for inland desalination. *World Water and Environmental Engineering*, 30(6), 28–29.
- 3. Bond, R., & Veerapaneni, S. (2008). Zeroing in on ZLD technologies for inland desalination. *Journal American Water Works Association*, 100, 76–89.
- 4. Chiam, C., & Sarbatly, R. (2011). Purification of aquacultural water: Conventional and new membrane-based techniques. *Separation & Purification Reviews*, 40(2), 126–160.
- 5. Roberts, D. A., Johnston, E. L., & Knott, N. A. (2010). Impacts of desalination plant discharges on the marine environment: A critical review of published studies. *Water Research*, 44(18), 5117–5128.* https://doi.org/10.1016/j.watres.2010.04.036
- 6. Tong, T., & Elimelech, M. (2016). The global rise of zero liquid discharge for wastewater management: Drivers, technologies, and future directions. *Environmental Science & Technology*, 50(13), 6846–6855.
- 7. Gadalla, M. A., Fatah, A. A., & Elazab, H. A. (2023). A novel renewable energy powered zero liquid discharge scheme for RO desalination applications. *Case Studies in Chemical and Environmental Engineering*, 8, 100407.
- 8. Lakshmanan, S., & Murugesan, T. (2014). The chlor-alkali process: Work in progress. Clean Technologies and Environmental Policy, 16, 225–234.
- 9. Jones, E. R., van Vliet, M. T. H., Qadir, M., & Bierkens, M. F. P. (2021). Country-level and gridded estimates of wastewater production, collection, treatment and reuse. *Earth System Science Data*, *13*, 237–254.
- 10. Korngold, E., Aronov, L., & Daltrophe, N. (2009). Electrodialysis of brine solutions discharged from an RO plant. *Desalination*, 242(1-3), 215-227.
- 11. Loganathan, K., Chelme-Ayala, P., & Gamal El-Din, M. (2016). Pilot-scale study on the treatment of basal aquifer water using ultrafiltration, reverse osmosis and evaporation/crystallization to achieve zero-liquid discharge. *Journal of Environmental Management*, 165, 213–223.
- 12. Panagopoulos, A., & Haralambous, K.-J. (2020). Minimal liquid discharge (MLD) and zero liquid discharge (ZLD) strategies for wastewater management and resource recovery Analysis, challenges and prospects. *Journal of Environmental Chemical Engineering*, 8(5).

- Panagopoulos, A. (2021). Energetic, economic and environmental assessment of zero liquid discharge (ZLD) brackish water and seawater desalination systems. *Energy* Conversion and Management, 235, 113957.
- 14. Petersen, K. L., *et al.* (2018). Impact of brine and antiscalants on reef-building corals in the Gulf of Aqaba Potential effects from desalination plants. *Water Research*, *144*, 183–191.
- 15. Wu, X., *et al.* (2019). Experimental and theoretical analysis of by-product formation process in Eaop for high salinity wastewater treatment. *Chemical Engineering Transactions*, 74, 1279–1284. https://doi.org/10.3303/CET1974214

EXPERIMENTAL INVESTIGATION OF 4-[(FURAN-2-YLMETHYLIDENE)AMINO]-5-METHYL-4H-1,2,4-TRIAZOLE-3-THIOL AS AN EFFICIENT CORROSION INHIBITOR ON MARAGING STEEL IN 1M HCL

Rachael N. Mary¹, Ronald Nazareth¹,

Deepa Urs Mysore Veeraraje Urs² and Suchetan P. Adimule*3

University College of Science, Tumkur University, Tumakuru-572103, India.

1. Introduction:

¹Department of Chemistry, St Aloysius (Deemed to be University), Mangaluru-575003, India.

²Department of Physics, The National Institute of Engineering, Mysore-570008, India.

³Department of Studies and Research in Chemistry,

^{*}Corresponding author E-mail: pasuchetan@gmail.com

Steel corrosion remains a significant global issue, particularly in industries where metals and alloys are exposed to various corrosive environments, including acids, bases and other aggressive agents. Acids of varying concentrations are commonly used in industrial processes such as descaling, acid cleaning, oil well acidizing, and pickling, all of which subject metals to highly corrosive conditions, making them vulnerable to degradation [Balangao (2024); Zulfareen *et al.* (2018); Kumar *et al.* (2014)]. To mitigate this, the most effective and widely adopted method for protecting metals against corrosion in acidic environments is the use of corrosion inhibitors. These inhibitors play a crucial role in reducing the corrosion rate, thereby extending the lifespan and reliability of metal structures [Kadhim *et al.* (2021); Obot *et al.* (2009)]

Many organic compounds serve as versatile anticorrosive agents, primarily by adsorbing onto metal surfaces. For a compound to be considered as an effective corrosion inhibitor, it typically requires the presence of atoms such as nitrogen, phosphorus, oxygen, or sulfur viz electron-donating atoms within its molecular structure. Additionally, compounds with π -electron systems, such as those containing double bonds, triple bonds, or aromatic rings, have been demonstrated to exhibit strong corrosion inhibition properties [Xu *et al.* (2014); Abdulridha *et al.* (2020); Singh *et al.* (2023); Huong *et al.* (2020); Savitha *et al.* (2016)]. Polymeric materials have also been extensively studied for their adsorption behaviour on metals and alloys, showing significant potential in corrosion prevention [Abd El-Lateef *et al.* (2022)].

Maraging steel, known for its extraordinary sturdiness and strength, is a high nickel, low-carbon iron-based combination. Additionally, to improve its strength, optional alloying components like molybdenum (Mo), cobalt (Co), and titanium (Ti) are added. The expansion in strength results from the precipitation of intermetallic compounds inside the Fe-Ni martensitic grid. Key properties of maraging steel incorporate high strength, moderate sturdiness, great weldability, fantastic thermal conductivity, high malleability, formability, and simplicity of manufacturing [Klobcar *et al.* (2008); Grum and Slab (2006)]. Maraging prepares are broadly utilized in aviation enterprises for rocket skins and rockets, as well as in the assembling of motor parts like direction, driving rods, and cog wheels, discharging pins in programmed weapons, careful instruments, and in atomic and gas turbine applications [Rezek *et al.* (1997)].

A review of the literature reveals numerous studies on the corrosion inhibition efficiency of organic compounds containing electron donating atoms on maraging steel in various acidic environments [Sanatkumar *et al.* (2012); Poornima *et al.* (2012); Naik *et al.* (2018); El-Sayed M Sherif (2014)]. These studies have demonstrated that the corrosion inhibition efficiency of these compounds increases with higher concentrations in the medium, identifying them as promising candidates for inhibiting corrosion. One such promising class of compounds are the Schiff bases.

They are characterized by an azomethine linkage (-C=N-), exhibit several notable properties, such as the ability to form complexes, and have applications in medicine, agriculture, catalysis, and the dye industry [Singh et al. (2015); Mushtaq et al. (2024)]. Based on corrosion inhibition studies, Schiff bases have been recognized as versatile and effective corrosion inhibitors in the field of corrosion research [Boulechfar et al. (2023); Emregul et al. (2003); Jamil et al. (2018)]. Schiff bases tend to form a positively charged species in acidic media resulting due to the protonation of the N atom in its imine group. This species is attracted electrostatically to the metal surface which is negatively charged, resulting in the physical adsorption of the species onto the metal. The protective layer formed through adsorption shields the metal surface from corrosive environment, thereby reducing corrosion. However, since physisorption is relatively a weaker adsorption, the aggressive nature of the environment in which the metals are handled may peel off this protective layer. Therefore, it is desirable to have a much robust mode of adsorption i.e. chemisorption. This can be achieved by incorporating electronegative atoms and π -electron systems to Schiff bases which enhances its ability to get chemically adsorbed onto the surface. In this aspect, we have earlier synthesized and studied the corrosion inhibitory activity of two closely related triazole-based Schiff bases **DBAMTT** $(4-\{[4-$ (dimethylamino)benzylidene|amino}-5-methyl-4H-1,2,4-triazole-3-thiol) and MTATT (5methyl-4-[(thiophene-2-ylmethylidene)amino]-4H-1,2,4-triazole-thiol). The efficiencies of these Schiff bases to inhibit corrosion of maraging steel by 1 M HCl and a 2:1 mixture of HCl and H₂SO₄ were studied [Mary et al. (2018), (2020), (2021)]. Both of them demonstrated significant corrosion inhibition efficiencies. Continuing our investigation into triazole-based Schiff bases, we have also reported the inhibition properties of FAMTT on maraging steel in a 2:1 mixture of HCl and H₂SO₄ [Mary et al. (2023)]. In our continued efforts, we, here in, report the results of our investigation of corrosion inhibition efficiency of FAMTT on maraging steel in 1M HCl solution. Also, the results are compared-experimentally as well as theoretically-with the results of our previous investigations with FAMTT, DBAMTT and MTATT to delineate the relation between molecular structures and corrosion inhibition efficiencies.

2. Experimental

2.1 Inhibitor Synthesis

Synthesis and purification of FAMTT (Fig. 1) was carried following the procedure outlined in our earlier work [Mary *et al.* (2018), (2020)]. Confirmation of product formation and its purity was verified by comparing the melting point of the recrystallized product with the reported value [Bai *et al.* (2008)].

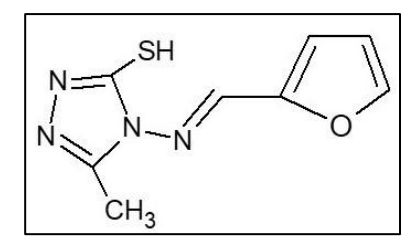


Figure 1: Structure of FAMTT

2.2. Medium

Acid stock solutions were prepared using Analar grade HCl, with double-distilled water as the solvent, and were standardized using standard Na₂CO₃ solution. Corrosion studies were conducted over a temperature range of 30–45°C (with an increment of 5°C) for electrochemical studies and at 30°C for weight loss studies. FAMTT concentrations were varied between 25 to 300 ppm.

2.3. Material

Composition of Maraging steel used in the current work: The sample was of M250 grade with composition (in wt%) - Ni-18%, Co-8.5%, Mo-5.2%, Ti-0.6%, Al-0.15%, Si-0.1%, Mn-0.1%, C-0.015%, S-0.01%, P-0.01%, N-30ppm, O-30ppm, H-2.0 ppm and remaining Fe.

2.4. Test Sample

The rod form of the test sample was epitomized in epoxy resin, leaving an uncovered surface area of 0.8910 cm² for electrochemical studies. The sample went through belt grinding followed by consecutive cleaning with emery papers of changing coarseness sizes (200, 400, 600, 800, 1000, 1200, and 1500) and was at last cleaned on a polishing wheel utilizing alumina to accomplish a mirror finish. The polished samples were then cleaned with acetone, flushed with double-distilled water, and dried prior to starting corrosion examination. The uncovered surface region of the test sample was 10.0572 cm² during weight loss study.

2.5. Weight Loss Method

For corrosion studies using weight loss method, the maraging steel was taken in the form of a coupon of known surface region. It was first cleaned, finely polished, dried, and weighed utilizing a computerized balance. It was then submerged in 100 mL of 1M HCl, at 30°C, both with and without FAMTT. The coupon was taken out from the medium after exposure for 4 hours, washed with water to eliminate the film of corrosion product, dried, and weighed again. The weight change was recorded for examination.

2.6. Electrochemical Measurements

Electrochemical analysis was conducted using a Gill AC electrochemical workstation equipped with the ACM instrument Version 5 program. The experimental setup included a three-electrode

glass cell with platinum as counter electrode, saturated Calomel as reference, and steel sample as the test electrode. To establish the open circuit potential (OCP), the cleaned and dried test sample was submerged in the corrosive medium, both with (different concentrations of FAMTT) and without the inhibitor. Analyses were performed at a proper temperature utilizing 100 mL of electrolyte under non-blended and normally circulated air through conditions. A scan rate of 1 mV/s was used to polarize the specimen over a range from +250 mV to -250 mV relative to the OCP, allowing for the recording of polarization curves. Additionally, a 10 mV AC signal amplitude was applied during electrochemical impedance spectroscopy (EIS) over a frequency range of 10 kHz to 0.01 Hz.

2.7. SEM-EDX Studies

SEM-EDX analysis were conducted using a Carl Zeiss instrument (USA) in conjunction with Oxford Instruments to observe changes in the morphology of the specimen's surface following exposure to the corrosive medium, both in the absence and presence of FAMTT.

2.8. DFT Calculations

Density functional theory (DFT) calculations on FAMTT and the related inhibitors DBAMTT & MTATT were performed using the basis set B3LYP/6-311++(d, p) available in the Gaussian 09 software package. Ground state optimized structures of all the inhibitors in the gas phase were obtained using which different properties were estimated. GaussView software was used for structure visualization [Becke (1993); Lee *et al.* (1988); Frisch *et al.* (2010); Dennington *et al.* (2009)].

3. Results and Discussion:

3.1. Weight Loss Studies

FAMTT demonstrated effective anticorrosion properties, as indicated by the weight loss test data presented in Table 1. A greater weight loss was observed in the blank solution compared to solutions containing FAMTT. In the presence of FAMTT, the corrosion rate significantly decreased, resulting in increased inhibition efficiencies as the concentration of the inhibitor was raised. The protective film formed on the metal surface by the adsorbed FAMTT molecules shields the metal surface from the aggressive medium, and thereby, acts as an efficient corrosion inhibitor [Yetri *et al.* (2014)]. As the concentration of FAMTT reaches 300 ppm, the weight loss, corrosion rate and inhibition efficiency reach a saturation limit (Fig. 2a), suggesting that FAMTT has adsorbed on to all the surface-active sites available on the maraging steel, and further increase in its concentration does not significantly improve the corrosion efficiency.

Table 1: Results of weight loss studies on maraging steel corrosion in 1M HCl with different FAMTT concentrations at 30°C

Immersion	[FAMTT]	Weight loss	Corrosion	Inhibition
time (hours)	(ppm)	(mg cm ⁻²)	rate (mm y ⁻¹)	efficiency (%)
	0	33.4	8.8473	
	25	6.4	1.6953	80.83
4	100	4.8	1.2714	85.62
	200	2.7	0.7152	91.91
	300	2.1	0.5562	93.71

The corrosion rate was calculated using the expression

$$CR = \frac{K.W}{A.D.T}(1)$$

where, corrosion rate in mmy⁻¹ is denoted as CR, K is a constant whose value is 87.6, weight loss of the metal in mg is denoted as W, surface area of the test coupon in in cm² is denoted as A, density of the metal in gcm⁻³ is denoted as D and time of exposure in hours as T [Fontana (2005a, (1987b)].

Equation (2) was used to calculate the inhibition efficiency, IE, in %.

IE (%) =
$$\frac{CR^o - CR}{CR^o} \times 100$$
 (2)

where, corrosion rates of the specimen immersed in the IM HCl solutions without and with FAMTT are denoted respectively as CR^o and CR.

The kinetics of the corrosion reaction concerning inhibitor concentrations was analysed based on the data presented above. The reaction exhibits simple kinetics, and the corrosion rate can be described by the following equation

$$v_{corr} = k [FAMTT]^n (3)$$

In the above equation, the rate constant and the order of the reaction with respect to the FAMTT concentration, are represented as k and n respectively.

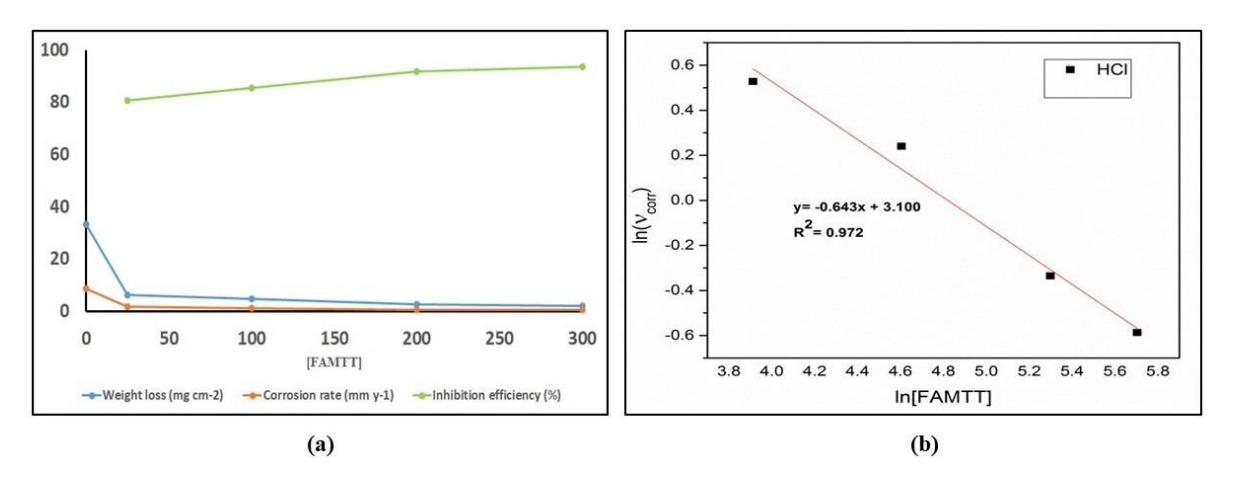


Figure 2: a) Variation of weight loss, corrosion rate and inhibition efficiency with FAMTT's concentration

b) Plot of ln(vcorr) vs ln[FAMTT] for maraging steel corrosion in 1M HCl.

The near-linear nature of the plot of $\ln \nu_{(corr)}$ vs \ln [FAMTT] (Fig. 2b) indicates that the corrosion reaction follows a simple kinetic model as expressed in Equation (3). From the slope and intercept of this plot, the order and the rate constant of the reaction were determined. The negative slope of the linear plot confirms FAMTT's inhibitory nature. The observed reaction order for FAMTT is -0.643.

Weight loss studies carried out in 1M HCl using DBAMTT and MTATT inhibitors also showed similar trend as FAMTT. For DBAMTT, inhibition efficiencies varied from 41.61% to 67.66% with inhibitor concentration ranging from 50 to 300 ppm, while, for MTATT, inhibition efficiencies varied from 68.26% to 76.64% with inhibitor concentration ranging from 10 to 300 ppm [Mary *et al.* (2020)]. The observed reaction order in the presence of DBAMTT was -0.304, with $\ln \nu_{(corr)}$ vs $\ln [DBAMTT]$ exhibiting a linear plot with negative slope, as in FAMTT. The corrosion reactions inhibited by MTATT did not follow simple kinetics as in equation (3), as the $\ln(\nu_{corr})$ vs $\ln [MTATT]$ plot was non-linear. A limiting behavior was observed at 100 ppm of MTATT, wherein a change in the order of the reaction was observed [Mary *et al.* (2020)]. Weight loss studies of FAMTT were also conducted in 2:1 mixture of HCl and H₂SO₄ [Mary *et al.* (2023)]. Saturation with respect to corrosion rate, weight loss and inhibition efficiency was achieved at very low concentration of 25 ppm at which the observe inhibition efficiency was 94.44%. The observed reaction order for FAMTT in acid mixture was -0.288.

3.2. Tafel Polarization Measurements

Potentiodynamic polarization studies provide valuable information about the corrosion behaviour of materials by evaluating their electrochemical response in a given environment. The experiments were conducted at temperatures ranging from 30°C to 45°C, which are commonly

used to simulate environmental or operational conditions. Fig. 3 illustrates the polarization curves recorded at 40°C for the corrosion of maraging steel in 1MHCl, both in the absence and presence of various concentrations of FAMTT.

The results of Tafel analysis are summarized in Table 2 and Fig. 4. At all temperatures, an increase in [FAMTT] decreases both i_{corr} and v_{corr} and increases the inhibition efficiency. The corrosion current density and potential (Fig. 4a and 4b), for a given FAMTT concentration, increase as temperature increases, and so does the corrosion inhibition efficiencies (Figure 4c). All these values attain saturation as the concentration of the inhibitor reaches 300 ppm, a trend similar to that observed in weight loss studies. These observations suggest that the inhibitor aims to reduce the corrosion rate, evident from changes in the anodic and cathodic branches of the polarization curves, where inhibited curves shift to low current density region. The parallel cathodic branches observed suggest that the cathodic reaction, primarily hydrogen evolution, is activation-controlled and remains unaffected by the presence of the inhibitor, indicating no alteration in the reduction mechanism [Chaitra *et al.* (2018)].

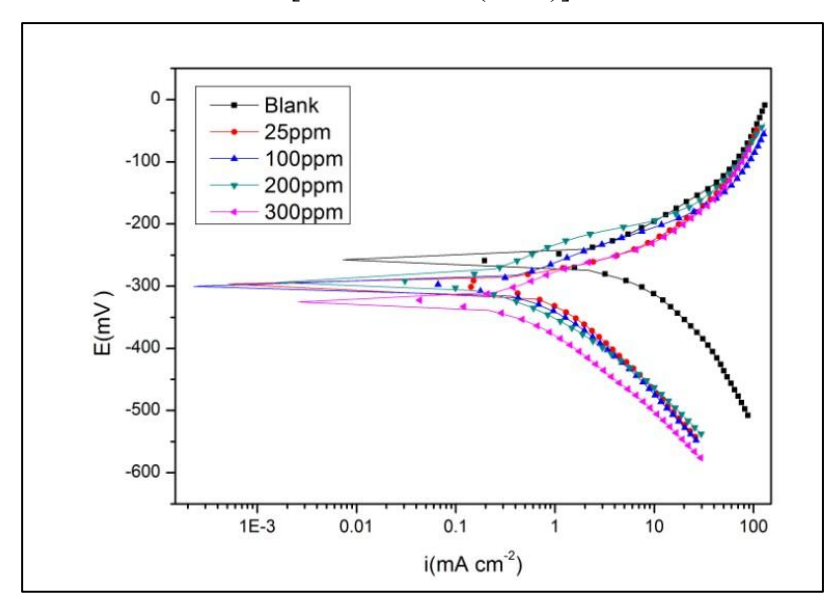


Figure 3: Tafel plots plotted for maraging steel corrosion with different inhibitor concentrations [FAMTT] at 40°C.

The rate of corrosion was calculated using the formula

$$CR = \frac{k \times E \times i_{corr}}{\rho} \tag{4}$$

where, corrosion rate in mm y⁻¹ is denoted as CR, k is a constant that defines the unit of corrosion rate whose value is 3270, the equivalent weight of the alloy is denoted as E, corrosion

current density in mA cm⁻² is denoted as i_{corr} , and density of the alloy in kg m⁻³ is denoted as ρ [Kumar *et al.* (2014)].

Equation (5) was used to calculate the inhibition efficiency η (%) [Prabhu et al.(2007)].

$$\eta(\%) = \frac{i_{corr} - i_{corr(inh)}}{i_{corr}} \times 100 (5)$$

Table 2: Results of Tafel polarization studies for the corrosion of maraging steel in 1M HCl containing different FAMTT concentrations at different temperatures

Temperature	[FAMTT]	Ecorr	-βc	İcorr	Vcorr	η (%)
°C	(ppm)	(mV/SCE)	(mV dec ⁻¹)	(mA cm ⁻²)	(mm y ⁻¹)	
	Blank	-261.6	122.46	1.9963	25.0181	
	25	-288.5	117.13	0.4839	6.0646	75.75
30	100	-298.3	123.41	0.2321	2.9088	88.37
	200	-294.6	132.32	0.2180	2.7332	89.07
	300	-304.5	117.29	0.1927	2.4152	90.34
	Blank	-257.4	149.24	3.4194	42.8527	
	25	-294.1	138.46	0.5281	6.6188	84.55
35	100	-287.9	116.35	0.3470	4.3496	89.84
	200	-282.4	116.26	0.3139	3.9346	90.81
	300	-332.6	122.19	0.2367	2.9671	93.07
	Blank	-257.2	177.38	5.8364	73.1432	
	25	-295.5	139.82	0.6697	8.3928	88.52
40	100	-300.5	124.87	0.5297	6.6392	90.92
	200	-325.9	124.05	0.4021	5.0400	93.10
	300	-295.3	105.07	0.3078	3.8578	94.72
	Blank	-255.2	177.63	9.4538	118.4773	
	25	-304.2	136.41	0.9005	11.2864	90.47
45	100	-301.0	129.51	0.6771	8.4861	92.83
	200	-324.8	110.17	0.5561	6.9698	94.11
	300	-295.7	113.42	0.3879	4.8622	95.89

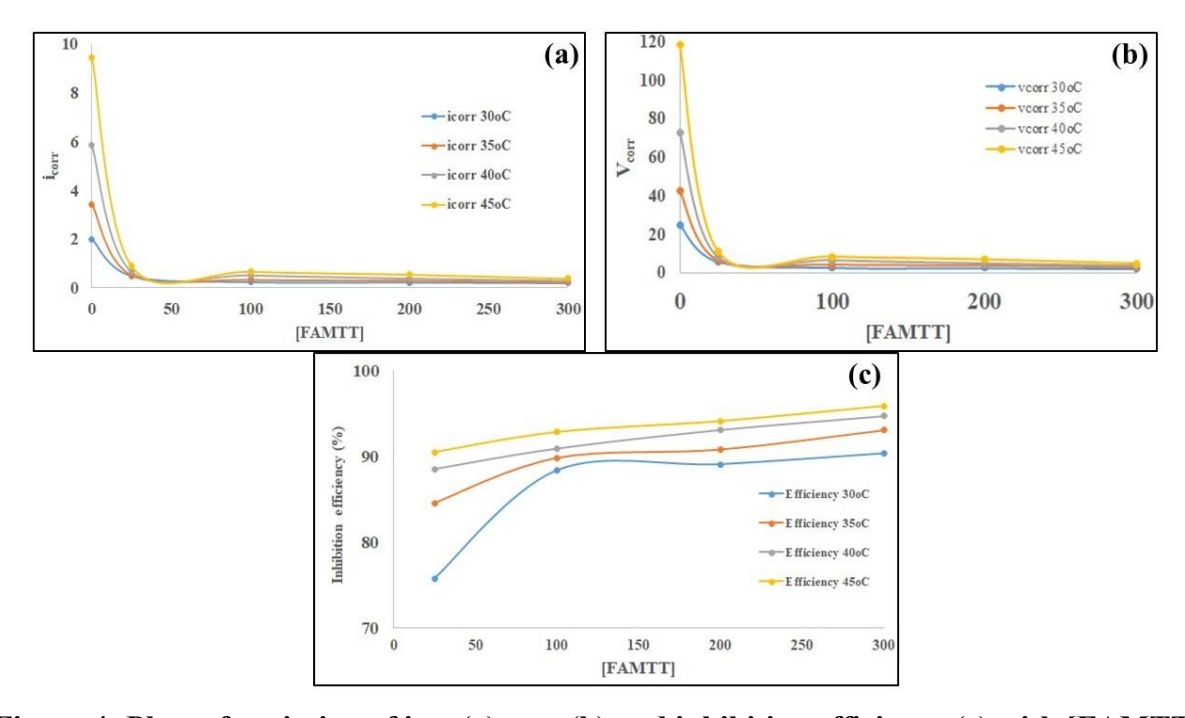


Figure 4: Plots of variation of i_{corr} (a) v_{corr} (b) and inhibition efficiency (c) with [FAMTT]. where, the corrosion current density obtained in uninhibited solution is denoted as i_{corr} , while, that for an inhibited solution is denoted as $i_{corr(inh)}$.

The corrosion potential E_{corr} showed a negative shift in its values upon addition of FAMTT to the corrosive medium. In order to classify an inhibitor as anodic or cathodic the displacement in the E_{corr} values should exceed ± 85 mV when compared to the blank solution. Here, the E_{corr} displacement in 1M HCl was approximately ± 68 mV, indicating that FAMTT exhibits mixed-type inhibitory behaviour [Li *et al.* (2007)]. i.e., FAMTT predominantly influences cathodic hydrogen evolution with the anodic metal dissolution reaction being affected as well. Furthermore, the slight variation in the cathodic Tafel slope β_c upon inhibitor addition highlights the impact of FAMTT on the kinetics of the cathodic reaction. The inhibitory action is attributed to the adsorption of FAMTT molecules on the metal surface, effectively shielding the metal from the corrosive environment [Vikneshvaran and Velmathi (2019)].

To evaluate the effect of concentration of FAMTT on the corrosion rate and analyse the reaction kinetics, plots of $ln(v_{corr})$ versus ln[FAMTT] were constructed at different temperatures (Fig. 5). The near linear correlation of the plots ($R^2 = 0.9937 - 0.9985$) observed at temperatures of 30 and 35°C indicates that the reaction adheres to simple kinetic behaviour as described by equation (3) within this temperature range.

At 40 and 45°C, the plots remain nearly linear up to a concentration of 200 ppm, with deviations from linearity observed beyond this point. This suggests a potential change in the reaction mechanism, with 200 ppm acting as a threshold concentration at these two temperatures. The

reaction order (*n*) shows slight dependence on temperature, though no consistent trend in its variation is observed. In all cases, the reaction order is close to -0.373, with the highest value recorded at 30°C. This indicates that increasing [FAMTT] at higher temperatures has a slightly reduced effect on inhibiting corrosion rates compared to its influence at lower temperatures. This is reflected in faster saturation reached in terms of i_{corr}, v_{corr} and efficiencies (Fig. 4).

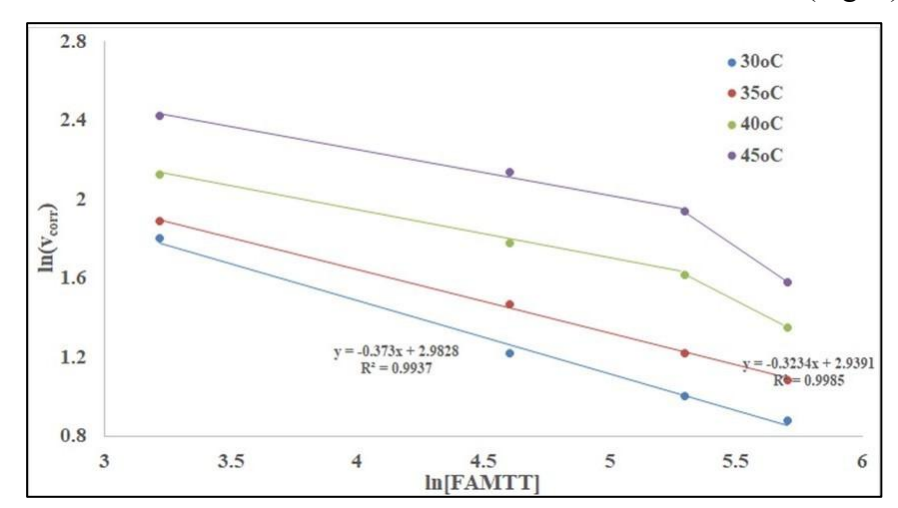


Figure 5: A plot of ln(vcorr) vs ln[FAMTT] at different temperatures in 1M HCl

For inhibitors DBAMTT and MTATT, the variation in Tafel parameters also showed same trend as observed in the current study exhibiting mixed type inhibitory behaviour. The maximum efficiency exhibited by DBAMTT was 87.69% at 45°C and 300ppm concentration. Unlike FAMTT, in the case of DBAMTT, the order of the reaction was temperature dependent and increased more negatively as the temperature was increased. In the case of MTATT, the maximum efficiency was 90.71% at 45°C and 300ppm concentration. As in weight loss studies, the reaction in the presence of MTATT did not follow simple kinetic behaviour. A limiting case is observed near 100 ppm inhibitor concentration suggesting a change in order at around this concentration at all temperatures. Below 100 ppm of MTATT, the order is almost independent of the temperature, while, above 100 ppm, temperature has a significant influence on order. It is observed that, at higher temperatures, increasing [MTATT] beyond 100 ppm induces a greater influence on inhibiting the corrosion rates than at lower temperatures. The inhibitory behaviour exerted by FAMTT in HCl and acid mixture is almost to the same extent, as the values of inhibition efficiencies obtained in both HCl and acid mixture are in the same range [Mary et al. (2023)].

3.2.1. Determination of Thermodynamic and Kinetic Parameters

Study of temperature effects on the rates of inhibited corrosion reactions aid in determination of key thermodynamic and kinetic parameters that decide the nature of metal-inhibitor interaction.

The Arrhenius equation and the transition state equation were used to assess the activation parameters for the metal dissolving process in 1M HCl both in the absence and presence of FAMTT. The Arrhenius equation (6) was used to get the activation energy (E_a) [Poornima *et al.* (2011)].

$$ln(v_{corr}) = B - \frac{Ea}{RT}(6)$$

where, R is universal gas constant, B is a constant whose values depends on the nature of the metal, and T is the absolute temperature. The plot of $ln(v_{corr})$ vs $\left(\frac{1}{T}\right)$ gives a straight line with slope $=\frac{Ea}{R}$, from which E_a for the corrosion process was calculated.

The transition state equation (7) was used to calculate enthalpy (ΔH^{\neq}) and entropy (ΔS^{\neq}) of activation for the corrosion process [Abdel Rehim *et al.* (1999)].

$$v_{corr} = \frac{RT}{Nh} exp \left(\frac{\Delta S^{\neq}}{R}\right) exp \left(\frac{-\Delta H^{\neq}}{RT}\right) (7)$$

where, h is Plank's constant and N is Avogadro's number.

The straight line obtained from the plot of $\ln(v_{\text{corr}}/T)$ vs $\left(\frac{1}{T}\right)$ was used to calculate the activation parameters ΔH^{\neq} and ΔS^{\neq} , since slope = $-\Delta H^{\neq}/R$ and intercept = $\ln(R/Nh) + \Delta S^{\neq}/R$.

The inhibition efficiency of the studied inhibitor increases with rising temperature, attributed to the presence of electron-rich sites within the inhibitor molecule. These sites enhance the inhibitor's ability to form strong bonds with the metal surface, facilitating chemisorption. Fig. 6 (a) represents Arrhenius plots and Fig. 6(b) represents Transition state plots for corrosion reactions in 1M HCl respectively. Table 3 give the activation parameters.

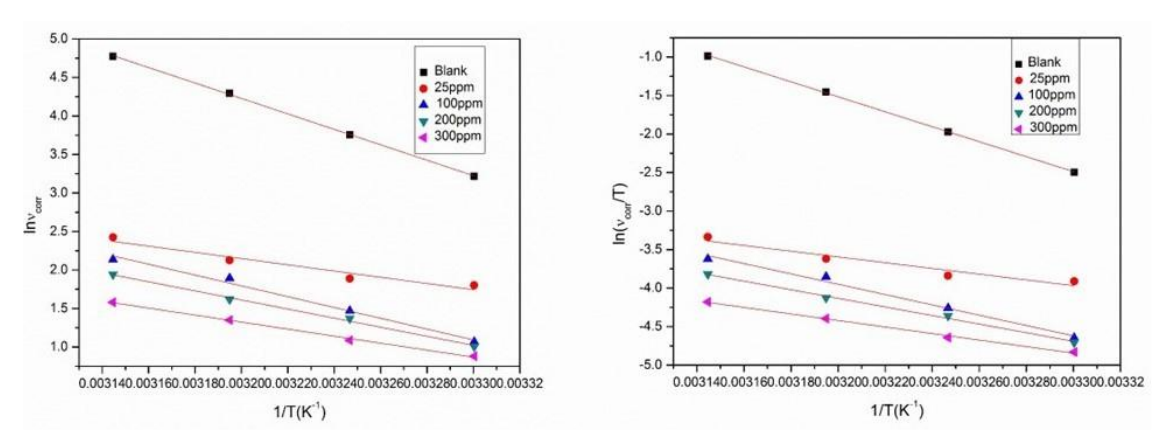


Figure 6: Arrhenius plots (a) and Transition state plots (b) for FAMTT in 1 M HCl.

There is a strong correlation between adsorption type and activation energy (E_a) values. Physisorption is ensued when an E_a value higher than that of the blank is observed, while, chemisorption is the case when a lower or unaltered E_a value for inhibited solution is obtained [Prabhu and Rao (2013)]. Here, as the inhibited solutions exhibit E_a values lesser than the

apparent activation energy (E_a) value of blank solution, FAMTT, is therefore, adsorbed over the metal surface preferentially by chemisorption as opposed to physisorption. This lowering is also correlated with the slower adsorption rate of the inhibitor [Hour and Holliday (1953)]. The overall corrosion processes, both inhibited and uninhibited, are endothermic as their $\Delta H^{\#}$ values are positive.

Table 3: Activation parameters for corrosion of maraging steel in 1M HCl containing different FAMTT concentrations

[FAMTT]	Ea	ΔH [≠]	$\Delta \mathbf{S}^{ eq}$
(ppm)	(kJ mol ⁻¹)	(kJ mol ⁻¹)	(J mol ⁻¹ K ⁻¹)
Blank	83.32	80.74	48.24
25	33.54	30.96	-128.33
100	58.30	55.72	-52.05
200	48.97	46.39	-83.44
300	37.81	35.26	-121.53

Compared to the activation energy (E_a) values, the ΔH^{\neq} values are lower in both the inhibited and uninhibited solutions, which is attributed to the hydrogen evolution reaction. Additionally, the difference between E_a and ΔH^{\neq} remains constant at 2.58 kJ in both cases, which matches the average value of RT = 2.5815 kJ under the current experimental conditions. This suggests a unimolecular corrosion reaction mechanism [Huong *et al.* (2019)]. A reduction in disorder observed during the formation of the activated complex in the rate-determining stage (indicated by the negative $\Delta S^{\#}$ values of inhibited solutions) suggests that formation of activated complex is through association, and not dissociation [Ameer *et al.* (2014)]. The adsorbed complexes formed on the metal surface is more stable owing to negative $\Delta S^{\#}$ values which justify the corrosion inhibition properties of FAMTT.

Inhibitors DBAMTT and MTATT also showed predominant chemisorption mode of adsorption as indicated by lower E_a values compared to blank [Mary *et al.* (2018), (2020)]. Also, the corrosion reaction was endothermic in nature as indicated by positive values of $\Delta H^{\#}$ for both the inhibited and uninhibited corrosion reactions. Entropy values were also negative suggesting stability of the adsorbed species on the metal surface. FAMTT in 2:1 mixture of acids also showed similar trend in activation and thermodynamic parameters as observed in 1M HCl.

3.2.2. Adsorption Isotherm

In order to further explore the nature of interaction between FAMTT and metal, adsorption isotherm studies were carried out. Results of Tafel polarization studies were used to determine

the amount of surface coverage (θ) at various FAMTT concentrations in solution (C_{inh}) using equation (8) [Poornima *et al.* (2011)]. Values of (θ) were then applied to various adsorption isotherms.

$$\theta = \frac{\eta \, (\%)}{100} \, (8)$$

Equations of various isotherms were put to test, but it was the Langmuir adsorption isotherm equation that gave the best fit. Fig.7 represents Langmuir adsorption isotherms of FAMTT in 1M HCl. Thermodynamic parameters are listed in Table 4. The plot of C_{inh}/θ vs C_{inh} gave a straight line, the intercept of which was used to calculate K_{ads} . The values of ΔG^o_{ads} were obtained from K_{ads} values by using equation [Franklin *et al.* (2012)].

$$K = \frac{1}{55.5} \exp\left(\frac{-\Delta G_{ads}^o}{RT}\right) (9)$$

where, R is the universal gas constant, 55.5 is the concentration of water in solution (in mol/dm³) and T is the absolute temperature.

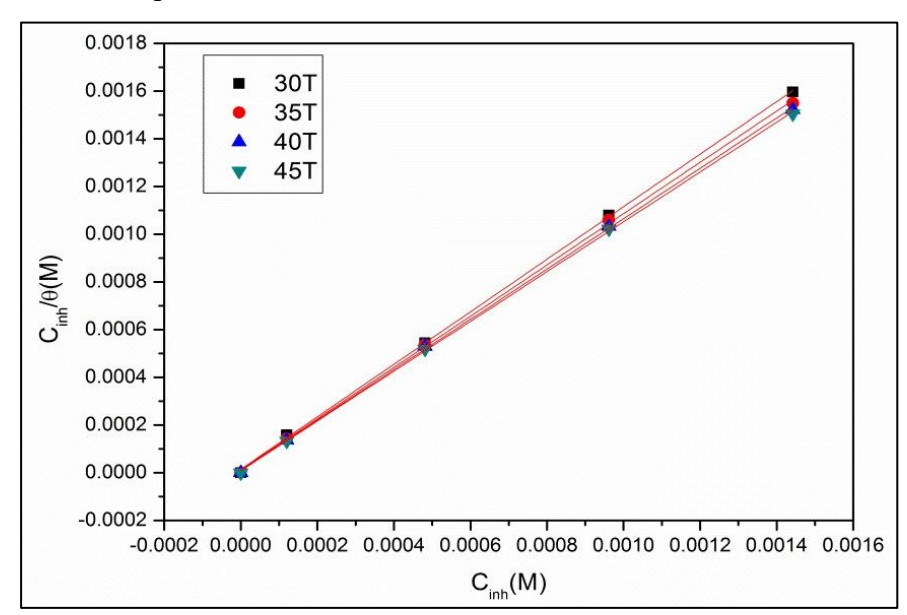


Figure 7: Langmuir adsorption isotherms of FAMTT

Table 4: Thermodynamic parameters for adsorption of FAMTT on surface of maraging steel in 1M HCl

Temperature	Kads	ΔG^o ads	ΔH^o_{ads}	ΔS^o ads
°С	(mol ⁻¹ L)	(kJ mol ⁻¹)	(kJ mol ⁻¹)	(J mol ⁻¹ K ⁻¹)
30	7.16×10^4	-38.27		
35	8.98 x 10 ⁴	-39.49	28.43	220.29
40	1.03×10^5	-40.47		
45	1.24×10^5	-41.61		

Equation (10) was used to calculate ΔH^o_{ads} and ΔS^o_{ads} viz standard enthalpy of adsorption and standard entropy of adsorption

$$\Delta G^{o}_{ads} = \Delta H^{o}_{ads} - T\Delta S^{o}_{ads} (10)$$

The variation of ΔG^o_{ads} with T gives a straight line with an intercept that equals ΔH^o_{ads} and a slope that equals ΔS^o_{ads} . The equilibrium constant K_{ads} showed high values indicating that FAMTT is strongly adsorbed to the metal surface i.e. chemisorption. The interaction between the metal surface and FAMTT is further fortified as the temperature is increased suggested by increase in K_{ads} values with increase in temperature [Bouklah *et al.* (2006)]. This is a typical character of chemical mode of adsorption. The stability and spontaneity of formation of the adsorbed layer is governed by negative ΔG^o_{ads} values. Furthermore, as the temperature rises, the ΔG^o_{ads} values become more negative, consistent with the increased inhibition efficiency seen at higher temperatures favoured by enhanced FAMTT adsorption.

The ΔG^{o}_{ads} values for the FAMTT range from -38.27 to -41.61 kJ/mol, indicating that FAMTT adsorbs through both physical and chemical modes, with a predominant chemisorption mechanism [Nnanna *et al.* (2010)]. Chemisorption is responsible for the endothermic nature of adsorption, which is revealed by a positive sign of ΔH^{o}_{ads} [Durnie *et al.* (1999)]. Adsorption is followed with an increase in entropy, as indicated by a positive value of ΔS^{o}_{ads} . This is because more water molecules are desorbing at the surface as opposed to fewer FAMTT molecules simultaneously adsorbing. One way to characterize this is [Mu *et al.* 2004)].

$$FAMTT_{(solution)} + xH_2O_{(adsorbed)} \longrightarrow FAMTT_{(adsorbed)} + xH_2O$$

where, *x* is the number of adsorbed water molecules being replaced by one molecule of FAMTT. This indicates that there is an increase in randomness of the system which drives the adsorption process.

The thermodynamic parameters analysed for inhibitors DBAMTT and MTATT [Mary *et al.* (2018), (2020)] in 1M HCl also showed strong adsorption behaviour with increase in temperature which corelates to the observed increased inhibition efficiency. Though the thermodynamic studies carried out with FAMTT in 2:1 acid mixture showed similar trend [Mary *et al.* (2023)] as in HCl, the K_{ads} values observed in the former case were higher compared to the present study since the inhibitor functions well in low concentrations in 2:1 acid mixture.

3.3. EIS Studies

Fig. 8 displays Nyquist graphs demonstrating the corrosion behaviour of maraging steel in 1M HCl at 40°C with different FAMTT concentrations. At different temperatures, similar Nyquist

graphs were also seen. The plots' constant shape, with and without the inhibitor, suggests that the underlying corrosion mechanism remains unchanged when FAMTT is added.

The diameter of the Nyquist plot semicircles increased with the addition of the inhibitor, indicating a decrease in the rate of corrosion. As the concentration of FAMTT increased, the efficiency of inhibition increased as well. Both with and without FAMTT, the Nyquist plots showed a depressed capacitive loop at high frequencies (HF), which is explained by charge transfer during corrosion and protective film generation [Pinto *et al.* (2016)]. The slightly depressed nature of the semicircles is frequently linked to solid electrodes and is explained by frequency dispersion brought on by surface irregularities and other irregularities on the electrode surface [Qiang *et al.* (2017)].

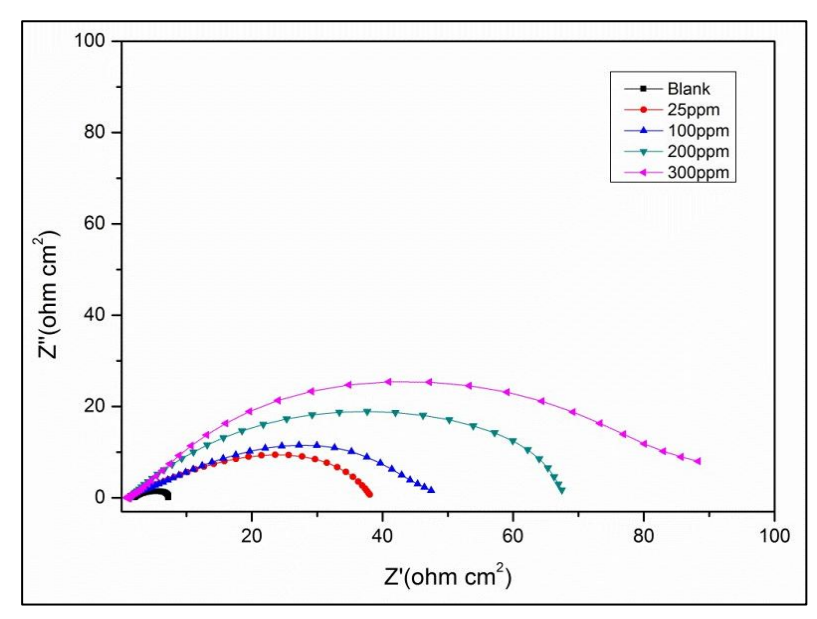


Figure 8: EIS curves for corrosion of maraging steel in 1M HCl containing different FAMTT concentrations at 40°C

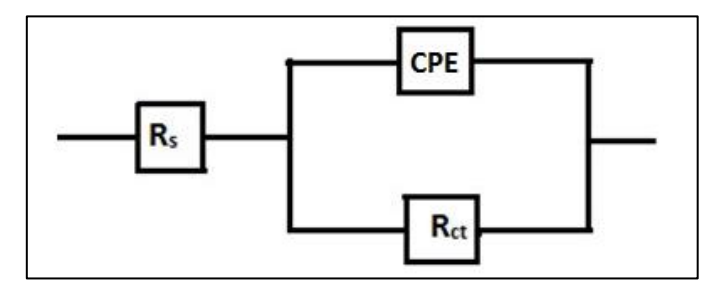


Figure 9: Equivalent circuit to fit the experimental EIS data for corrosion of maraging steel in 1M HCl

The impedance parameters are summarized in Table 5, while Fig. 9 illustrates the proposed equivalent circuit used to interpret the Nyquist spectra. The circuit comprises R_s , R_{ct} , and Q_{dl} . Due to surface roughness at the metal-solution interface, the double layer exhibits deviations from ideal capacitive behaviour. To account for this, a constant phase element (CPE) was

incorporated into the equivalent circuit to achieve a more accurate fit [Emregul and Atakol (2003)].

Table 5: Results of EIS studies for the corrosion of maraging steel in 1M HCl containing different FAMTT concentrations

Temperature	[FAMTT]	Rct	C _{dl} x 10 ³	η (%)
°C	(ppm)	(ohm cm ²)	(F cm ⁻²)	
	Blank	11.38	27.57	
30	25	51.19	9.29	77.76
	100	90.92	7.65	88.01
	200	110.50	3.42	89.70
	300	136.41	1.44	91.65
	Blank	7.44	42.11	
35	25	48.04	9.45	84.50
	100	64.56	7.85	88.47
	200	95.31	6.16	92.19
	300	116.6	1.63	93.61
	Blank	5.79	48.19	
40	25	39.43	11.74	85.31
	100	49.93	6.25	88.39
	200	69.63	8. 53	91.68
	300	89.77	2.24	93.54
	Blank	3.30	72.91	
45	25	33.24	12.62	90.04
	100	40.59	9.92	91.84
	200	48.44	3.46	93.16
	300	71.94	4.37	95.40

The charge transfer resistance R_{ct} shows an increase in inhibited solutions which is a result of the formation of a barrier by the inhibitor to the charge transfer reaction. The adsorption of FAMTT molecules onto the metal surface results in increase of thickness of electrical double layer at the metal-electrolyte interface, thereby, reducing the double layer capacitance C_{dl} [Finley and Hackerman (1960)]. FAMTT molecules may dislodge the water molecules and get adsorbed onto the metal surface to form a protective coating, and thereby, slowing the rate of metal dissolution,

as indicated by the rise in R_{ct} and the concomitant drop in C_{dl} [Vikneshvaran and Velmathi (2019)].

Equation (11) was used to calculate the inhibitor efficiency, $\eta(\%)$:

$$\eta~(\%~) = \frac{R_{ct(inh)} - R_{ct}}{R_{ct(inh)}} \times 100~(11)$$

where, the charge transfer resistances obtained in inhibited and uninhibited solutions are denoted as $R_{ct(inh)}$ and R_{ct} respectively. C_{dl} values were calculated using the equation

$$C_{dl} = Q(\omega_{max})^{n-1} (12)$$

where, the Constant Phase Element (CPE) constant is denoted as Q, the frequency at which the imaginary part of impedance (- Z_i) has a maximum value is denoted as ω_{max} , and CPE exponent is denoted as n. The value of n signifies surface homogeneity [Huong *et al.* (2019)].

The corrosion inhibition efficiencies at all temperatures reach saturation values when the inhibitor's concentrations reach very close to 300 ppm. This is very similar to that observed in weight loss and polarization studies.

3.4. SEM-EDX Analysis

Changes in the surface morphology of the specimens exposed to the acidic media, both with and without the FAMTT inhibitor, were investigated by SEM-EDX analysis. The samples were finely polished and left in the acidic medium for six hours before being subjected to SEM-EDS analysis. Fig. 10 and Fig.11 present the SEM and EDX images of the maraging steel surfaces under various exposure conditions. The SEM image of the uninhibited maraging steel sample revealed a rough surface with visible cracks and pits. In contrast, the inhibited samples exhibited a smoother surface, attributed to the adsorption of the inhibitor onto the metal surface.

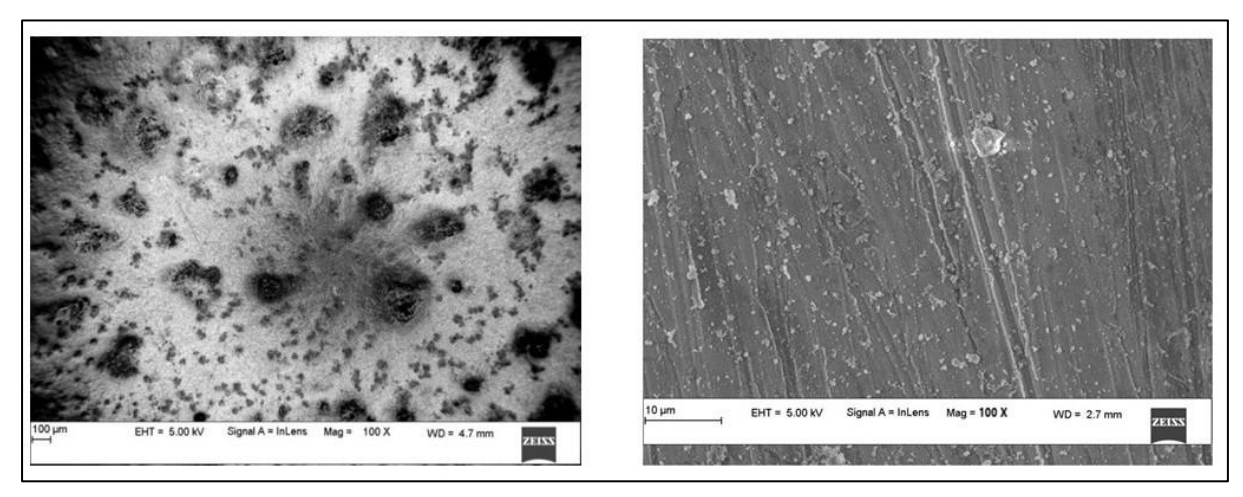


Figure 10: SEM images of maraging steel immersed in aggressive medium without any inhibitor (a) containing FAMTT with concentration 300 ppm (b)

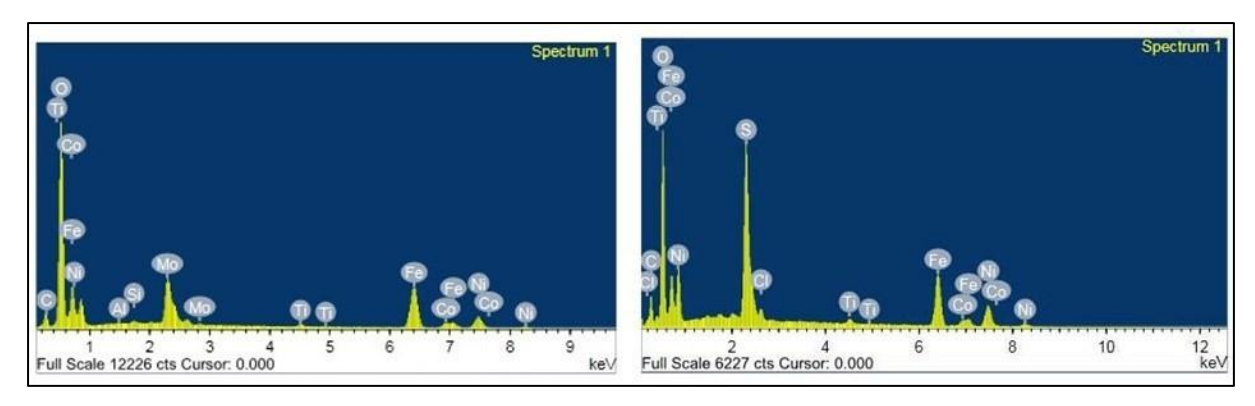


Figure 11: EDX spectrum of maraging steel without any inhibitor (a) containing FAMTT with concentration 300 ppm (b)

The EDX spectrum of the uninhibited sample (Figure 11a) showed no sulphur peaks, whereas the spectrum of the inhibited sample displayed a sulphur peak along with a high-intensity oxygen peak which can be attributed to the adsorbed FAMTT molecules on the maraging steel surface and thereby explaining its inhibition efficiency.

3.5. Corrosion Inhibition Mechanism

Organic molecules such as FAMTT with several hetero atoms and π -electron systems inhibit metal corrosion in suitable media through their ability to adsorb onto the metal surface. Greater the electron density within the molecule and the electron cloud surrounding donor atoms, stronger is the adsorption. This leads to the formation of a barrier-like film on the sample's surface.

The adsorption has characteristics of both physisorption as well as chemisorption, but largely chemisorption. Physisorption results due to the alignment of positively charged FAMTT molecules (which is due to the protonation of FAMTT in 1M HCl) closer to the oppositely charged metal surface. The remaining FAMTT molecules that remain neutral in the solution take up exposed adsorption sites on the surface leading to chemisorption via sharing of electrons between the donor atoms of FAMTT and the metal surface. The strength of chemisorption is further enhanced by the fact that iron's unoccupied d-orbitals encourage donor-acceptor interactions between the π -electrons of the aromatic rings of FAMTT and the metal surface [Faiz *et al.* (2024)].

For iron and steel corrosion, in acid medium, the mechanism suggested is shown below [Obot *et al.* (2011)].

 $Fe + H_2O FeOH_{ads} \rightarrow H^+ + e^-$

FeOH_{ads} FeOH⁺ + **→** (rate determining step)

 $FeOH^+ + H^+ Fe^{2} + H_2O$

Following are the steps for cathodic hydrogen evolution:

Bhumi Publishing, India October 2025

```
Fe + H<sup>+</sup> (FeH<sup>+</sup>)<sub>ads</sub> \rightarrow

(FeH<sup>+</sup>)<sub>ads</sub> + e<sup>-</sup> (FeH)<sub>ads</sub>

(FeH)<sub>ads</sub> + H<sup>+</sup> + e<sup>-</sup>Fe\rightarrow H<sub>2</sub>
```

The mechanism suggested above is validated not just by experimental data but also by theoretical calculations. DFT studies were conducted on FAMTT and other related inhibitors and results were presented in our previous work [Mary *et al.* (2023)]. Different properties/parameters of FAMTT and related Schiff bases DBAMTT & MTATT were computed by DFT method using B3LYP/6-311++g(d,p) basis set and reported [Mary *et al.* (2023)].

According to the HOMO-LUMO study, the FAMTT molecule has an energy gap of 3.9987 eV with a greater E_{HOMO} value (-6.3720 eV) and a lower E_{LUMO} value (-2.3733) [Mary *et al.* (2023)]. While lower values of E_{LUMO} are more likely to be associated with the molecule's capacity to take electrons [Fang and Li (2002), Ebenso *et al.* (2010)], higher values of E_{HOMO} indicate greater chances of the electrons being donated to the empty molecular orbital of a suitable acceptor molecule having lower energy [Udhayakala *et al.* 2012)]. The energy gap between HOMO and LUMO can be used to evaluate the compound's chemical behaviour.

A deeper analysis of the HOMO and LUMO of FAMTT shows that the HOMO is distributed over the triazole ring and partially on the benzofuran ring, whereas, the LUMO is distributed over the furan ring and partially on the triazole ring. This suggests a charge transfer from the triazole ring of FAMTT through unsaturation (C = N) group to the furan ring. According to DFT computation, the presence of electron-rich sites helps FAMTT attach to the metal surface by donating electrons, whereas the presence of electron-deficient sites allows the molecule to simultaneously take electrons from the metal and display back bonding. This facilitates a stronger interaction of FAMTT molecule with the steel surface the surface of the steel thereby ensuring chemisorption. Further, other computed parameters, namely, Ionization potential (I), Electron affinity (A), Electronegativity (χ), Global hardness (η), Chemical softness (ν), Chemical potential (μ), Electrophilicity index (ω), the fraction of electrons transferred (ΔN) and backdonation (ΔE) also signify greater binding capacity of FAMTT on steel surface and, thereby, justify good corrosion inhibition efficiency shown by FAMTT [Mary *et al.* (2023)].

Conclusion:

Weight loss, Tafel, and EIS tests were employed to assess various parameters for the corrosion inhibition of maraging steel by FAMTT in 1M HCl medium. Since each result displayed comparable variances, they are all in good agreement with one another. FAMTT demonstrated improved corrosion inhibition properties at higher temperatures and concentration. Mixed type inhibitory action was demonstrated by Tafel experiments. The inhibiting property of FAMTT

may be attributed to its adsorption following Langmuir adsorption isotherm onto the metal surface. Based on thermodynamic calculations, the chemisorption mode of adsorption was found to be predominant. SEM-EDX examination revealed differences in the surface morphology of the inhibited and uninhibited samples. There is a correlation between the experimental data and DFT simulations, suggesting that FAMTT has strong inhibitory power. Based on weight loss and electrochemical measurements, in 1M HCl, FAMTT demonstrated better inhibition efficiency than those of structurally close molecules DBAMTT and MTATT, with the overall order of performance being FAMTT>MTATT>DBAMTT. Though the prediction about inhibition efficiencies made from DFT calculations do not exactly fit with the experimental results, there are similarities among the theoretical and experimental results based on certain estimated parameters. This discrepancy is largely because of the fact that neutral molecules in gas phase were used for computational purpose while, in the experimental conditions, the molecules existed even in the protonated form due to the acidic nature of the medium.

References:

- 1. Balangao, J. K. B. (2024). Corrosion of metals: Factors, types and prevention strategies. *Journal of Chemical Health Risks*, 14, 79–87.
- 2. Zulfareen, N., Venugopal, T., & Kannan, K. (2018). Experimental and theoretical studies on the corrosion inhibition of brass in hydrochloric acid by N-(4-((4-benzhydryl piperazin-1-yl) methyl carbamoyl) phenyl) furan-2-carboxamide. *International Journal of Corrosion*, Article ID 9372804.
- 3. Kumar, P., & Shetty, A. N. (2014). Corrosion inhibition effect of 2,5-bis (3,4,5-trimethoxy phenyl)-1,3,4-oxadiazole (BTPO) on 18 Ni M250 grade welded maraging steel in 1.0 M sulphuric acid medium. *Journal of Materials and Environmental Science*, 5, 873–886.
- 4. Kadhim, A., Al-Amiery, A. A., Alazawi, R., Al-Ghezi, M. K. S., & Abass, R. H. (2021). Corrosion inhibitors: A review. *International Journal of Corrosion and Scale Inhibition*, 10, 54–67.
- 5. Obot, I. B., Obi-Egbedi, N. O., & Umoren, S. A. (2009). Antifungal drugs as corrosion inhibitors for aluminium in 0.1 M HCl. *Corrosion Science*, *51*, 1868–1875.
- 6. Xu, B., Yang, W., Liu, Y., Yin, X., Gong, W., & Chen, Y. (2014). Experimental and theoretical evaluation of two pyridine carboxaldehyde thiosemicarbazone compounds as corrosion inhibitors for mild steel in hydrochloric acid solution. *Corrosion Science*, 78, 260–268.
- Abdulridha, A. A., Allah, M. A. A. H., Makki, S. Q., Sert, Y., Salman, H. E., & Balakit, A.
 A. (2020). Corrosion inhibition of carbon steel in 1 M H₂SO₄ using new azo Schiff

- compound: Electrochemical, gravimetric, adsorption, surface and DFT studies. *Journal of Molecular Liquids*, 315, 113690.
- 8. Singh, A., Ansari, K. R., Ali, I. H., Ibrahimi, B. E., Sharma, N. R., Bansal, A., Alanazi, A. K., Younas, M., Alamri, A. H., & Lin, Y. (2023). Heteroatomic organic compound as a novel corrosion inhibitor for carbon steel in sulfuric acid: Detailed experimental, surface, molecular docking and computational studies. *Colloids and Surfaces A: Physicochemical and Engineering Aspects*, 673, 131692.
- 9. Huong, D. Q., Huong, N. T. L., Nguyet, T. T. A., Duong, T., Tuan, D., Thong, N. M., & Nam, P. C. (2020). Pivotal role of heteroatoms in improving the corrosion inhibition ability of thiourea derivatives. *ACS Omega*, *5*, 27655–27666.
- 10. Savitha, Mourya, P., Choubey, N., Singh, V. K., & Singh, M. M. (2016). Eco-friendly inhibitors for copper corrosion in nitric acid: Experimental and theoretical evaluation. *Metallurgical and Materials Transactions B*, 47, 47–57.
- 11. Abd El-Lateef, H. M., Shalabi, K., Sayed, A. R., Gomha, S. M., & Bakir, E. M. (2022). The novel polythiadiazole polymer and its composite with α-Al(OH)₃ as inhibitors for steel alloy corrosion in molar H₂SO₄: Experimental and computational evaluations. *Journal of Industrial and Engineering Chemistry*, 105, 238–250.
- 12. Klobčar, D., Tušek, J., Taljat, B., Kosec, L., & Pleterski, M. (2008). Aging of maraging steel welds during aluminium alloy die casting. *Computational Materials Science*, 44, 515–522.
- Grum, J., & Slabe, J. M. (2006). Effect of laser-remelting of surface cracks on microstructure and residual stresses in 12Ni maraging steel. *Applied Surface Science*, 252, 4486–4492.
- 14. Rezek, J., Klein, I. E., & Yahalom, J. (1997). Structure and corrosion resistance of oxides grown on maraging steel in steam at elevated temperatures. *Applied Surface Science*, 108, 159–165.
- 15. Sanatkumar, B. S., Nayak, J., & Shetty, A. N. (2012). The corrosion inhibition of maraging steel under weld-aged condition by 1(2E)-1-(4-aminophenyl)-3-(2-thienyl)prop-2-en-1-one in 1.5 M hydrochloric acid medium. *Journal of Coatings Technology and Research*, 9, 483–493.
- 16. Poornima, T., Nayak, J., & Shetty, A. N. (2012). Corrosion inhibition of the annealed 18 Ni 250 grade maraging steel in 0.67 M phosphoric acid by 3,4-dimethoxybenzaldehyde thiosemicarbazone. *Chemical Science International Journal, CSJ-69*.

- 17. Naik, P., Nayak, J., Girish, L. V., Somashekhar, T. M., Bhanuprakash, S. H., & Rahul, S. (2018). Effect of 1,2,3-benzotriazole on the corrosion of aged 18Ni250 grade maraging steel in phosphoric acid solution. *IOP Conference Series: Materials Science and Engineering*, 376, 012107.
- 18. El-Sayed, M. Sherif. (2014). Corrosion inhibition in 2.0 M sulphuric acid solutions of high strength maraging steel by aminophenyl tetrazole as a corrosion inhibitor. *Applied Surface Science*, 292, 190–196.
- 19. Singh, K. C., Sharma, M., & Singh, K. K. (2015). Applications of Schiff bases and their metal complexes: A short review. *International Journal of Emerging Technologies and Innovative Research*, 2, 2215–2219.
- 20. Mushtaq, I., Ahmad, M., Saleem, M., & Ahmed, A. (2024). Pharmaceutical significance of Schiff bases: An overview. *Future Journal of Pharmaceutical Sciences*, 10, 16.
- 21. Boulechfar, C., Ferkous, H., Delimi, A., Berredjem, M., Kahlouche, A., Madaci, A., Djellali, S., Boufas, S., Djedouani, A., Errachid, A., Khan, A. A., Boublia, A., Lemaoui, T., & Benguerba, Y. (2023). Corrosion inhibition of Schiff base and their metal complexes with [Mn(II), Co(II) and Zn(II)]: Experimental and quantum chemical studies. *Journal of Molecular Liquids*, 378, 121637.
- 22. Emregul, K. C., Kurtaran, R., & Atakol, O. (2003). An investigation of chloride-substituted Schiff bases as corrosion inhibitors for steel. *Corrosion Science*, *14*, 2803–2817.
- Jamil, D. M., Al Okbi, A. K., Al Baghdadi, S. B., Al Amiery, A. A., Kadhim, A., Gaaz, T. S., Kadhum, A. A. H., & Mohamad, A. B. (2018). Experimental and theoretical studies of Schiff bases as corrosion inhibitors. *Chemistry Central Journal*, 12, 7.
- 24. Mary, R. N., Nazareth, R., & Suchetan, P. A. (2018). Inhibition effect of 4-{[4-(dimethylamino)benzylidene]amino}-5-methyl-4H-1,2,4-triazole-3-thiol on the corrosion of maraging steel in 1.5 M HCl. *Journal of Applied Chemistry*, 7, 1713–1727.
- 25. Mary, R. N., Nazareth, R., Murthy, P. K., & Suchetan, P. A. (2020). Experimental and theoretical study of corrosion behavior of maraging steel in 1 M HCl in the presence of 5-methyl-4-[(E)-(thiophen-2-ylmethylidene)amino]-4H-1,2,4-triazole-3-thiol. *Asian Journal of Chemistry*, 32(4), 845–852.
- 26. Mary, R. N., Nazareth, R., Murthy, P. K., & Suchetan, P. A. (2021). Investigation of corrosion inhibition property of triazole-based Schiff bases on maraging steel in acid mixtures. *Journal of Failure Analysis and Prevention*, 21(2), 547–562.

- 27. Mary, R. N., Nazareth, R., Murthy, P. K., & Suchetan, P. A. (2023). Schiff bases derived from triazoles as corrosion inhibitors for maraging steel in acid mixtures: Experimental and theoretical studies. *Polycyclic Aromatic Compounds*, 43(3), 2788–2809.
- 28. Bai, Y., Zhao, G., Li, C., Zhao, S., & Shi, Z. (2008). Microwave-enhanced reactions of 4-amino-5-mercapto-1,2,4-triazoles with benzoyl chloride and aromatic aldehydes. *Synthetic Communications*, 38(19), 3311–3319.
- 29. Beck, A. D. (1993). Density functional thermochemistry. III. The role of exact exchange. *Journal of Chemical Physics*, 98, 5648–5652.
- 30. Lee, C., Yang, W., & Parr, G. (1988). Development of the Colle–Salvetti correlation-energy formula into a functional of the electron density. *Physical Review B: Condensed Matter and Material Physics*, *37*, 785–789.
- 31. Frisch, M. J., Trucks, G. W., Schlegel, H. B., Scuseria, G. E., Robb, M. A., Cheeseman, J. R., Scalmani, G., Barone, V., Mennucci, B., Petersson, G. A., *et al.* (2010). *Gaussian 09, Revision B.01*. Wallingford, CT: Gaussian, Inc.
- 32. Dennington, R., Keith, T., & Millam, J. (2009). *GaussView, Version 5*. Shawnee Mission, KS: Semichem Inc.
- 33. Yetri, Y., Emriadi, Jamarun, N., & Gunawarman. (2014). Corrosion inhibition efficiency of mild steel in hydrochloric acid by adding *Theobroma cacao* peel extract. *International Conference on Biological, Chemical and Environmental Sciences (BCES-2014)*, June 14–15. (a) Fontana, M. G. (2005). *Corrosion testing in corrosion engineering* (3rd ed.). New Delhi: Tata McGraw Hill. (b) Fontana, M. G. (1987). *Corrosion engineering* (3rd ed.). New York: McGraw-Hill International Edition.
- 34. Chaitra, K. T., Mohana, K. N., & Tandon, H. C. (2018). Evaluation of newly synthesized hydrazones as mild steel corrosion inhibitors by adsorption, electrochemical, quantum chemical and morphological studies. *Arab Journal of Basic and Applied Sciences*, 25, 45–55.
- 35. Prabhu, R. A., Shanbhag, A. V., & Venkatesh, T. V. (2007). Influence of tramadol on corrosion inhibition of mild steel in acidic media. *Journal of Applied Electrochemistry*, 37, 491–497.
- 36. Li, W. H., He, Q., Pei, C. L., & Hou, B. R. (2007). Experimental and theoretical investigation of adsorption behavior of new triazole derivatives as inhibitors for mild steel corrosion in acid media. *Electrochimica Acta*, *52*, 6386–6397.

- 37. Vikneshvaran, S., & Velmathi, S. (2019). Schiff bases of 2,5-thiophenedicarboxaldehyde as corrosion inhibitor for stainless steel under acidic medium: Experimental, quantum chemical and surface studies. *Chemistry A European Journal, 4*, 387–392.
- 38. Poornima, T., Nayak, J., & Shetty, A. N. (2011). 3,4-Dimethoxy benzaldehyde thiosemicarbazone as corrosion inhibitor for aged 18Ni 250 grade maraging steel in 0.5 M sulphuric acid. *Journal of Applied Electrochemistry*, 41, 223–233.
- 39. Abdel Rehim, S. S., Magdy, A. M., & Ibrahim, K. F. (1999). 4-aminoantipyrine as an inhibitor of mild steel corrosion in HCl solutions. *Journal of Applied Electrochemistry*, 29, 593–599.
- 40. Prabhu, D., & Rao, P. (2013). *Coriandrum sativum* L.—A novel green inhibitor for the corrosion inhibition of aluminium in 1.0 M phosphoric acid solution. *Journal of Environmental Chemical Engineering*, 1, 676–683.
- 41. Hour, T. P., & Holliday, R. D. (1953). The inhibition by quinolones and thioureas on the acid dissolution of mild steel. *Journal of Applied Chemistry*, 3, 502–513.
- 42. Huong, D. Q., Duong, T., & Nam, P. C. (2019). Effect of the structure and temperature on corrosion inhibition of thiourea derivatives in 1.0 M HCl solution. *ACS Omega*, 4, 14478–14489.
- 43. Ameer, M. A., Fekry, A. M., & Othman, A. (2014). Electrochemical investigation of green inhibitor adsorption on low carbon steel in produced water. *International Journal of Electrochemical Science*, *9*, 1964–1985.
- 44. Franklin, T. S., Rajesh, A., Mideen, S., Karthikeyan, J., & Anitha, S. (2012). Inhibitive effect of N,N-bis(2-chloroethylaminobenzaldehyde) ethylthiosemicarbazone on the corrosion of mild steel in 1N H₂SO₄. *Journal of Science and Technology*, *5*, 2810–2815.
- 45. Bouklah, M., Benchat, N., Hammouti, B., Aouniti, A., & Kertit, S. (2006). Thermodynamic characterization of steel corrosion and inhibitor adsorption of pyridazine compounds in 0.5 M H₂SO₄. *Materials Letters*, 60, 1901–1905.
- 46. Nnanna, L. A., Onwuagba, B. N., Mejeha, I. M., & Okeoma, K. B. (2010). Inhibition effects of some plant extracts on the acid corrosion of aluminium alloy. *African Journal of Pure and Applied Chemistry*, 4, 11–16.
- 47. Durnie, W., De Marco, R., Jefferson, A., & Kinsella, B. (1999). Development of a structure–activity relationship for oil field corrosion inhibitors. *Journal of Electrochemical Society*, *146*, 1751–1756.

- 48. Mu, G. N., Li, X., & Li, F. (2004). Synergistic inhibition between o-phenanthroline and chloride ion on cold rolled steel corrosion in phosphoric acid. *Materials Chemistry and Physics*, 86, 59–68.
- 49. Pinto, G. M., Nazareth, R. A., Shetty, A. N., & Nayak, J. (2016). Electrochemical, SEM/EDX study of 3-ethyl-4-amino-5-mercapto-1,2,4-triazole as inhibitor for corrosion of 6061 Al–15 vol. pct. SiC(p) composite and its base alloy in sulphuric acid medium. *Journal of Chemical and Pharmaceutical Research*, 8, 84–106.
- 50. Qiang, Y., Zhang, S., Yan, S., Zou, X., & Chen, S. (2017). Three indazole derivatives as corrosion inhibitors of copper in a neutral chloride solution. *Corrosion Science*, 126, 295–304.
- 51. Emregul, K. C., & Atakol, O. (2003). Corrosion inhibition of mild steel by Schiff base compounds in 1 M HCl. *Materials Chemistry and Physics*, 82, 188–193.
- 52. Finley, H. F., & Hackerman, N. (1960). Effect of adsorption of polar organic compounds on the reactivity of steel. *Journal of Electrochemical Society*, 107, 259–263.
- 53. Faiz, M., Zahari, A., Awang, K., & Hussin, H. (2020). Corrosion inhibition on mild steel in 1 M HCl solution by *Cryptocarya nigra* extracts and three of its constituents (alkaloids). *RSC Advances*, 10, 6547–6562.
- 54. Obot, I. B., Obi-Egbedi, N. O., & Eseola, A. O. (2011). Anti-corrosion potential of 2-mesityl-1H-imidazo[4,5-f][1,10]-phenanthroline on mild steel in sulphuric acid solution: Experimental and theoretical study. *Industrial & Engineering Chemistry Research*, 50, 2098–2110.
- 55. Fang, J., & Li, J. (2002). Quantum chemistry study on the relationship between molecular structure and corrosion inhibition efficiency of amides. *Journal of Molecular Structure: THEOCHEM*, 593, 179–185.
- 56. Ebenso, E. E., Isabirye, D. A., & Eddy, N. O. (2010). Adsorption and quantum chemical studies on the inhibition potentials of some thiosemicarbazides for the corrosion of mild steel in acidic medium. *International Journal of Molecular Sciences*, 11, 2473–2498.
- 57. Udhayakala, P., Rajendiran, T. V., & Gunasekaran, S. (2012). Density functional theory investigations for the adsorption of some oxadiazole derivatives on mild steel. *Journal of Advanced Scientific Research*, 3, 67–74.

SYNTHESIS OF TETRAPHENYLETHYLENE-

AND OLIGOPHENYLENEVINYLENE-CORED DENDRIMERS

Priyabrata Roy

Department of Chemistry,

Victoria Institution (College), 78B, A.P.C. Road, Kolkata 700009, India

Corresponding author E-mail: priyo chem@yahoo.co.in

Abstract:

Dendritic π -conjugated materials represent an important class of organic semiconductors with wide-ranging applications in optoelectronics, particularly in organic light-emitting devices (OLEDs). This chapter details the synthesis of two families of conjugated dendrimers constructed on tetraphenylethylene (TPE) and oligophenylenevinylene (OPV) scaffolds. The TPE-cored stilbenoid dendrimers were assembled via multifold Heck coupling of tetraiodo-TPE with either simple styrene or pre-functionalized stilbenoid dendrons, yielding dendrimers of varying steric complexity. In parallel, OPV-based dendrimers were synthesized through a modular route involving Horner-Wadsworth-Emmons condensation to prepare a tetrabromo-OPV core, followed by functionalization via Suzuki-Miyaura and Buchwald-Hartwig crosscoupling with thiophene, triphenylamine, and carbazole substituents. Comprehensive characterization was carried out using NMR spectroscopy, MALDI-TOF mass spectrometry, and elemental analysis. The synthetic strategies highlight complementary strengths: while TPE dendrimers showcase the versatility of multifold Heck reactions, OPV dendrimers demonstrate higher yields, modularity, and improved solubility, simplifying purification and processing. Together, these methods establish TPE and OPV as robust scaffolds for dendrimer construction, offering tunable optoelectronic properties. The presented synthetic approaches provide scalable and versatile routes toward conjugated dendrimers, making them valuable platforms for advancing OLED technology and other organic electronic applications.

Keywords: Tetraphenylethylene, Oligophenylenevinylene, Dendrimers, Heck coupling, Suzuki–Miyaura coupling, Buchwald–Hartwig amination, OLEDs.

1. Introduction:

Organic light-emitting devices (OLEDs) have emerged as promising candidates for flat-panel display technologies.¹,² Among the three primary colors, efficient blue-light emitters are particularly critical for full-color display applications^{3–8} and as donor materials for generating white-light OLEDs through exothermic energy transfer.^{9–13} However, achieving high-

performance blue emitters that simultaneously offer strong color purity, stability, and high fluorescence efficiency remains a challenge.

One important subclass of conjugated organic materials is dendritic poly(phenylenevinylenes), also known as stilbenoid dendrimers. Their highly branched structures with conjugated backbones have been applied as molecular wires,¹⁴ active layers in light-emitting diodes,¹⁵ organic lasers,¹⁶ and optoelectronic devices.^{16c} A particularly useful scaffold for such systems is tetraphenylethylene (TPE), which allows diagonal, lateral, and cross conjugation due to its four phenyl substituents. When substituted with stilbenoid dendrons, these TPE-based dendrimers exhibit unique electronic interactions, with the dendritic arms serving as light-harvesting antennae.^{15b}

In parallel, oligophenylenevinylene (OPV) scaffolds represent another class of versatile π conjugated frameworks. Their modular design allows functionalization at the para positions with
electron-donating substituents such as triphenylamine (TPA), thiophene (T), and carbazole (C).
Such substitutions strongly influence π -delocalization, especially at the para position, and often
lead to enhanced conjugation compared to ortho or meta substitution.¹⁷

This chapter describes the synthesis of two families of dendrimers:

- 1. **TPE-cored stilbenoid dendrimers** via multifold Heck coupling.
- 2. **OPV-cored dendrimers** via Suzuki–Miyaura and Buchwald–Hartwig cross-coupling.

2. Synthetic Strategy

The overall synthetic design involves two components:

- **Preparation of dendrons and functionalized cores** through halogenation, substitution, Arbuzov, Wittig, and Horner–Wadsworth–Emmons (HWE) reactions.
- **Pd-catalyzed coupling reactions** (Heck, Suzuki–Miyaura, and Buchwald–Hartwig) for the assembly of dendrimers.

The stilbenoid dendrimers were synthesized by attaching stilbenoid dendrons to a tetraiodo-TPE scaffold through a fourfold Heck reaction (Schemes 1–2). The OPV-based dendrimers were constructed by preparing a tetrabromo-OPV core via HWE condensation, followed by Suzuki–Miyaura and Buchwald–Hartwig couplings with donor groups (Schemes 3–4).

3. Experimental Section

3.1 Synthesis of Stilbenoid Dendrons (Scheme 1)

The synthesis began with methyl anthranilate (1), which was subjected to dibromination followed by diazotization—deamination with *tert*-butyl nitrite in DMF. This transformation furnished methyl 3,5-dibromobenzoate (2) in 65% yield. Compound 2 underwent twofold Heck coupling with 4-*tert*-butylstyrene under Jeffery's phase-transfer conditions (Pd(OAc)₂, n-Bu₄NBr, KOAc, DMF, 100 °C), providing derivative 3 in 75% yield. Subsequent reduction of 3

with LiAlH₄ in THF gave benzyl alcohol 4 in 78% yield. Oxidation of 4 with pyridinium dichromate (PDC) followed by a Wittig reaction using methyltriphenylphosphonium bromide/NaH produced the terminal olefin dendron 5 in 66% yield.¹⁹

Scheme 1: Reagents and conditions: (a) (i) Br₂, HOAc; (ii) t-BuONO, DMF, 60°C; (b) 4-t-butylstyrene, Pd(OAc)₂, n Bu₄NBr, KOAc, DMF, 90°C, 24h; (c) LiAlH₄, THF, rt; (d) PDC, CH₂Cl₂, rt; (e) Ph₃P+MeI¹, n-BuLi, THF, -20°C.

Scheme 2. Reagents and conditions: (a) 4-t-butylstyrene, Pd(OAc)₂, n-Bu₄NBr, PPh₃, KOAc, DMF, 100°C, 24 h, 45%; (b) 5, Pd(OAc)₂, n-Bu₄NBr, PPh₃, KOAc, DMF, 100°C, 48 h, 21%

3.2 Synthesis of Tetraiodo-TPE Core

Tetraphenylethylene (TPE) was iodinated with I₂–PhI(OAc)₂ in dichloromethane at room temperature for 60 h under dark conditions, affording tetraiodide 6 in 76% yield.²⁰,²¹

3.3 Construction of Stilbenoid Dendrimers (Scheme 2)

Fourfold Heck coupling of tetraiodide 6 with 4-tert-butylstyrene using Pd(OAc)₂, n-Bu₄NBr, and KOAc in DMF at 100 °C afforded dendrimer 7 in 45% yield. Under the same conditions, coupling of 6 with dendron 5 gave the X-shaped meta-branched dendrimer 8 in 21% yield.²²

3.4 Synthesis of OPV Core (Scheme 3)

Starting from 1,4-bisdodecyloxybenzene (9),²³ bis-bromomethylation using paraformaldehyde and HBr produced dibromide 10. Arbuzov reaction with triethyl phosphite afforded diphosphonate 11, which was then reacted with 4,4'-dibromobenzophenone in a Horner–Wadsworth–Emmons (HWE) condensation to yield the tetrabromo-OPV core 12.²⁴

Scheme 3: Reagents and conditions: (a) paraformaldehyde, 50% HBr in acetic acid, AcOH, 80 °C, 5 h; (b) Triethyl phosphite, 150 °C, 12 h; (c) 4,4′-dibromobenzophenone, *t*-BuOK, THF, 20 h, rt.

3.5 Functionalization of OPV Core (Scheme 4)

- Suzuki–Miyaura coupling of 12 with 2-thienylboronic acid yielded **OPV-T** (13) in 74% yield.
- Coupling of 12 with 4-(diphenylamino)phenylboronic acid produced OPV-TPA (14) in 71% yield.
- Buchwald–Hartwig amination of 12 with carbazole (prepared according to literature procedure¹⁴) using Pd(OAc)₂/P(t-Bu)₃ and NaOt-Bu in toluene gave **OPV-C** (15) in 76% yield.

All final dendrimers were purified by column chromatography and fully characterized by ¹H and ¹³C NMR spectroscopy, MALDI-TOF mass spectrometry, and elemental analysis.

Scheme 4: Reagents and conditions: (a) 2-thienylboronic acid, Pd(PPh₃)₄, K₂CO₃, toluene, H₂O, Aliquat 336, 90 °C, 16 h; (b) 4-(diphenylamino)phenylboronic acid, Pd(PPh₃)₄, K₂CO₃, toluene, H₂O, Aliquat 336, 90 °C, 16 h; (c) carbazole, Pd(OAc)₂, P(t-Bu)₃, NaOt-Bu, toluene, 100 °C, 3 days

4. Results and Discussion:

The synthetic routes demonstrate complementary strategies for accessing dendritic conjugated materials.

For the TPE-cored dendrimers, the Heck coupling methodology provided direct access to stilbenoid dendrimers. The use of simple styrene gave dendrimer 7 in moderate yield (45%), while the sterically demanding stilbenoid dendron reduced the yield of dendrimer 8 (21%), consistent with incomplete coupling due to steric hindrance.²²

In contrast, the OPV-cored dendrimers were obtained in higher yields (71–76%) owing to the robustness of Suzuki–Miyaura and Buchwald–Hartwig cross-coupling strategies. Importantly, the OPV derivatives exhibited excellent solubility in organic solvents (CHCl₃, CH₂Cl₂, THF, toluene), simplifying purification by column chromatography instead of sublimation.

Thus, while TPE-based dendrimers highlight the versatility of multifold Heck reactions, OPV-based dendrimers demonstrate superior synthetic efficiency, modularity, and processability.

Conclusion:

Two complementary synthetic approaches were developed for dendrimer construction:

- 1. TPE-based stilbenoid dendrimers via fourfold Heck coupling reactions.
- 2. OPV-based dendrimers via Suzuki-Miyaura and Buchwald-Hartwig reactions.

These strategies establish tetraphenylethylene and oligophenylenevinylene as valuable scaffolds for the creation of conjugated dendrimers. The methodologies described here provide reliable, scalable, and versatile routes for synthesizing dendrimers suitable for applications in organic optoelectronics.

References:

- 1. Fuhrmann, T., & Salbeck, J. (2003). MRS Bulletin, 28, 354.
- 2. Tang, C. W., & Van Slyke, S. A. (1987). Applied Physics Letters, 51, 913.
- 3. Hosokawa, C., Eida, M., Matsuura, M., Fukuoka, K., Nakamura, H., & Kusumoto, T. (1997). *Synthetic Metals*, 91, 3.
- 4. Duan, Y., Zhao, Y., Chen, P., Li, J., Liu, S. Y., He, F., & Ma, Y. G. (2006). *Applied Physics Letters*, 88, 263503.
- 5. Shih, H.-T., Lin, C.-H., Shih, H.-H., & Cheng, C.-H. (2002). *Advanced Materials*, 14, 1409.
- 6. Shen, J. Y., Lee, C. Y., Huang, T.-H., Lin, J. T., Tao, Y.-T., Chien, C.-H., & Tsai, C. T. (2005). *Journal of Materials Chemistry*, 15, 2455.
- 7. Wu, C.-C., Lin, Y.-T., Wong, K.-T., Chen, R.-T., & Chien, Y.-Y. (2004). *Advanced Materials*, 16, 61.
- 8. Chiechi, R. C., Tseng, R. J., Marchioni, F., Yang, Y., & Wudl, F. (2006). *Advanced Materials*, 18, 325.
- 9. Jou, J.-H., Chiu, Y.-S., Wang, R.-Y., Hu, H.-C., Wang, C.-P., & Lin, H.-W. (2006). Organic Electronics, 7, 8.
- 10. Chuen, C. H., Tao, Y. T., Wu, F. I., & Shu, C. F. (2004). Applied Physics Letters, 85, 4609.
- 11. Galer, P., Korošec, R. C., Vidmar, M., & Šket, B. (2014). *Journal of the American Chemical Society*, 136, 7383.
- 12. Llanes-Pallas, A., Yoosaf, K., Traboulsi, H., Mohanraj, J., Seldrum, T., Dumont, J., Minoia, A., Lazzaroni, R., Armaroli, N., & Bonifazi, D. (2011). *Journal of the American Chemical Society*, 133, 15412.
- 13. Thompson, B. C., Kim, Y.-G., McCarley, T. D., & Reynolds, J. R. (2006). *Journal of the American Chemical Society*, 128, 12714.
- 14. Liégault, B., Lee, D., Huestis, M. P., Stuart, D. R., & Fagnou, K. (2008). *Journal of Organic Chemistry*, 73, 5022.
- 15. Bloor, D. (1995). Introduction to molecular electronics. In M. C. Petty, M. R. Bryce, & D. Bloor (Eds.), *Introduction to molecular electronics* (pp. 1–28). Edward Arnold: London.

- (a) Pillow, J. N. G., Halim, M., Lupton, J. M., Burn, P. L., & Samuel, I. D. W. (1999). *Macromolecules*, 32, 5985.
- (b) Halim, M., Pillow, J. N. G., Samuel, I. D. W., & Burn, P. L. (1999). *Advanced Materials*, 11, 371.
- (c) Tolosa, J., Romero-Nieto, C., Díez-Barra, E., Sánchez-Verdú, P., & Rodríguez-López, J. (2007). *Journal of Organic Chemistry*, 72, 3847.
- Dodabalapur, A., Berggren, M., Slusher, R. E., Bao, Z., Timko, A., Schiortino, P., Laskowski, E., Katz, H. E., & Nalamasu, O. (1998). *IEEE Journal on Selected Topics in Quantum Electronics*, 4, 67.
 - (b) Berggren, M., Dodabalapur, A., Bao, Z., & Slusher, R. E. (1997). *Advanced Materials*, 9, 968.
 - (c) Oldham, W. J. Jr., Lachicotte, R. J., & Bazan, G. C. (1998). *Journal of the American Chemical Society*, 120, 2987.
 - (d) Maddux, T., Li, W., & Yu, L. (1997). Journal of the American Chemical Society, 119, 844.
- 17. Sengupta, S., Sadhukhan, S. K., & Singh, R. S. (2002). Tetrahedron Letters, 43, 1117.
- 18. Jeffery, T. (1996). In S. L. Liebeskind (Ed.), *Advances in metal-organic chemistry* (Vol. 5, p. 153). JAI Press: Greenwich, CT.
- 19. Buckles, R. E., & Matlock, G. M. (1963). Organic Syntheses Collective Volume IV, 914.
- 20. Sengupta, S. (2004). Synlett, 7, 1191.
- 21. Wang, S., Oldham, W. J. Jr., Hudack, R. A. Jr., & Bazan, G. C. (2000). *Journal of the American Chemical Society*, 122, 5695.

NONLINEAR OPTICAL PROPAGATION: SELF-FOCUSING, BEAM COLLAPSE, AND FILAMENTATION IN KERR MEDIA

Swagatam Deva Nath*1 and Chiranjit Hazarika2

Abstract:

This chapter presents a comprehensive introduction to the fundamental principles underlying nonlinear optical phenomena, particularly self-focusing, beam collapse, and multiple filamentation in Kerr media. Beginning with a historical overview of light-matter interaction and the advent of laser technology, the discussion highlights how high-intensity laser beams induce nonlinear responses in optical materials. The nonlinear polarization is described using a power series expansion of the electric field, leading to the definition of higher-order susceptibilities and the characterization of the optical Kerr effect. The chapter examines how the intensity-dependent refractive index causes self-focusing and the subsequent formation of spatial solitons when nonlinear focusing counterbalances diffraction. The concepts of critical power and threshold power are introduced to determine the onset of beam collapse. The nonlinear Schrödinger equation (NLSE) is presented as a universal model governing these processes, with emphasis on its role in predicting self-focusing dynamics and singularity formation. Analytical and numerical approaches, including the split-step Fourier method and variational techniques, are discussed for modelling nonlinear propagation. The chapter concludes with an overview of multiple filamentation arising from high-power laser beams and methods to control filamentation through tailored beam shaping. Overall, this chapter establishes the theoretical framework necessary for understanding the nonlinear propagation of intense laser beams and sets the foundation for subsequent analysis and modelling.

Introduction:

Since antiquity, humans have been fascinated by the nature and behaviour of light - a fascination that has evolved into the scientific study of optics, cantered on understanding how light interacts with matter. When a light wave propagates through an optical medium, the oscillating electromagnetic field exerts a polarizing force on the electrons of the medium.

In ordinary light sources, the radiation fields are much smaller than the fields that bind electrons to atoms, and polarization is directly proportional to the electric field of the light wave - this

¹Department of Physics, Nanda Nath Saikia College, Titabar, Assam, India

²Department of Physics, Mariani College, Mariani, Assam, India

^{*}Corresponding author E-mail: swgtmdvnth@gmail.com

phenomenon is known as linear optics. Various light sources such as sunlight, burning torches, and excited matter have been used to study optical phenomena. Properties such as *monochromaticity*, *coherence*, and *directionality* are key components in optical communication and other applications of optics [1].

While early optics was confined to the linear regime, the invention of the laser by *Theodore H. Maiman* in 1960 opened an entirely new field—nonlinear optics—where light itself modifies the properties of the medium through which it propagates. Lasers emit coherent light and can achieve extremely high intensities, leading to strong nonlinear light–matter interactions. These interactions give rise to new optical phenomena such as optical harmonic generation, combination frequency production, and optical rectification [2].

1.1 Nonlinear Optics

Nonlinear optics (NLO) is a branch of physical optics that describes the behaviour of light in nonlinear media—media in which the dielectric polarization responds nonlinearly to the electric field [3]. Nonlinear effects of various kinds are observed at sufficiently high light intensities in all materials.

The response of a medium can be mathematically expressed as a power series in the electric field E:

$$P = \varepsilon_0 (\chi^{(1)}E + \chi^{(2)}E^2 + \chi^{(3)}E^3 + \cdots)$$

Here, $\chi^{(1)}$, $\chi^{(2)}$, and $\chi^{(3)}$ are the linear, second-order, and third-order susceptibilities, respectively.

- The second-order nonlinear phenomena are observed in non-centrosymmetric materials (without inversion symmetry) and include effects such as *electro-optic modulation*, *second-harmonic generation*, and *three-wave mixing*.
- Third-order nonlinear effects dominate in materials with inversion symmetry such as amorphous solids, liquids, or gases where $\chi^{(2)} = 0$. Examples include the *Kerr effect*, third-harmonic generation, four-wave mixing, and stimulated Raman scattering [4,5].

At low intensities, only the first term contributes, producing effects such as refraction and absorption. At higher intensities, higher-order terms become non-negligible, giving rise to phenomena where the medium's response depends on light intensity.

1.2 Optical Kerr Effect

The Kerr effect arises from third-order nonlinearity and leads to an intensity-dependent refractive index. In a Kerr medium, the nonlinear polarization is dominated by $\chi^{(3)}$ and results in:

$$n = n_0 + n_2 I$$

where n_0 is the linear refractive index, n_2 is the Kerr coefficient, and I is the light intensity [6]. As the intensity increases, the refractive index of the medium changes, altering the propagation of the beam. This phenomenon can lead to self-focusing or self-defocusing, depending on the sign of n_2 .

The Kerr effect is central to self-focusing, since it effectively creates a light-induced lens whose focal length depends on the beam's intensity distribution.

1.3 Kerr Nonlinearity

In Kerr materials, the refractive index depends on the light intensity. The nonlinear refractive index change is proportional to n_2I , and the nonlinear polarization can be expressed as:

$$P_{NL} = \varepsilon_0 \chi^{(3)} \mid E \mid^2 E$$

For positive n_2 , the refractive index increases with intensity, resulting in self-focusing; for negative n_2 , it decreases, resulting in self-defocusing.

Most materials have very small nonlinear coefficients ($n_2 \approx 10^{-16}$ to 10^{-14} cm²/W), requiring very high light intensities to observe measurable nonlinear effects. Excessively high intensities, however, can damage the material. Hence, developing materials with larger nonlinear coefficients has been a major research focus [6].

1.4 Self-Focusing

Self-focusing is a nonlinear optical phenomenon occurring in media with positive nonlinearity. A high-intensity laser beam causes a local increase in refractive index, effectively turning the medium into a waveguide that traps light within its high-intensity core.

In such a medium, the refractive index varies spatially according to the beam's intensity profile, $n = n_0 + n_2 I(r)$, where I(r) is the radial intensity distribution. The center of a Gaussian beam, being more intense, has a higher refractive index than its edges, causing the beam to focus.

When the nonlinear focusing balances diffraction spreading, self-trapping occurs, resulting in a non-spreading optical beam [8,9].

1.5 Critical Power

A light beam propagating in a Kerr medium will self-focus if its power exceeds a critical power P_{cr} , given by [6]:

$$P_{cr} = \frac{\alpha \lambda^2}{4\pi n_0 n_2}$$

where λ is the laser wavelength, n_0 is the linear refractive index, and n_2 characterizes the Kerr nonlinearity, α is a dimensionless constant depending on beam shape (for a Gaussian beam, $\alpha \approx 1.896$).

The critical power represents the threshold above which self-focusing dominates diffraction. It marks the onset of nonlinear beam collapse. When $P_0 > P_{cr}$, nonlinear effects dominate, leading to self-focusing. If $P_0 \gg P_{cr}$, the beam typically breaks up into multiple filaments, each carrying approximately the critical power [11].

1.6 Nonlinear Schrödinger Equation (NLSE)

The Nonlinear Schrödinger Equation (NLSE) is derived from Maxwell's equations and serves as a universal model describing nonlinear wave propagation in various fields including optics, acoustics, plasma physics, and hydrodynamics [11].

For an intense laser beam in a Kerr medium, the two-dimensional NLSE is expressed as:

$$\frac{\partial \psi}{\partial z} = \frac{1}{2jk_0} \nabla_t^2 \psi - j \frac{n_2}{n_0} k_0 |\psi|^2 \psi$$

where ψ is the complex field amplitude, k_0 the wave number, and ∇_t^2 the transverse Laplacian. This equation effectively models self-focusing and filamentation phenomena.

1.7 Optical Beam Collapse and Singularities

Optical beam collapse is an intrinsic feature of many nonlinear systems. It occurs when the nonlinear self-focusing overcomes diffraction, leading to a concentration of energy into a singular point [12–15].

Kelly [4] showed that diffraction cannot always prevent collapse in a Kerr medium and derived the self-focusing distance, beyond which the beam intensity grows catastrophically. Numerical and analytical studies [16–18] have since refined this understanding, yielding accurate formulas for predicting the collapse distance and threshold conditions.

1.8 Threshold Power

The threshold power for beam collapse or filamentation is slightly above the critical power. For a Gaussian input beam, it is approximately 1.8% higher, and for a super-Gaussian beam about 8.8% higher [17]. The threshold depends on the beam shape and ellipticity—elliptic beams require slightly higher power due to energy loss as they evolve into a radially symmetric (Townes) profile.

1.9 Optical Filaments

Optical filaments are narrow, high-intensity light channels that can propagate over distances much longer than the Rayleigh range without diffracting [10,11]. They result from a dynamic

balance between Kerr self-focusing and defocusing mechanisms such as plasma generation, nonlinear losses, or group velocity dispersion.

Filamentation gives rise to phenomena like supercontinuum generation, coloured conical emission, and nonlinear plasma channels. Though the Townes profile theoretically represents a stationary state, it is unstable in practice, so external mechanisms or saturation effects are necessary to sustain filaments.

1.10 Position of Nonlinear Focus

When a beam passes through a lens and propagates in a nonlinear medium, the nonlinear focus is shifted closer to the lens compared to the linear case. For a collimated beam, the focus distance is given by:

$$z_{sf} = 0.367 z_R / \sqrt{(P/P_{cr}) - 0.852}$$

where z_R is the Rayleigh range and P is the beam power.

If $P > P_{cr}$, the nonlinear effects cause earlier focusing and can lead to collapse or filamentation [6].

1.11 Numerical Methods

Analytical solutions to the Maxwell wave equation in nonlinear systems are rarely possible due to their complexity. Numerical methods such as finite difference, pseudo-spectral, variational, and split-step Fourier methods (SSFM) are widely used to solve the NLSE.

The SSFM is especially effective and computationally efficient. It separates the linear (diffraction) and nonlinear (self-action) effects, solving them alternately in small propagation steps. The variational method is another useful analytical approach, based on the *calculus of variations* and *Euler–Lagrange equations*, allowing approximate solutions with trial functions.

1.12 Multiple Filamentation

When beam power greatly exceeds P_{cr} , the beam may break up into several long, narrow filaments, a process known as multiple filamentation [11]. This phenomenon arises from symmetry-breaking mechanisms, such as input beam noise or beam ellipticity, since ideal Kerr media preserve radial symmetry.

- Noise-induced filamentation produces random, shot-to-shot variations in filament patterns [11].
- **Deterministic filamentation**, however, can be induced by beam ellipticity or polarization effects, resulting in reproducible filament structures [10].

Experimental observations confirm that increasing beam ellipticity lowers the threshold for multiple filamentation and that the filamentation pattern rotates with the input beam orientation [10].

1.13 Tailored Filaments and Control of Multiple Filamentation

Filamentation control—tailored filamentation—has become an active area of research, driven by applications such as *attosecond pulse generation*, *remote sensing*, *terahertz radiation generation*, and *laser-induced discharge guidance*.

Methods for controlling filamentation include introducing amplitude masks, phase modulation, or astigmatism (e.g., via a tilted lens). Experiments show that these techniques can stabilize or steer filamentation patterns [10].

Conclusion:

This chapter established the fundamental framework of nonlinear optics, emphasizing how the Kerr effect leads to self-focusing, beam collapse, and multiple filamentation in high-intensity laser propagation. It explained the role of the nonlinear Schrödinger equation as a universal model describing these dynamics and introduced analytical and numerical techniques for their analysis. The concepts of critical and threshold powers were defined to determine the onset of collapse. Finally, the discussion of filamentation and its control methods highlighted the intricate interplay between nonlinear self-action and external modulation, setting the stage for advanced studies in nonlinear beam dynamics.

References:

- 1. Boyd, R. W. (Ed.). (2009). *Self-focusing: Past and present* (Vol. 114, Chapter 4). Springer Science.
- 2. Gedalin, M., Scott, T. C., & Band, Y. B. (1997). Self-focusing and collapse of optical beams. *Physical Review Letters*, 78, 448.
- 3. Bloembergen, N. (1965). *Nonlinear optics*. W. A. Benjamin Inc.
- 4. Kelly, P. L. (1965). Self-focusing of optical beams. *Physical Review Letters*, 15, 1005–1008.
- 5. Centurion, M., Pu, Y., & Psaltis, D. (2005). Self-organization of spatial solitons. *Optics Express*, 12, 6202–6211.
- 6. Boyd, R. W. (2003). Nonlinear optics (3rd ed.). Academic Press.
- 7. Fibich, G. (2015). The nonlinear Schrödinger equation: Singular solutions and wave collapse. Springer.
- 8. Hercher, M. (1964). Laser-induced damage in transparent media. *Journal of the Optical Society of America*, 54, 563.

- 9. Chiao, R. Y., Garmire, E., & Townes, C. H. (1965). Self-trapping of optical beams. *Physical Review Letters*, *13*, 479–482.
- 10. Dubietis, A., Tamosauskas, G., Fibich, G., & Ilan, B. (2004). Multiple filamentation induced by input beam ellipticity. *Optics Letters*, 29, 1126–1129.
- 11. Bespalov, V. I., & Talanov, V. I. (1966). Filamentary structure of light beams in nonlinear media. *JETP Letters (Translated)*, *3*, 307–310.
- 12. Gedalin, M., Scott, T. C., & Band, Y. B. (1997). Nonlinear evolution and wave collapse. *Physical Review Letters*, 78, 448.
- 13. Ruprecht, P. A., Holland, M. J., Burnett, K., & Edwards, M. (1995). Time-dependent solution for collapsing Bose–Einstein condensates. *Physical Review A*, *51*, 4704.
- 14. Bradley, C., Sackett, C. A., Tollett, J. J., & Hulet, R. G. (1995). Evidence of Bose–Einstein condensation in an atomic gas with attractive interactions. *Physical Review Letters*, 75, 1687.
- 15. Mio, K., Ogino, T., Minami, K., & Takeda, S. (1976). Modified nonlinear Schrödinger equation for Alfvén waves propagating along the magnetic field in cold plasmas. *Journal of the Physical Society of Japan*, 41, 265.
- 16. Dawes, E. L., & Marburger, J. H. (1969). A computer study of self-focusing. *Physical Review*, 179, 862–868.
- 17. Fibich, G., & Papanicolaou, G. C. (1999). Self-focusing in the perturbed and unperturbed nonlinear Schrödinger equation in critical dimension. *SIAM Journal on Applied Mathematics*, 60, 183–240.
- 18. Fibich, G., Sivan, Y., & Weinstein, M. I. (2005). Self-focusing distance of very high-power laser pulses. *Optics Express*, *13*, 5897–5899.

(ISBN: 978-81-994425-3-5)

FOUNDATIONS OF MOLECULAR THERMODYNAMICS THROUGH STATISTICAL PARTITION FUNCTIONS

Naveen Awasthi

Department of Chemistry,

Janta College Bakewar (206124), Etawah, India

Corresponding author E-mail: nvn awsthi@rediffmail.com

Abstract:

The partition function is a fundamental concept in statistical thermodynamics that encapsulates how microscopic energy states of molecules determine macroscopic thermodynamic properties. This chapter examines the statistical basis of partition functions, including the Boltzmann distribution, canonical ensemble, and contributions from translational, rotational, Vibrational, and electronic energy modes. It discusses how partition functions allow calculation of essential quantities such as internal energy, free energy, entropy, and equilibrium constants. Examples from molecular systems highlight the quantitative impact of quantum effects and degeneracy, and the chapter also considers practical aspects such as symmetry and high-temperature behavior. The objective is to provide a cohesive theoretical foundation for understanding how partition functions bridge molecular behavior and observable thermodynamics.

Keywords: Quantum Effects and Degeneracy, Partition Functions, Translational, Rotational **Introduction:**

Thermodynamics describes how energy moves, how work is done, and how matter responds in macroscopic systems—predicting pressure, temperature, entropy, free energy, etc. However,

macroscopic systems—predicting pressure, temperature, entropy, free energy, etc. However, these macroscopic quantities emerge from the behavior of incredibly many molecules, each with discrete quantum energy levels. *Statistical thermodynamics* provides the formal machinery to connect the microscopic (molecules, atoms, energy levels) with the macroscopic (pressure, entropy, free energy). At the heart of this connection lies the partition function, a sum (or integral, in continuum limits) over all accessible quantum states of the system, weighted by the Boltzmann factor ($e^{-\beta \epsilon_{tx,l}}$). The canonical partition function, (Q), formally defined for a system at fixed temperature (T), volume (V), and particle number (N), plays several roles. First, it normalizes the probabilities of different energy states under thermal equilibrium. Second, it is the generator of thermodynamic observables: internal energy (U), Helmholtz free energy (A), entropy (S), which can be expressed as derivatives or functions of (Q). Third, for molecular systems, the partition function decomposes into separate contributions from translational,

rotational, Vibrational, and electronic motions each with distinct quantum features, degeneracy, and temperature dependence. In molecular gases especially, the translational contribution often dominates under standard conditions, but rotational and Vibrational modes can become significant at lower or higher temperatures, or when molecular symmetry, anharmonicity, or electronic excitation alter level spacing and degeneracy. Additionally, proper treatment of symmetry (e.g. indistinguishability in identical molecules), high-temperature limits, and cutoffs for electronic states are necessary to avoid divergences or large errors (as discussed in recent works, for example, in hydrogen partition function studies) [1-2]. Several other researchers also work on rotational partition function [3-4 and the relations with thermodynamic functions [5-6]. The aim of this chapter is to build up from the basic statistical postulates (microstates, ensembles, Boltzmann law) through explicit derivation of molecular partition functions, to show how these lead to observable thermodynamic properties and applications. Topics include translational partition function in an ideal gas, quantum rotational levels and symmetry corrections, Vibrational partition functions, electronic states, and issues such as convergence and approximations. Examples and problem cases are included to illustrate quantitative effects in real molecules.

Boltzmann Distribution Law

According to Boltzmann statistics, the number of molecules occupying a particular energy level depends on the energy of that level and the system's temperature.

The distribution is given as:

$$\frac{n_i}{n} = \frac{g_i e^{-\beta E_i}}{\sum_i g_i e^{-\beta E_i}} (1)$$

Where,

 \triangleright n_i = number of molecules in the i^{th} energy level,

 \rightarrow n = total number of molecules,

 \triangleright E_i = energy of the i^{th} level,

 \Rightarrow $\beta = \frac{1}{kT}$, with k as Boltzmann constant and T as absolute temperature.

This shows that the fraction of molecules in a particular energy state decreases exponentially with increasing energy. Lower energy states are therefore more populated than higher energy states.

The denominator of the above equation is called the Partition Function, denoted as Q.

$$Q = \sum_{i} g_i e^{-\beta E_i} (2)$$

where,

 \triangleright g_i = degeneracy (i.e., number of different states having the same energy E_i).

Thus, the Boltzmann distribution law can be written as:

$$\frac{n_i}{n} = \frac{g_i e^{-\beta E_i}}{O}$$

or equivalently,

$$n_i = n \cdot \frac{g_i e^{-\beta E_i}}{O}$$

Significance

- \triangleright The partition function Q acts as a normalization factor, ensuring that the total probability of all energy states is equal to 1.
- \triangleright The population of a level increases with higher degeneracy (g_i) and decreases with increasing energy (E_i) .
- At high temperature, molecules distribute more evenly among the available states, while at low temperature they tend to remain in the lowest energy states.

Expression in Terms of Zero Energy Level

From Boltzmann distribution law:

$$n_i = n_0 \cdot \frac{g_i}{g_0} e^{-\beta(E_i - E_0)}$$

where:

- n_i = number of molecules in energy state i,
- $rack{rack}{n_0}$ = number of molecules in reference state (taken as zero energy),
- \Rightarrow g_i , g_0 = degeneracies of levels i and 0,
- \triangleright E_i , E_0 = energies of levels i and 0.

Summation Over All States

The total number of molecules is:

$$n=\sum_{i}n_{i}$$

Substituting the expression for n_i :

$$n = n_0 \sum_{i} \frac{g_i}{g_0} e^{-\beta(E_i - E_0)}$$

Factorizing terms:

$$n = n_0 \cdot \frac{1}{g_0} e^{\beta E_0} \sum_i g_i e^{-\beta E_i}$$

Since the summation is defined as the Partition Function Q:

$$n = n_0 \cdot Q$$

or,

$$Q = \frac{n}{n_0}$$

This shows that the Partition Function is the ratio of:

$$Q = \frac{\text{Total number of molecules}}{\text{Number of molecules in the zeroeth (lowest) energy level}}$$

- At absolute zero (0 K): all molecules occupy the lowest energy state. Hence, $n = n_0$ and Q = 1.
- At higher temperatures: more molecules occupy higher energy states, so $n_0 < n$, and therefore Q > 1.

Thus, as temperature increases, partition function increases.

Importance of Partition Function

- \triangleright Q is a dimensionless quantity.
- It depends on molecular weight, molar volume, and temperature.
- It forms a link between microscopic properties (energy levels of molecules) and macroscopic properties (entropy, polarization, internal energy, free energy, etc.).

Partition Function for Molecules with Different Types of Energy

The total energy of a molecule includes contributions from:

$$E = E_t + E_r + E_v + E_e + E_0$$

Where:

- \triangleright E_t = translational energy,
- \triangleright E_r = rotational energy,
- \triangleright E_{v} = vibrational energy,
- \triangleright E_e = electronic excitation energy,
- \triangleright E_0 = zero-point energy.

Hence, the partition function can be expressed as:

$$Q = \sum_{i} g_i e^{-\beta E_i} = Q_t \cdot Q_r \cdot Q_v \cdot Q_e \cdot Q_{nuc}$$

This shows that the total partition function is the product of contributions from different types of molecular motion.

Translational Partition Function

A particle can move in x, y, z directions. For translational motion along x-axis, the partition function is:

$$Q_{tx} = \sum_{i} e^{-\beta \epsilon_{tx,i}}$$

where:

 $\epsilon_{tx,i}$ = translational energy along x-direction,

$$\beta = \frac{1}{kT}.$$

If each translational level has statistical weight factor = 1, this reduces to:

$$Q_{tx} = \sum_{i} e^{-\beta \epsilon_{tx,i}}$$

Derivation of Translational Energy Levels

From de Broglie's relation:

$$\lambda_x = \frac{h}{p_x}$$

Where:

 ho_x = momentum along x-axis,

 \rightarrow h = Planck's constant.

So,

$$p_x = \frac{h}{\lambda_x}$$

But momentum is also:

$$p_x = mv_x$$

Where m = mass of particle, $v_x = \text{velocity along x-axis}$.

Thus,

$$v_x = \frac{h}{m\lambda_x}$$

The translational energy along x-axis is:

$$\epsilon_{tx} = \frac{1}{2}mv_x^2$$

Substitute $v_x = \frac{p_x}{m}$:

$$\epsilon_{tx} = \frac{1}{2}m\left(\frac{p_x}{m}\right)^2 = \frac{p_x^2}{2m}$$

But since $p_x = \frac{h}{\lambda_x}$:

$$\epsilon_{tx} = \frac{1}{2m} \left(\frac{h}{\lambda_x}\right)^2$$

Allowed wavelengths in a box are:

Bhumi Publishing, India October 2025

$$\lambda_x = \frac{2L_x}{n_x}, \quad n_x = 1,2,3,...$$

Thus,

$$p_x = \frac{n_x h}{2L_x}$$

Substitute into energy:

$$\epsilon_{tx} = \frac{1}{2m} \left(\frac{n_x h}{2L_x}\right)^2 = \frac{n_x^2 h^2}{8mL_x^2}$$

$$Q_{trans,x} = \sum_{n_x=1}^{\infty} \exp\left(-\frac{n_x^2 h^2}{8ml_x^2 k_B T}\right)$$

Since energy levels are very closely spaced at ordinary temperatures, the sum is replaced by an integral:

$$Q_{trans,x} = \int_0^\infty \exp\left(-\frac{n_x^2 h^2}{8ml_x^2 k_B T}\right) dx$$

After solving using Gaussian integrals:

$$Q_{trans,x} = \left(\frac{2\pi m k_B T}{h^2}\right)^{\frac{1}{2}} l_x$$

Similarly, for y and z directions:

$$Q_{trans,y} = \left(\frac{2\pi m k_B T}{h^2}\right)^{\frac{1}{2}} l_y$$

$$Q_{trans,z} = \left(\frac{2\pi m k_B T}{h^2}\right)^{\frac{1}{2}} l_z$$

Net Translational Partition Function: Multiplying all three directions:

$$Q_{trans} = Q_x \cdot Q_y \cdot Q_z$$

$$Q_{trans} = \left(\frac{2\pi m k_B T}{h^2}\right)^{\frac{3}{2}} V$$

Where $V = l_x l_y l_z$ is the volume of the box.

Conclusion:

The partition function represents the essential link between microscopic molecular behavior and macroscopic thermodynamic observables. It encapsulates the statistical distribution of molecules among available energy states and translates this information into measurable quantities such as internal energy, entropy, and free energy. Within this framework, each component translational, rotational, Vibrational, and electronic—contributes distinctively to the overall thermodynamic behavior of a system. By connecting molecular energy levels with

ensemble properties, the statistical—thermodynamic approach provides a coherent understanding of how order and randomness coexist in physical systems. The translational partition function describes the freedom of molecular motion in space, while the rotational and Vibrational parts account for the quantized nature of molecular motion and internal structure. Together, these aspects illustrate how macroscopic equilibrium arises from the probabilistic behavior of countless microscopic entities. Ultimately, the study of partition functions reinforces the unifying principle of statistical mechanics: that the collective properties of matter can be derived from the statistical treatment of its microscopic components. This understanding not only strengthens the theoretical basis of thermodynamics but also supports modern applications such as molecular simulations, reaction kinetics, and the modeling of materials at the atomic level. The partition function thus remains an indispensable tool for interpreting, predicting, and rationalizing the energetic behavior of molecular systems across disciplines.

References:

- 1. Popovas, A., & Jørgensen, U. G. (2016). Partition functions I. Improved partition functions and thermodynamic quantities for normal, equilibrium, and ortho and para molecular hydrogen. *Astronomy & Astrophysics*, 595, A130. https://doi.org/10.1051/0004-6361/201527209
- 2. Ab initio partition functions and thermodynamic quantities for the molecular hydrogen isotopologues. (n.d.). *The Journal of Physical Chemistry A*. https://doi.org/10.1021/acs.jpca.1c06468
- 3. McDowell, R. S. (1988). Rotational partition functions for linear molecules. *Journal of Chemical Physics*. https://doi.org/10.1063/1.454608
- 4. McDowell, R. S. (1990). Rotational partition functions for symmetric-top molecules. *Journal of Chemical Physics*. https://doi.org/10.1063/1.458865
- 5. Stowe, K. (2012). The partition function. In *An introduction to thermodynamics and statistical mechanics*. Cambridge University Press. https://doi.org/10.1017/CBO9780511801570.019
- 6. Burgot, J.-L. (2017). Classical statistical mechanics, configuration, and classical canonical partition function. In *The notion of activity in chemistry*. Springer. https://doi.org/10.1007/978-3-319-46401-5 27

THE FUTURE OF MATERIALS SCIENCE: CONVERGENCE OF CHEMISTRY, PHYSICS, AND ARTIFICIAL INTELLIGENCE

Rajesh Kumar Mishra¹, Divyansh Mishra² and Rekha Agarwal³

¹ICFRE-Tropical Forest Research Institute

(Ministry of Environment, Forests & Climate Change, Govt. of India)

P.O. RFRC, Mandla Road, Jabalpur, MP-482021, India

²Department of Artificial Intelligence and Data Science,

Jabalpur Engineering College, Jabalpur, MP

³Government Science College, Jabalpur, MP, India- 482 001

Corresponding author E-mail: rajeshkmishra20@gmail.com, rajesh.mishra0701@gov.in,

divyanshspps@gmail.com, rekhasciencecollege@gmail.com

Abstract:

The evolution of materials science in the 21st century is characterized by the unification of chemistry, physics, and computational intelligence into a data-driven, predictive, and sustainable research paradigm. Traditional experimental methodologies are now augmented by computational modeling, machine learning (ML), and high-throughput simulations that enable accelerated discovery and design of novel materials. This chapter explores the scientific, technological, and philosophical foundations of this convergence. It highlights how atomic-level quantum chemistry, mesoscale physical modeling, and AI-driven data analytics collectively define the next frontier in materials innovation. The integration of materials informatics, autonomous laboratories, and digital twins is transforming the discipline into an intelligent ecosystem capable of continuous self-improvement. Future directions include explainable AI, multi-scale modeling, and sustainable material lifecycle management, ensuring that materials science becomes both predictive and responsible in addressing global challenges in energy, environment, and health.

Keywords: Convergence, Artificial Intelligence, Materials Informatics, Quantum Chemistry, Machine Learning, Multi scale Modeling, Digital Twins, Sustainable Materials

Introduction:

Materials science has traditionally evolved at the intersection of chemistry, which governs atomic bonding and synthesis pathways, and physics, which explains structure–property relationships through thermodynamics and quantum mechanics. In the modern era, a third dimension—artificial intelligence (AI)—has emerged, offering data-driven insights that

transcend human intuition. This triad of chemistry, physics, and AI represents a new

epistemological framework for materials discovery and understanding. According to the Materials Genome Initiative (MGI, 2011), the goal of accelerating materials innovation from discovery to deployment has catalyzed interdisciplinary collaboration between experimentalists, theorists, and data scientists. Over the past decade, advances in high-performance computing, automated synthesis, and deep learning have transformed how we perceive and design materials. Today, the convergence of quantum chemical theory, physical modeling, and AI-assisted decision-making enables the prediction of material behavior before experimental realization, marking a paradigm shift from empirical to computational and autonomous materials science. The future of materials science lies in the seamless convergence of chemistry, physics, and artificial intelligence (AI) — a triad that is redefining how we design, synthesize, and understand matter. Historically, materials discovery was guided by chemical intuition and physical experimentation, where breakthroughs often emerged through decades of empirical research. While chemistry provides the molecular and electronic foundation of materials behavior, and physics elucidates their structural, thermodynamic, and functional phenomena, artificial intelligence introduces a transformative third dimension: data-driven reasoning and predictive power. The integration of these disciplines enables a paradigm shift from conventional trial-anderror discovery toward autonomous, computation-guided innovation. With the advent of highthroughput simulations, quantum mechanical modeling, and materials informatics, scientists can now navigate chemical composition spaces of billions of potential compounds with unprecedented speed and accuracy. AI algorithms, particularly machine learning (ML) and deep learning (DL) models, learn complex non-linear relationships between structure and properties — predicting outcomes that were once computationally prohibitive or experimentally inaccessible. These predictive capabilities have been instrumental in identifying new highentropy alloys, energy storage materials, and photo catalysts, compressing discovery timelines from decades to months (Butler et al., 2018; Ward et al., 2016). Furthermore, this convergence extends beyond theory into experimental realization through autonomous laboratories equipped with robotic synthesis and real-time optimization systems. Such self-driving labs embody the "closed-loop discovery" concept, where AI continuously analyzes experimental feedback to refine hypotheses and direct subsequent synthesis efforts (MacLeod et al., 2022). As data becomes the new language of materials research, cross-disciplinary collaboration among chemists, physicists, data scientists, and engineers is essential. The result is a new scientific paradigm — intelligent materials design — where the boundaries between computation, experimentation, and intuition blur, giving rise to an era of rapid, sustainable, and innovation-driven materials science.

Foundations of the Convergence Paradigm

The convergence paradigm in materials science represents a transformative integration of chemistry, physics, and artificial intelligence (AI) — forming a unified framework for the discovery, designs, and deployment of next-generation materials. At its core, this paradigm stems from the recognition that material behavior cannot be fully described by any single discipline. Chemistry governs atomic bonding, reaction kinetics, and electronic interactions; physics explains macroscopic phenomena such as elasticity, conductivity, and magnetism; and AI acts as the cognitive layer that learns from experimental and computational data to predict and optimize material properties. The synergy of these domains establishes a closed knowledge loop, where theoretical predictions, data-driven learning, and experimental validations iteratively reinforce each other to accelerate innovation. From a chemical standpoint, the convergence paradigm builds upon the molecular understanding of structure-property relationships. Quantum chemistry, density functional theory (DFT), and molecular dynamics simulations provide atomistic insight into bonding environments, reaction pathways, and energetics (Curtarolo et al., 2013). When combined with AI-driven modeling, these chemical data sources enable highfidelity predictions of thermodynamic stability, catalytic activity, and defect formation energies across vast chemical spaces. Machine learning models trained on ab initio data — such as neural network potentials and graph-based learning architectures — have achieved near-DFT accuracy while reducing computational cost by orders of magnitude (Schütt et al., 2018). This coupling allows chemists to move beyond intuition-based discovery toward algorithmic design guided by predictive analytics. From a physical perspective, convergence leverages theoretical and experimental physics to describe emergent phenomena arising from atomic interactions. Techniques such as X-ray diffraction, spectroscopy, and electron microscopy generate rich multidimensional datasets that capture the structural, optical, and mechanical attributes of materials at different scales. AI techniques, including convolutional neural networks (CNNs) and unsupervised feature extraction, have proven essential for interpreting such complex data, enabling automated phase identification, defect analysis, and microstructure classification (Ziletti et al., 2018). This integration of physics-informed modeling and data-driven reasoning leads to "physics-aware AI" — models that not only predict outcomes but also adhere to fundamental physical laws, ensuring interpretability and robustness.

At the computational and algorithmic layer, AI serves as the unifying force bridging chemistry and physics. Modern materials informatics pipelines combine data preprocessing, feature

engineering, and surrogate modeling to map the structure–property–performance landscape. Knowledge graphs and generative AI architectures (e.g., variational auto encoders and diffusion models) now enable inverse materials design, where desired properties drive the identification of candidate compositions and structures (Noé *et al.*, 2020). This convergence supports the emergence of autonomous materials intelligence — systems capable of hypothesizing, simulating, synthesizing, and characterizing new materials with minimal human intervention. In essence, the foundations of this convergence paradigm rest on three pillars: (i) theoretical frameworks that describe atomic and mesoscale behavior, (ii) computational and data infrastructures that enable large-scale simulation and analysis, and (iii) AI-driven learning systems that connect theory with experiment in a feedback loop. Together, these components are redefining the materials research ecosystem from a fragmented discipline into a cohesive, interdisciplinary enterprise, fostering an era of intelligent materials discovery and knowledge-guided innovation.

Chemical Principles: From Bonding to Design

At the molecular level, materials design begins with understanding chemical bonding, coordination environments, and reactivity. Quantum chemical tools such as Density Functional Theory (DFT) and Hartree-Fock methods have provided atomistic insights into electronic structures, potential energy surfaces, and reaction mechanisms. These calculations are now integrated with AI-assisted potential energy mapping (e.g., SchNet, DeepMD) to accelerate the search for stable compositions and phases. The chemical foundation of materials science remains the cornerstone of understanding how atomic interactions dictate macroscopic behavior, forming the bridge between fundamental bonding mechanisms and rational materials design. At the most basic level, chemical bonding — covalent, ionic, metallic, and van der Waals — defines the stability, electronic configuration, and reactive nature of materials. The hybridization of atomic orbital, electron density distributions, and the resulting potential energy surfaces determine how atoms assemble into functional structures. Advances in quantum chemistry and density functional theory (DFT) have enabled precise calculation of electronic band structures, charge transfer processes, and reaction energetics, providing predictive insights into chemical reactivity and material performance (Kohn & Sham, 1965). These principles not only govern simple molecular systems but extend to complex crystalline solids, surfaces, and interfaces where catalytic, optical, and electronic phenomena emerge. In the era of computational materials design, chemical intuition is increasingly complemented by data-driven approaches. Traditional design strategies based on heuristic rules—such as the Hume-Rothery criteria for alloys or Pauling's rules for ionic compounds—are now augmented by machine learning algorithms capable of identifying hidden correlations within high-dimensional chemical spaces (Rajan, 2005). By analyzing descriptors like electro negativity, atomic radii, oxidation states, and coordination environments, AI models can predict formation energies, band gaps, and adsorption affinities with remarkable accuracy. For instance, feature-engineered learning algorithms have been used to screen millions of hypothetical compounds to identify promising candidates for solid-state electrolytes and perovskite solar absorbers, accelerating discovery cycles by several orders of magnitude (Jain et al., 2013). Furthermore, chemistry-informed neural networks and graph-based molecular representations have revolutionized how chemical bonding information is encoded for computational learning. Graph neural networks (GNNs), in particular, treat atoms as nodes and bonds as edges, enabling direct learning from molecular topology and electronic features (Gilmer et al., 2017). This approach allows models to generalize across different chemical families and predict molecular properties with near-quantum accuracy, without explicit solution of Schrödinger's equation. Such integration of chemical theory and AI transforms the traditional "forward design" problem—predicting properties from structure—into an inverse design problem, where desired functionality drives the automated generation of novel compositions and architectures. The transition from bonding principles to materials design represents a fundamental evolution of chemistry itself: from a descriptive to a prescriptive science. The combination of quantum-mechanical modeling, big chemical data, and AI-guided synthesis is ushering in a new era of rational, autonomous materials design. In this vision, chemical bonding is no longer viewed merely as a static property of matter but as a tunable parameter in a multidimensional optimization landscape, enabling precise control over reactivity, selectivity, and performance across applications ranging from catalysis and energy conversion to biomaterials and nanotechnology.

Physical Principles: From Microstructure to Macro scale

Physics provides the link between microscopic and macroscopic behavior through thermodynamics, kinetics, and statistical mechanics. For instance, phase-field modeling and molecular dynamics (MD) simulations predict grain growth, diffusion, and phase stability. The inclusion of machine learning into these frameworks (e.g., Gaussian process regression for force fields) enables faster and more accurate simulations over large configuration spaces. The physical principles underpinning materials science establish the critical link between atomic-scale phenomena and macroscopic performance, translating fundamental interactions into observable mechanical, electrical, optical, and thermal behaviors. At the micro structural level, materials are characterized by their crystalline order, grain boundaries, dislocation networks, and phase distributions, all of which govern their macroscopic properties. The arrangement and

evolution of these micro structural features are dictated by thermodynamics and kinetics — parameters that control processes such as nucleation, diffusion, and phase transformation. Classical frameworks like Gibbs free energy minimization, Fick's laws of diffusion, and phase-field theory have long provided the physical foundation for understanding how materials evolve under external stimuli such as temperature, stress, or irradiation (Porter & Easterling, 1992). These principles enable the prediction of structure-property correlations that define the strength, ductility, conductivity, or optical transparency of a material.

At the meso scale, where micro structural entities interact, complex collective phenomena emerge. Grain growth, texture formation, and crack propagation illustrate the multi scale coupling between atomic and continuum physics. Here, computational physics and multi scale modeling techniques, including molecular dynamics (MD), finite element analysis (FEA), and phase-field simulations, play pivotal roles in bridging scales from nanometers to millimeters (Farkas, 2004). Recent advances in AI-assisted simulations and physics-informed neural networks (PINNs) have further enabled the accurate prediction of stress–strain behavior, thermal conductivity, and fatigue life, integrating experimental and theoretical knowledge into unified predictive frameworks (Karniadakis *et al.*, 2021). Such models not only accelerate the simulation of deformation and failure processes but also ensure compliance with conservation laws, energy principles, and symmetry constraints—key requirements for physical realism.

At the macro scale, materials exhibit emergent properties that define their engineering applications — from the toughness of composite structures to the piezoelectric response of functional ceramics. The transition from micro- to macro scale behavior is governed by scaling laws and continuum mechanics, where constitutive equations relate stress, strain, and deformation fields. AI and data-driven modeling are increasingly being used to extract these relationships directly from experimental datasets, enabling the discovery of new constitutive models for nonlinear or anisotropic materials (Bessa *et al.*, 2017). For example, surrogate models trained on large-scale mechanical testing data can predict performance under complex loading conditions, supporting real-time optimization of additive manufacturing and materials processing pipelines.

Moreover, advanced characterization techniques such as 3D X-ray tomography, transmission electron microscopy (TEM), and atom probe tomography (APT) now generate terabytes of micro structural data. Coupled with machine learning, these tools enable automated segmentation, defect recognition, and feature quantification, linking structure to function with unprecedented precision (Holm *et al.*, 2020). Thus, the physical perspective completes the materials triad by connecting atomic-level interactions (dictated by chemistry) to system-level performance

(guided by AI). Through this integration, modern materials science transcends descriptive analysis to achieve predictive and prescriptive control of materials behavior across all length scales — from electrons to engineered components.

Artificial Intelligence: The Third Pillar

AI acts as the bridge that integrates chemistry and physics via data-centric modeling. Machine learning algorithms can infer patterns from massive datasets derived from experiments and simulations, predicting material properties such as bandgap, hardness, or catalytic activity. Recent works (Butler et al., 2018; Ward et al., 2020) have demonstrated AI's ability to autonomously propose new compositions and structures, effectively redefining the scientific discovery process. Artificial Intelligence (AI) has emerged as the third and transformative pillar of modern materials science, complementing chemistry and physics by introducing an unprecedented capacity for data-driven reasoning, prediction, and automation. Unlike traditional approaches that rely solely on empirical experimentation or first-principles calculations, AI systems learn directly from massive, heterogeneous datasets — encompassing computational simulations, spectroscopic measurements, and high-throughput experiments — to uncover hidden patterns and correlations within the structure-property-performance landscape. This capability enables researchers to predict material properties, design novel compounds, and optimize synthesis routes with remarkable speed and accuracy (Butler et al., 2018). Machine learning (ML), deep learning (DL), and reinforcement learning (RL) algorithms have been successfully applied across diverse domains, from predicting band gaps and formation energies to accelerating molecular dynamics and identifying optimal process parameters.

At the algorithmic level, AI's strength lies in its ability to generalize from limited data and operate across multiple scales. For example, supervised learning models can be trained on databases such as the Materials Project or AFLOW to forecast stability and mechanical performance of untested compounds (Jain *et al.*, 2013), while unsupervised learning aids in clustering unknown crystal structures or detecting anomalies in diffraction data. Deep neural networks (DNNs) and graph neural networks (GNNs) have further revolutionized materials informatics by directly encoding atomic and bonding information into predictive architectures that achieve near quantum-chemical accuracy (Xie & Grossman, 2018). These models bridge the gap between quantum chemistry and condensed matter physics, enabling inverse design—where desired functional targets drive the identification or generation of novel materials through AI-guided search and optimization. Beyond prediction, AI facilitates autonomous experimentation through closed-loop integration with robotics, sensors, and laboratory automation platforms. The concept of the self-driving laboratory, wherein AI algorithms plan experiments, analyze real-

time data, and iteratively refine hypotheses, exemplifies this paradigm shift (MacLeod *et al.*, 2022). Such systems can explore vast chemical and processing parameter spaces with minimal human intervention, achieving orders-of-magnitude improvements in discovery efficiency. Reinforcement learning frameworks, in particular, enable adaptive control of synthesis conditions, guiding robotic instruments toward optimal compositions or morphologies in real time. Crucially, AI is not merely a computational tool but a cognitive framework for scientific discovery — capable of integrating physical laws, chemical rules, and empirical data into unified models of materials behavior. The emergence of physics-informed machine learning (PIML) and knowledge-graph-based reasoning ensures that AI models retain physical interpretability and causality, avoiding "black-box" limitations. This synthesis of data-driven and physics-constrained modeling signifies the maturation of AI as an epistemological partner in materials research, rather than a computational assistant.

There is a pressing need for advanced materials in various areas such as technology, transportation, infrastructure, energy, and healthcare. Yet, conventional methods of finding and investigating novel materials face constraints because of the intricate nature of chemical compositions, structures and desired characteristics. Additionally, innovative materials should not just allow for new uses, but also incorporate eco-friendly methods for their production, utilization, and disposal. In order to address technological and environmental challenges, alloys are becoming more complex in terms of their composition, synthesis, processing, and recycling due to the increasing need for diverse material properties (Mishra *et al.*, 2024). Artificial Intelligence (AI) has witnessed rapid advancements in recent years, transforming various sectors by enhancing efficiency, automating tasks, and enabling more intelligent decision-making processes (Mishra *et al.*, 2025a; Mishra *et al.*, 2025b; Mishra *et al.*, 2025c; Mishra *et al.*, 2025d; Mishra *et al.*, 2025f; Mishra *et al.*, 2025f; Mishra *et al.*, 2025h;
In sum, AI represents the intelligent layer of the materials science trinity. It transforms how knowledge is generated, validated, and applied — bridging microscopic theory and macroscopic application through automation, reasoning, and prediction. As the third pillar, AI not only accelerates discovery but redefines the scientific method itself, heralding a new era of autonomous, explainable, and intelligent materials innovation.

Data-Driven Materials Discovery

The paradigm of data-driven materials discovery marks a pivotal transition in the way scientists explore, understand, and design new materials. Traditionally, materials innovation relied heavily on empirical experimentation and theoretical intuition — processes constrained by time, cost,

and human bias. In contrast, the data-driven approach leverages large-scale computational databases, advanced analytics, and machine learning (ML) to identify complex correlations between composition, structure, and properties across vast materials spaces (Rajan, 2005). This transformation is fueled by the rise of the Materials Genome Initiative (MGI) and the establishment of open-access repositories such as the Materials Project, AFLOW, OQMD, and NOMAD, which collectively contain millions of computed and experimentally validated data points (Jain *et al.*, 2013; Curtarolo *et al.*, 2012). These datasets serve as training grounds for AI algorithms capable of predicting thermodynamic stability, electronic structure, and functional performance before a material is ever synthesized, effectively transforming the traditional discovery pipeline into a virtual laboratory.

At the core of data-driven discovery lies the integration of materials informatics—the science of extracting actionable insights from heterogeneous datasets. Using feature engineering techniques, descriptors such as atomic number, electronegativity, ionic radius, and valence electron configuration are converted into numerical representations that capture the essence of chemical and physical behavior. These descriptors feed into supervised learning algorithms (e.g., random forests, gradient boosting, neural networks) to construct predictive models for key material properties such as band gap, hardness, elasticity, or catalytic activity (Ward et al., 2016). In parallel, unsupervised learning techniques help uncover hidden patterns and classify material families, revealing new design heuristics beyond human intuition. Data-driven discovery extends beyond property prediction to enable inverse design and optimization, where AI models are tasked with proposing new materials that meet predefined performance objectives. Generative models, including variational auto encoders (VAEs), generative adversarial networks (GANs), and diffusion-based architectures, are now capable of creating entirely novel compounds and crystal structures that balance multiple target attributes — such as high strength, low density, and thermal stability (Sanchez-Lengeling & Aspuru-Guzik, 2018). Combined with Bayesian optimization and active learning frameworks, these systems autonomously explore chemical design spaces, focusing computational and experimental resources on the most promising candidates.

Importantly, the success of data-driven materials discovery depends on data quality, diversity, and interoperability. Integrating experimental and computational datasets requires careful curation, uncertainty quantification, and the adoption of standardized ontologies such as OPTIMADE and FAIR (Findable, Accessible, Interoperable, and Reusable) data principles (Wilkinson *et al.*, 2016). Emerging efforts in self-driving laboratories further close the discovery loop, where AI continuously analyzes experimental feedback, refines its models, and guides

subsequent synthesis and characterization (Häse *et al.*, 2019). This synergy between automation, informatics, and machine intelligence is redefining the scientific method — transforming materials discovery from a linear, trial-based process into an adaptive, autonomous discovery ecosystem capable of accelerating innovation by orders of magnitude.

Materials Databases and Informatics

Global databases—such as the Materials Project, AFLOW, OQMD, and NOMAD—contain millions of computed materials entries derived from DFT and experimental validation. These datasets serve as the foundation for materials informatics, where data mining and machine learning extract hidden correlations among structure, composition, and performance. The emergence of materials databases and informatics has fundamentally reshaped the landscape of modern materials science by providing a structured, data-centric foundation for discovery, design, and deployment. These databases—housing terabytes of computational and experimental data—form the digital backbone of the materials research ecosystem. They enable scientists to store, retrieve, and analyze chemical compositions, crystal structures, thermodynamic properties, and electronic characteristics in a machine-readable and interoperable format. The evolution of this field was catalyzed by the Materials Genome Initiative (MGI), launched in 2011, which sought to accelerate the discovery-deployment cycle of advanced materials by integrating computation, experimentation, and data sharing (Holdren, 2011). Today, platforms such as The Materials Project, AFLOWLIB, Open Quantum Materials Database (OQMD), NOMAD Laboratory, and JARVIS-DFT collectively offer millions of pre computed and experimentally validated material entries, transforming how researchers access and interpret materials knowledge (Jain et al., 2013; Curtarolo et al., 2012; Draxl & Scheffler, 2019).

Each of these repositories contributes uniquely to the informatics ecosystem. For instance, The Materials Project integrates density functional theory (DFT)-based calculations with user-friendly visualization tools, allowing rapid screening of electronic, elastic, and thermodynamic properties across tens of thousands of compounds. AFLOWLIB provides high-throughput computational workflows for generating and standardizing materials data, while OQMD focuses on thermodynamic phase stability and reaction energetics. The NOMAD Repository, a European initiative, emphasizes reproducibility and transparency by storing raw DFT data and providing an infrastructure for data reusability under the FAIR principles—Findable, Accessible, Interoperable, and Reusable (Wilkinson *et al.*, 2016). Together, these platforms promote open science, democratizing access to materials data for researchers, industry, and educators alike. At the heart of materials informatics lays the process of data curation, representation, and analysis. Informatics transforms raw numerical or categorical data into knowledge by employing feature

engineering, dimensionality reduction, and pattern recognition techniques. Descriptors derived from chemical composition (e.g., electro negativity, valence electrons) and crystal structure (e.g., coordination number, lattice symmetry) are encoded into feature vectors that serve as inputs to machine learning models. This structured representation allows for predictive analytics, where AI models can estimate material properties such as band gaps, formation energies, and diffusion coefficients with high accuracy (Ward *et al.*, 2016). Moreover, knowledge graphs and ontology-based frameworks are increasingly being developed to integrate diverse data sources—linking computational predictions, experimental observations, and literature metadata into unified networks of materials knowledge (Kim *et al.*, 2020).

The future of materials databases lies in their interoperability, automation, and intelligence. Efforts such as OPTIMADE (Open Databases Integration for Materials Design) aim to create standardized APIs that enable cross-platform querying and data exchange, while AI-assisted database mining identifies trends, anomalies, and design principles hidden in multidimensional datasets (Andersen *et al.*, 2021). Furthermore, integration with autonomous laboratories allows for closed-loop data pipelines where newly synthesized materials are automatically characterized, analyzed, and added back into the database for continuous learning and model refinement. Thus, materials databases and informatics are evolving from static repositories into active, self-learning ecosystems that form the foundation of next-generation autonomous materials discovery.

Predictive Modeling and Inverse Design

The classical forward design problem—predicting properties from structures—is now complemented by inverse design, where desired properties guide the generation of candidate materials. Generative AI techniques (e.g., variational auto encoders, graph neural networks) can create hypothetical materials with optimized band gaps or formation energies before laboratory synthesis. Predictive modeling and inverse design lie at the heart of the modern transformation in materials science, where artificial intelligence (AI), machine learning (ML), and computational physics converge to accelerate discovery and optimization processes. Traditionally, materials development followed a forward design paradigm, in which researchers began with known compositions and structures, tested their properties experimentally or computationally, and iteratively refined them to achieve desired performance. However, this approach is time-consuming and often limited by human intuition. In contrast, predictive modeling leverages AI algorithms trained on extensive datasets—from density functional theory (DFT) calculations to high-throughput experimental results—to establish quantitative relationships between material descriptors (composition, structure, processing parameters) and target properties such as band

gap, mechanical strength, or catalytic activity (Butler *et al.*, 2018). These models can rapidly screen vast chemical spaces, identifying promising candidates before synthesis, thereby reducing the traditional trial-and-error bottleneck in materials design.

The emergence of inverse design frameworks marks an even more revolutionary shift. Instead of predicting properties from known materials, inverse design approaches start with a desired set of functionalities—such as high thermal stability, optical absorption, or ion conductivity—and use generative algorithms to propose novel material structures likely to meet those specifications. Techniques like Bayesian optimization, genetic algorithms, and deep generative models (e.g., variational auto encoders and generative adversarial networks) have been successfully applied to generate new alloys, catalysts, and polymers with tailor-made properties (Sanchez-Lengeling & Aspuru-Guzik, 2018). In particular, graph neural networks (GNNs) and transformer architectures trained on crystal structure databases, such as the Materials Project and Open Quantum Materials Database (OQMD), can directly learn the mapping from atomic connectivity to property spaces, enabling both prediction and generation of unseen materials (Xie & Grossman, 2018).

Moreover, the integration of predictive modeling with multi-objective optimization has enabled the simultaneous tuning of competing properties—such as strength versus ductility or stability versus conductivity—within a unified computational framework. This holistic perspective is critical in advanced applications like solid-state batteries, high-entropy alloys, and thermoelectric materials, where performance depends on complex interdependencies among structural, chemical, and physical parameters. The coupling of first-principles calculations, statistical learning, and Bayesian inference ensures that predictions are not only data-driven but also physically interpretable and uncertainty-aware, fostering trust in AI-assisted decision-making. In essence, predictive modeling and inverse design embody a paradigm shift from empirical discovery to autonomous innovation, paving the way for self-driving laboratories capable of iterative learning from real-time experiments. This closed-loop system—linking simulation, data, and experimentation—promises to shorten the materials development cycle from decades to days, heralding a new era of computationally guided, AI-driven materials innovation.

High-Throughput and Autonomous Laboratories

Automated robotics and closed-loop experimentation have given rise to self-driving laboratories (Jain *et al.*, 2019), where AI controls synthesis parameters in real-time, learning from experimental feedback. For example, the integration of Bayesian optimization allows continuous refinement of synthesis conditions to achieve optimal microstructures. The advent of high-throughput experimentation (HTE) and autonomous laboratories represents one of the most transformative developments in modern materials science. These systems combine robotic

synthesis, automated characterization, and AI-driven decision-making to accelerate the discovery and optimization of new materials far beyond traditional laboratory workflows. High-throughput methodologies allow researchers to simultaneously fabricate and test hundreds or thousands of material compositions, systematically mapping composition–property relationships across vast chemical design spaces (Jain *et al.*, 2013). This approach has been instrumental in identifying novel catalysts, alloys, and energy materials, dramatically reducing the time from concept to functional prototype. For instance, combinatorial materials libraries generated using automated sputtering or solution deposition techniques enable rapid screening of compositionally complex materials such as high-entropy alloys (HEAs) and perovskite photovoltaics (Gregoire *et al.*, 2013).

The evolution from high-throughput to autonomous laboratories is driven by the integration of robotics with machine learning algorithms that can interpret results, refine hypotheses, and plan new experiments in real time. In this closed-loop experimental framework, AI models guide the selection of synthesis parameters, predict likely outcomes, and iteratively improve performance by learning from experimental feedback—a process known as active learning or Bayesian optimization (Raccuglia *et al.*, 2016). Such systems can autonomously identify optimal compositions or processing routes while minimizing the number of experiments required, thereby saving time, cost, and resources. For example, the Berkeley Lab's A-Lab and the University of Toronto's Self-Driving Laboratory exemplify this approach, using robotic platforms capable of continuous operation to synthesize, characterize, and analyze materials 24/7 without human intervention.

A key feature of autonomous materials laboratories is their reliance on real-time data analytics and adaptive control systems, where experimental data are instantly processed and integrated into predictive models. Advances in computer vision, spectral analysis, and automated microscopy enable autonomous recognition of micro structural patterns, defect formations, and phase transitions, transforming raw data into actionable scientific insight. Furthermore, cloud-based materials informatics infrastructures, such as AiiDA, Citrine Informatics, and the Materials Acceleration Platform (MAP), provide interoperable frameworks for managing, sharing, and analyzing experimental data streams. This ensures that discoveries made in one laboratory can immediately inform global research efforts through standardized data protocols and FAIR (Findable, Accessible, Interoperable, and Reusable) principles (Himanen *et al.*, 2019).

The convergence of automation, AI, and robotics in materials research is leading toward the concept of "self-driving laboratories" (SDLs)—fully autonomous research ecosystems capable of performing the complete scientific cycle: hypothesize, design, synthesize, test, and learn. Such

laboratories hold immense potential for tackling grand challenges in energy materials, carbon capture, quantum materials, and biocompatible polymers. As these systems evolve, they not only promise exponential gains in discovery speed but also redefine the scientific method itself—transforming materials science into a data-centric, continuously learning discipline that seamlessly bridges computation and experiment.

Multi scale Modeling: Bridging Chemistry and Physics

Multi scale modeling stands as a cornerstone of modern materials science, serving as the critical bridge between the quantum-scale phenomena governed by chemistry and the continuum-scale behaviors described by physics. The fundamental challenge in materials design lies in the fact that properties and performance emerge from interactions across vastly different spatial and temporal scales—from electronic bonding at the ångström level to mechanical deformation at the macro scale. Traditional single-scale approaches, such as molecular dynamics or finite element analysis, are often limited in scope, unable to fully capture this cross-scale coupling. Multi scale modeling overcomes this limitation by integrating diverse computational frameworks—quantum mechanics, atomistic simulations, meso scale models, and continuum mechanics—into a unified hierarchical or concurrent modeling paradigm (Fish, 2014). At the smallest scales, quantum mechanical methods such as density functional theory (DFT) and Hartree-Fock calculations provide essential insights into electronic structure, charge distribution, and chemical bonding. These results inform classical molecular dynamics (MD) simulations, where inter atomic potentials derived from quantum calculations govern the dynamic behavior of thousands to millions of atoms. Moving upward in scale, coarse-grained molecular dynamics and phase-field modeling capture meso scale processes such as grain growth, phase segregation, and defect evolution, which directly influence macroscopic properties like toughness, ductility, and conductivity (Karma, 2001). Finally, continuum-level models, implemented through finite element or finite volume methods, describe the large-scale mechanical, thermal, and electronic behavior of engineered materials under realistic loading conditions.

Recent developments in AI-augmented multi scale modeling have significantly accelerated this workflow. Machine learning algorithms can interpolate between scales by learning effective potentials, surrogate functions, or constitutive relations directly from simulation data. For instance, neural network potentials (NNPs) and Gaussian approximation potentials (GAPs) trained on DFT data now enable atomistic simulations of systems containing millions of atoms with near-quantum accuracy, bridging the gap between ab initio precision and classical efficiency (Behler & Parrinello, 2007). Similarly, physics-informed neural networks (PINNs)

integrate governing equations such as Schrödinger's or Navier–Stokes equations into the learning process, ensuring physically consistent predictions across scales (Raissi *et al.*, 2019).

The convergence of chemistry and physics through multi scale modeling is particularly transformative for the design of functional materials such as battery electrodes, semiconductors, and structural composites, where electron-level interactions dictate macroscopic reliability and efficiency. For example, in solid-state batteries, multi scale models can simulate ionic transport at the atomic level, phase transitions at the meso scale, and stress evolution at the macro scale to predict lifetime and safety under real operating conditions (Zhang et al., 2020). These integrated insights enable a predictive understanding of how chemical composition and microstructure influence emergent physical properties—turning multi scale modeling into a powerful tool for rational materials designs. In essence, multi scale modeling represents the fusion of chemical accuracy and physical realism, offering a holistic framework for understanding and engineering materials from the atom up to the device. When coupled with data-driven learning and high-performance computing, it provides a path toward truly predictive, first-principles-informed materials engineering, capable of unifying the microscopic laws of chemistry with the macroscopic principles of physics.

Quantum-to-Continuum Modeling

At the atomic scale, quantum mechanical methods describe bonding and electronic states; at the meso scale, phase-field and finite element methods capture morphology evolution. The challenge is to couple these scales seamlessly. Emerging hybrid frameworks—such as QM/MD coupling and coarse-grained neural networks—enable accurate transfer of information from electrons to devices. Quantum-to-continuum modeling represents the pinnacle of multi scale materials simulation, providing a seamless framework that connects electronic-scale phenomena with macroscopic material behavior. This approach addresses one of the central challenges in materials science: how to translate the fundamental quantum mechanical interactions of electrons and atoms into continuum-level predictions that are relevant for engineering applications. At the quantum scale, density functional theory (DFT) and wave function-based methods capture the intricacies of chemical bonding, electron density distributions, and potential energy surfaces, enabling precise prediction of properties such as band gaps, defect formation energies, and catalytic activity (Kohn & Sham, 1965). However, the computational cost of quantum calculations limits their direct application to systems containing thousands of atoms or larger device-scale structures.

To bridge this gap, atomistic simulations using classical or semi-empirical potentials are employed. Inter atomic potentials can be parameterized directly from quantum mechanical

calculations, ensuring that molecular dynamics (MD) or Monte Carlo simulations retain quantum-informed accuracy while scaling to millions of atoms. Techniques such as neural network potentials (NNPs) and Gaussian approximation potentials (GAPs) now allow near-DFT accuracy in large-scale atomistic simulations, capturing dynamic processes like diffusion, phase transitions, and dislocation motion (Behler & Parrinello, 2007). These atomistic insights are then coarse-grained into meso scale models, such as phase-field methods or crystal plasticity simulations, which describe the evolution of microstructures and the collective behavior of defects, grains, and interfaces.

At the continuum scale, principles of solid mechanics, thermodynamics, and transport phenomena are applied to predict macroscopic properties like elasticity, plasticity, thermal conductivity, and fracture toughness. Quantum-to-continuum frameworks use homogenization techniques or multi scale finite element methods to propagate atomic and meso scale information upward, ensuring that continuum predictions are grounded in the fundamental physics of materials (Fish, 2014). Furthermore, physics-informed machine learning models can accelerate this scale-bridging by learning surrogate relationships between quantum-level descriptors and continuum responses, enabling rapid evaluation of material performance under complex conditions (Raissi *et al.*, 2019).

Applications of quantum-to-continuum modeling span a wide range of advanced materials. For example, in semiconductor devices, quantum calculations determine electronic band structure and defect states, which influence device-scale charge transport and thermal management. In structural composites and alloys, atomic-scale predictions of bonding and dislocation behavior inform meso scale stress distributions, which are ultimately used to design macro scale components with optimized mechanical performance. By integrating quantum mechanics, atomistic modeling, and continuum mechanics into a unified predictive framework, quantum-to-continuum modeling enables rational, first-principles-driven materials design, reducing reliance on empirical testing while enhancing predictive confidence for novel materials and devices.

Digital Twins of Materials

The concept of a digital twin—a virtual replica of a material or device that evolves in real time—extends multi scale modeling into the predictive domain. Digital twins integrate sensor data, simulation outputs, and machine learning predictions to continuously assess material performance under operational conditions (Rao *et al.*, 2023). Such systems allow lifetime prediction of batteries, structural composites, and semiconductor devices with unprecedented accuracy. The concept of digital twins has emerged as a transformative paradigm in materials science, offering a virtual representation of physical materials that evolves in tandem with its

real-world counterpart. A digital twin integrates experimental data, computational models, and real-time sensor inputs to simulate, predict, and optimize the behavior of materials across their lifecycle. Unlike traditional modeling approaches that provide static predictions, digital twins are dynamic, data-driven, and continuously updated, enabling predictive maintenance, performance optimization, and accelerated materials innovation (Grieves & Vickers, 2017). In essence, they serve as an intelligent bridge between physical reality and computational insight, merging chemistry, physics, and AI into a unified framework for materials management.

At the core of materials digital twin is the fusion of multi scale modeling and real-time data acquisition. Quantum-level simulations, molecular dynamics, and meso scale phase-field models provide foundational understanding of structural, electronic, and thermal properties, while sensors embedded in materials or components supply continuous feedback on stress, strain, temperature, and chemical degradation. This integration enables the twin to capture both intrinsic material properties and environmental influences, allowing for predictive modeling of failure mechanisms, degradation kinetics, or performance under variable operating conditions (Negri et al., 2017). Machine learning algorithms continuously analyze these data streams, updating predictive models and enabling proactive adjustments in material design, processing, or usage. Digital twins are particularly impactful in applications requiring high reliability and performance optimization. In aerospace and automotive industries, digital twins of composite materials can predict fatigue life and micro crack evolution, informing maintenance schedules and component redesign. In energy materials, digital twins of battery electrodes or solid electrolytes can simulate ion transport, structural degradation, and thermal management under realistic cycling conditions, enabling design adjustments that improve longevity and efficiency. Beyond prediction, the integration of inverse design algorithms with digital twins allows for autonomous materials optimization, where AI suggests modifications to composition, microstructure, or processing parameters to meet predefined performance goals (Kritzinger et al., 2018).

The development of materials digital twins relies on interoperable data infrastructures and standardized modeling frameworks, which ensure that heterogeneous datasets from simulations, experiments, and sensors can be seamlessly integrated. Initiatives such as Materials Acceleration Platforms (MAPs) and FAIR data principles facilitate this integration; supporting reproducible, transparent, and scalable twin models (Wilkinson *et al.*, 2016). As computational power, AI algorithms, and sensor technologies advance, digital twins are poised to evolve from predictive tools into autonomous, decision-making entities that actively guide materials discovery, processing, and lifecycle management. Ultimately, digital twins embody the convergence of

physical, chemical, and computational sciences, enabling a new era of intelligent, adaptive, and resilient materials engineering.

Applications and Technological Frontiers

Energy Materials

Al-driven design is revolutionizing energy storage and conversion systems, from solid-state electrolytes to photo catalytic semiconductors. For instance, graph neural networks trained on DFT data predict ionic conductivity in solid electrolytes with >90% accuracy (Zuo et al., 2021). Hybrid computational—experimental approaches now guide the synthesis of high-entropy oxides for oxygen evolution and carbon capture. The convergence of chemistry, physics, and artificial intelligence has propelled materials science into an era of unprecedented technological innovation, where the integration of multi scale modeling, data-driven discovery, and autonomous experimentation enables transformative applications across diverse domains. One of the most impactful areas is energy materials, including advanced battery chemistries, solid electrolytes, and photovoltaic absorbers. Al-guided design and high-throughput screening have accelerated the discovery of next-generation lithium-ion, sodium-ion, and solid-state batteries, optimizing parameters such as ionic conductivity, electrode stability, and charge—discharge efficiency (Goodenough & Park, 2013). Similarly, perovskite and organic photovoltaic materials have benefited from predictive modeling and inverse design, leading to materials with improved light absorption, charge transport, and long-term stability.

In aerospace and structural engineering, materials with tailored mechanical, thermal, and fatigue properties are being developed using a combination of multi scale modeling, high-throughput experimentation, and digital twins. High-entropy alloys (HEAs), ultralight composites, and additive-manufactured metallic structures exemplify this trend, where predictive modeling informs micro structural design, and autonomous laboratories enable rapid prototyping (Gludovatz *et al.*, 2014). Beyond mechanical performance, smart materials with stimuli-responsive behavior—such as piezoelectric sensors, shape-memory alloys, and self-healing polymers—are being designed using AI-augmented simulations and data-driven optimization, opening new frontiers in robotics, wearable electronics, and adaptive architectures.

In the catalysis and chemical process industries, AI-driven materials discovery has accelerated the development of heterogeneous catalysts, electro catalysts, and photo catalysts. Machine learning models predict adsorption energies, reaction pathways, and selectivity, reducing reliance on time-consuming trial-and-error experimentation (Jiang *et al.*, 2019). This approach has been pivotal in designing catalysts for green hydrogen production, CO₂ reduction, and ammonia synthesis, where reaction efficiency and material stability are critical. Furthermore, the

integration of digital twins in process monitoring enables real-time optimization of catalytic performance, ensuring that lab-scale discoveries translate efficiently into industrial operations. Emerging quantum materials and nano-engineered systems represent another frontier. Materials with tailored topological properties, quantum coherence, or nano scale hetero structures are being designed for applications in quantum computing, spintronics, and next-generation sensors. Multi scale modeling and AI-guided inverse design allow for precise control over electronic band structures, defect states, and interfacial phenomena, accelerating the realization of functional quantum devices (Arute *et al.*, 2019).

Finally, the convergence of materials science with AI and automation has catalyzed sustainable and circular materials development. Predictive modeling enables optimization of resource-efficient synthesis pathways, reduction of hazardous byproducts, and lifecycle assessment of material performance. The integration of high-throughput experimentation, autonomous laboratories, and digital twins ensures that sustainability metrics are embedded into the design process from inception, supporting the transition toward environmentally responsible materials innovation (Chen *et al.*, 2022). In summary, the applications and technological frontiers of modern materials science are defined by the seamless integration of chemical insight, physical modeling, and artificial intelligence. This convergence is driving faster discovery, enhanced performance, and sustainable innovation across energy, aerospace, catalysis, quantum technologies, and beyond, heralding a new era in which materials are designed not only for function but also for adaptability, efficiency, and global impact.

Quantum and Electronic Materials

Quantum materials—such as topological insulators and Weyl semimetals—require precise control of composition and symmetry. Physics-based simulations coupled with AI-optimized synthesis are enabling targeted control over spin—orbit coupling, electron mobility, and quantum coherence. AI is also being used to explore emergent phenomena such as superconductivity and quantum entanglement, bridging condensed matter physics and machine intelligence. Quantum and electronic materials form the foundation of modern technologies, ranging from high-performance semiconductors to quantum computing devices. These materials are characterized by their electronically tunable properties, such as band structure, carrier mobility, spin states, and topological features, which are critical for applications in electronics, optoelectronics, spintronics, and quantum information processing. Advances in materials design, computational modeling, and artificial intelligence (AI) have accelerated the discovery and optimization of such materials, enabling precise control over electronic behavior at atomic and nano scales (Arute *et al.*, 2019; Xie & Grossman, 2018).

At the heart of electronic materials are semiconductors, including silicon, gallium arsenide, and emerging two-dimensional (2D) materials such as graphene, transition metal dichalcogenides (TMDs), and phosphorene. These materials' electronic properties, including band gap, effective mass, and excitonic behavior, can be predicted through density functional theory (DFT) and enhanced via machine learning-based surrogate models that rapidly screen large material spaces for optimal performance (Butler et al., 2018). AI-assisted inverse design and high-throughput computational methods have been pivotal in identifying new 2D semiconductors and hetero structures with tailored band alignments, enabling applications in ultra-thin transistors, flexible electronics, and photo detectors. Quantum materials represent an emerging frontier where electron correlations, topology, and quantum coherence dictate functionality. Materials such as topological insulators, superconductors, and spin liquids exhibit exotic phenomena like edgestate conductivity, Majorana modes, and long-range entanglement, which are essential for quantum computing, spintronic devices, and fault-tolerant information processing (Sarma et al., 2015). Multi scale modeling, spanning ab initio calculations to tight-binding models, combined with AI-guided discovery, has enabled the prediction of new quantum phases, optimal dopants, and defect engineering strategies to stabilize quantum states under realistic conditions.

Additionally, functional oxides and perovskites have received significant attention for their tunable electronic, ferroelectric, and ionic transport properties. These materials serve as active components in resistive switching devices, memristors, and solid-state electrolytes, where a combination of quantum simulations, machine learning models, and high-throughput experimentation enables rapid exploration of composition–structure–property relationships (Zheng *et al.*, 2020). Integration of digital twins and real-time characterization further allows predictive monitoring of device performance, degradation, and optimization of fabrication parameters. In conclusion, quantum and electronic materials exemplify the synergy of chemistry, physics, and AI-driven design, enabling the development of next-generation devices with unprecedented performance, efficiency, and functionality. By combining predictive modeling, multiscale simulations, and autonomous experimentation, researchers can engineer materials at the quantum level while ensuring scalable, application-ready solutions for electronics, energy, and information technologies.

Bio inspired and Sustainable Materials

Integrating AI with chemical biology opens routes for bio inspired materials that emulate natural functions—self-healing, hierarchical structuring, and adaptability. AI-guided molecular modeling accelerates the design of biodegradable polymers and bio mimetic composites, contributing to circular materials engineering. Bio inspired and sustainable materials represent a

rapidly growing frontier in materials science, where principles observed in natural systems guide the design of environmentally friendly, high-performance materials. Drawing inspiration from biological structures and processes—such as the hierarchical architecture of bone, the toughness of nacre, or the self-healing mechanisms in plant tissues—researchers are developing materials that combine mechanical efficiency, adaptability, and multi functionality while minimizing environmental impact (Fratzl & Weinkamer, 2007). These materials aim not only to replicate the extraordinary properties found in nature but also to address the global challenges of resource efficiency, circular economy, and sustainability.

The design of bio inspired materials often relies on hierarchical structuring across multiple scales, from nano scale reinforcement to macro scale architectures. For example, nacre-mimetic composites utilize layered organic-inorganic assemblies to achieve exceptional toughness and impact resistance, while self-healing polymers emulate biological repair mechanisms to extend service life and reduce material waste (Bertoldi *et al.*, 2020). Similarly, bio mineralization-inspired processes have been applied to fabricate ceramics, glasses, and composites under mild, environmentally benign conditions, replacing high-energy synthesis routes with aqueous, room-temperature pathways. Sustainability in materials design is increasingly enabled by computational modeling, machine learning, and high-throughput experimentation. AI algorithms predict optimal combinations of natural or biodegradable polymers, nano cellulose, and metal-organic frameworks for applications in packaging, water purification, and energy storage, minimizing trial-and-error synthesis (Chen *et al.*, 2022). Digital twins and data-driven workflows further allow continuous monitoring and optimization of material performance and lifecycle impact, ensuring that bio inspired materials meet stringent ecological and functional criteria. In energy, bio inspired electrodes and membranes improve the efficiency and durability of

batteries and fuel cells. In healthcare, biodegradable scaffolds and hydrogels mimic extracellular matrices for tissue engineering. In environmental applications, bio inspired filtration systems and catalysts facilitate water purification and pollutant degradation using renewable materials. Collectively, these innovations demonstrate that mimicking nature is not merely aesthetic but a strategic approach to achieving high performance with minimal environmental footprint. In summary, bio inspired and sustainable materials exemplify the integration of chemical ingenuity, physical understanding, and data-driven design to create functional, resilient, and eco-friendly materials. By leveraging hierarchical architectures, natural mechanisms, and AI-augmented discovery, this class of materials offers a pathway toward responsible innovation, combining human ingenuity with nature's design principles to meet the technological and ecological demands of the 21st century.

Challenges and Ethical Considerations

As materials science advances toward the integration of chemistry, physics, and artificial intelligence (AI), it faces a range of technical, societal, and ethical challenges that must be carefully navigated. One primary challenge is data quality, standardization, and accessibility. Machine learning and data-driven approaches depend heavily on large, high-fidelity datasets; however, experimental variability, incomplete reporting, and proprietary restrictions often limit the reliability and reproducibility of models (Wilkinson *et al.*, 2016). Ensuring FAIR (Findable, Accessible, Interoperable, Reusable) data practices is essential not only for scientific rigor but also for equitable access to knowledge across academia and industry. Another key challenge is the complexity of multi scale and autonomous systems. Bridging quantum-scale phenomena with macroscopic material behavior, or implementing autonomous laboratories, requires integration of heterogeneous modeling frameworks, high-performance computing infrastructure, and robotics. Misalignment between scales, algorithmic biases, or insufficient physical constraints can lead to erroneous predictions or unintended material failures, potentially causing costly or hazardous outcomes (Fish, 2014; Häse *et al.*, 2019). Developing robust validation protocols and uncertainty quantification methods is therefore critical for trust in AI-driven materials discovery.

Ethical considerations extend beyond technical challenges. Dual-use concerns arise when novel materials, such as advanced explosives, high-strength alloys, or quantum devices, can be misapplied for military or surveillance purposes. There is also the environmental impact of new materials to consider; even as sustainable and bio inspired materials are prioritized, computational predictions must be coupled with lifecycle assessments to avoid unintended ecological harm (Chen et al., 2022). Additionally, the increasing automation of discovery through AI and robotics raises questions about human oversight, workforce displacement, and equitable access to technology. Ensuring that AI augments rather than replaces human expertise, and that benefits of accelerated materials innovation are broadly shared, is essential for responsible research. Finally, there are challenges related to intellectual property and open science. While open databases like the Materials Project and NOMAD promote transparency, tensions exist between proprietary industrial research and academic data sharing. Ethical frameworks must balance innovation incentives with collaborative scientific progress, ensuring that AI-driven materials discoveries contribute to societal advancement rather than exacerbate inequalities. In conclusion, while the convergence of chemistry, physics, and AI offers transformative potential for materials science, it necessitates careful attention to technical, ethical, and societal dimensions. Addressing data integrity, model reliability, environmental impact, dual-use potential, and equitable access will ensure that the next generation of materials discovery is not only rapid and efficient but also responsible, safe, and sustainable.

Future Outlook

The future of materials science lies at the convergence of chemical insight, physical understanding, and artificial intelligence, heralding a new era of predictive, adaptive, and sustainable materials innovation. Over the next decade, advances in machine learning, highthroughput experimentation, and autonomous laboratories are expected to accelerate the pace of discovery by orders of magnitude, transforming the traditional trial-and-error paradigm into a closed-loop, self-optimizing workflow. Materials that once required decades to discover may soon be designed, synthesized, and characterized within weeks or even days, with AI models continuously refining predictions through real-time experimental feedback (Häse et al., 2019). The expansion of digital twins and multiscale modeling will further enhance predictive capabilities, enabling the simulation of material behavior across atomic, meso scale, and macro scale domains under realistic operating conditions. Such integrated frameworks will facilitate the rational design of next-generation materials for energy storage, catalysis, quantum computing, aerospace, and bioengineering, allowing engineers to optimize performance, durability, and sustainability simultaneously. Moreover, the incorporation of uncertainty quantification and physics-informed machine learning will increase the reliability and interpretability of predictions, fostering broader trust in AI-guided materials discovery.

Sustainability and circular economy considerations will increasingly shape materials research. Data-driven lifecycle assessments, combined with bio inspired and environmentally friendly design principles, will prioritize resource efficiency, recyclability, and reduced environmental footprint, aligning materials innovation with global sustainability goals (Chen *et al.*, 2022). Additionally, emerging quantum and electronic materials will underpin revolutionary technologies such as quantum computers, spintronic devices, and ultrafast optoelectronics, redefining the boundaries of computing, sensing, and communication. The democratization of materials discovery is another anticipated trend. Open-access databases, interoperable software platforms, and cloud-based simulation tools will allow researchers worldwide to participate in accelerated innovation, reducing the reliance on specialized infrastructure and promoting equitable access to advanced materials technology. At the same time, ethical frameworks will be increasingly integrated into research planning, addressing dual-use concerns, data privacy, workforce implications, and environmental responsibility. In summary, the future outlook for materials science is transformative and multidisciplinary, combining AI, chemistry, physics, and automation to create a predictive, sustainable, and socially responsible materials ecosystem. The

coming era promises not only rapid technological advancement but also a more informed, holistic approach to materials design—one where scientific discovery is guided by both performance and responsibility, shaping a resilient and innovative technological landscape for the 21st century.

Conclusions:

The convergence of chemistry, physics, and artificial intelligence is redefining the landscape of materials science, transforming it from a largely empirical discipline into a predictive, datadriven, and multi scale field. Through the integration of quantum simulations, atomistic and meso scale modeling, high-throughput experimentation, and AI-driven predictive tools, researchers can now explore vast chemical and structural spaces with unprecedented speed and precision. Techniques such as inverse design, digital twins, and autonomous laboratories enable not only the rapid discovery of new materials but also the optimization of their performance under realistic operating conditions. This paradigm shift accelerates innovation across diverse sectors, including energy storage, catalysis, quantum devices, aerospace, electronics, and sustainable materials. Key insights from this convergence highlight the synergistic interplay between fundamental understanding and computational capability. Chemical principles inform the selection and tuning of material compositions, physical modeling elucidates structure property relationships, and AI enables intelligent exploration of complex material landscapes. Moreover, the integration of data-driven methodologies with experimental feedback loops fosters adaptive learning systems that continuously refine predictions, paving the way for self-driving laboratories and predictive materials ecosystems.

Despite these advances, challenges remain, including data quality, reproducibility, ethical considerations, and environmental impact. Addressing these concerns will require robust validation frameworks, FAIR data practices, and a commitment to sustainable and responsible innovation. At the same time, emerging frontiers—such as quantum materials, bio inspired systems, and circular-materials design—illustrate the transformative potential of this integrated approach. In conclusion, the future of materials science is interdisciplinary, accelerated, and intelligent. By unifying chemical insight, physical modeling, and AI-driven discovery, researchers are not only shortening the path from concept to application but also enabling smarter, more sustainable, and socially responsible materials development. This convergence paradigm promises to redefine what is possible in materials innovation, offering tools and frameworks capable of meeting the technological and environmental challenges of the 21st century.

Acknowledgement:

Authors are very much thankful to the authors of different publications as many new ideas are abstracted from them. Authors also express gratefulness to their colleagues and family members for their continuous help, inspirations, encouragement, and sacrifices without which this work could not be executed. Finally, the main target of this work will not be achieved unless it is used by research institutions, students, research scholars, and authors in their future works. The authors will remain ever grateful to Dr. Neelu Singh, Director, ICFRE Tropical Forest Research Institute, Jabalpur, Principal, Jabalpur Engineering College, Jabalpur & Principal Government Science College, Jabalpur who helped by giving constructive suggestions for this work. The authors are also responsible for any possible errors and shortcomings, if any in the chpter, despite the best attempt to make it immaculate.

References:

- 1. Andersen, C. W., Schütt, O., & Schmidt, J. (2021). Toward data-driven materials design: The role of artificial intelligence in materials informatics. *Advanced Intelligent Systems*, 3(8), 2000229.
- 2. Arute, F., Arya, K., Babbush, R., Bacon, D., Bardin, J. C., Barends, R.,... & Martinis, J. M. (2019). Quantum supremacy using a programmable superconducting processor. *Nature*, *574*(7779), 505–510.
- 3. Behler, J., & Parrinello, M. (2007). Generalized neural-network representation of high-dimensional potential-energy surfaces. *Physical Review Letters*, 98(14), 146401.
- 4. Bertoldi, K., Vitelli, V., Christensen, J., & van Hecke, M. (2020). Flexible mechanical metamaterials. *Nature Reviews Materials*, 2(11), 17066.
- Bessa, M. A., Bostanabad, R., Liu, Z., Hu, A., Apley, D. W., Brinson, C., Chen, W., & Liu, W. K. (2017). A framework for data-driven analysis of materials under uncertainty: Countering the curse of dimensionality. *Computer Methods in Applied Mechanics and Engineering*, 320, 633–667.
- 6. Butler, K. T., Davies, D. W., Cartwright, H., Isayev, O., & Walsh, A. (2018). Machine learning for molecular and materials science. *Nature*, 559, 547–555.
- 7. Chen, P., Li, Z., Li, W., & Wolverton, C. (2022). Materials informatics for sustainable materials design. *Advanced Materials*, *34*(5), 2106825.
- 8. Curtarolo, S., *et al.* (2013). The high-throughput highway to computational materials design. *Nature Materials*, *12*(3), 191–201.

- 9. Curtarolo, S., Setyawan, W., Wang, S., Xue, J., Yang, K., Taylor, R. H.,... & Morgan, D. (2012). AFLOWLIB.org: A distributed materials properties repository from high-throughput ab initio calculations. *Computational Materials Science*, 58, 227–235.
- 10. Draxl, C., & Scheffler, M. (2019). The NOMAD laboratory: From data sharing to artificial intelligence. *Journal of Physics: Materials*, 2(3), 036001.
- 11. Farkas, D. (2004). Atomistic and mesoscale modeling of mechanical behavior of nanostructured materials. *Current Opinion in Solid State and Materials Science*, 8(4), 287–293.
- 12. Fish, J. (2014). *Practical multiscaling*. John Wiley & Sons.
- 13. Floridi, L., *et al.* (2022). Ethics of artificial intelligence for sustainable science. *Nature Machine Intelligence*, *4*, 89–96.
- 14. Fratzl, P., & Weinkamer, R. (2007). Nature's hierarchical materials. *Progress in Materials Science*, 52(8), 1263–1334.
- 15. Gilmer, J., Schoenholz, S. S., Riley, P. F., Vinyals, O., & Dahl, G. E. (2017). Neural message passing for quantum chemistry. *Proceedings of the 34th International Conference on Machine Learning*, 70, 1263–1272.
- 16. Gludovatz, B., Hohenwarter, A., Catoor, D., Chang, E. H., George, E. P., & Ritchie, R. O. (2014). A fracture-resistant high-entropy alloy for cryogenic applications. *Science*, 345(6201), 1153–1158.
- 17. Goodenough, J. B., & Park, K. S. (2013). The Li-ion rechargeable battery: A perspective. Journal of the American Chemical Society, 135(4), 1167–1176.
- 18. Gregoire, J. M., Xiang, C., Liu, X., Marcin, M., & Jin, J. (2013). Scanning droplet cell for high throughput electrochemical and photoelectrochemical measurements. *Review of Scientific Instruments*, 84(2), 024102.
- 19. Grieves, M., & Vickers, J. (2017). Digital twin: Mitigating unpredictable, undesirable emergent behavior in complex systems. In *Transdisciplinary perspectives on complex systems* (pp. 85–113).
- 20. Häse, F., Roch, L. M., & Aspuru-Guzik, A. (2019). Next-generation experimentation with self-driving laboratories. *Trends in Chemistry*, 1(3), 282–291.
- 21. Himanen, L., Geurts, A., Foster, A. S., & Rinke, P. (2019). Data-driven materials science: Status, challenges, and perspectives. *Advanced Science*, *6*(21), 1900808.
- 22. Holdren, J. P. (2011). *Materials Genome Initiative for Global Competitiveness*. Executive Office of the President, National Science and Technology Council.

- 23. Holm, E. A., Li, R., & Rollett, A. D. (2020). The role of machine learning in constructing the structure–property link. *Annual Review of Materials Research*, 50, 1–22.
- 24. Jain, A., *et al.* (2019). The Materials Project: A materials genome approach to accelerating materials innovation. *APL Materials*, 7, 011002.
- 25. Jiang, T., Miao, R., & Chen, W. (2019). Machine learning in catalysis and materials science. *Catalysis Science & Technology*, *9*, 5463–5478.
- 26. Karma, A. (2001). Phase-field formulation for quantitative modeling of alloy solidification. *Physical Review Letters*, 87(11), 115701.
- 27. Karniadakis, G. E., Kevrekidis, I. G., Lu, L., Perdikaris, P., Wang, S., & Yang, L. (2021). Physics-informed machine learning. *Nature Reviews Physics*, *3*(6), 422–440.
- 28. Kim, E., Huang, K., Saunders, A., McCallum, A., Ceder, G., & Olivetti, E. (2020). Materials synthesis insights from scientific literature via text extraction and machine learning. *Chemistry of Materials*, 32(4), 1536–1547.
- 29. Kitchin, J. R. (2018). Thinking about the ethical implications of AI for science. *Nature Machine Intelligence*, *I*(1), 1–2.
- 30. Kohn, W., & Sham, L. J. (1965). Self-consistent equations including exchange and correlation effects. *Physical Review*, *140*(4A), A1133–A1138.
- 31. Kritzinger, W., Karner, M., Traar, G., Henjes, J., & Sihn, W. (2018). Digital twin in manufacturing: A categorical literature review and classification. *IFAC-PapersOnLine*, 51(11), 1016–1022.
- 32. MacLeod, B. P., Parlane, F. G. L., Morrissey, T. D., Häse, F., Roch, L. M., Dettelbach, K. E.,... & Cronin, L. (2022). Self-driving laboratory for accelerated discovery of thin-film materials. *Science Advances*, 8(4), eabl5546.
- 33. Mishra, R. K., Mishra, D., & Agarwal, R. (2024). An artificial intelligence-powered approach to material design. In *Cutting-edge research in chemical and material science* (pp. 61–89). ISBN: 978-93-95847-39-1.
- 34. Mishra, R. K., Mishra, D., & Agarwal, R. (2025a). Environmental sustainability and ecological balance. In *Implementation of innovative strategies in integral plant protection* (pp. 81–96). ISBN: 978-93-48620-22-4.
- 35. Mishra, R. K., Mishra, D., & Agarwal, R. (2025b). Advanced simulation techniques for forest fire and natural hazard prediction: A computational science perspective. *Journal of Science Research International (JSRI)*, 11(4), 20–34.

- 36. Mishra, R. K., Mishra, D., & Agarwal, R. (2025c). Digital guardians of nature: Emerging AI technologies in plant and animal surveillance. In *Advances in plant and animal sciences* (Vol. I, pp. 12–35). ISBN: 978-93-49938-62-5.
- 37. Mishra, R. K., Mishra, D., & Agarwal, R. (2025d). Artificial intelligence and machine learning in plant identification and biodiversity conservation: Innovations, challenges, and future directions. In *Botanical insights: From traditional knowledge to modern science* (Vol. I, pp. 7–31). ISBN: 978-81-981142-3-5.
- 38. Mishra, R. K., Mishra, D., & Agarwal, R. (2025e). Digital guardians of nature: Emerging AI technologies in plant and animal surveillance. In *Advances in plant and animal sciences* (Vol. I, pp. 12–35). ISBN: 978-93-49938-62-5.
- 39. Mishra, R. K., Mishra, D., & Agarwal, R. (2025f). Advanced simulation techniques for forest fire and natural hazard prediction: A computational science perspective. *Journal of Science Research International (JSRI)*, 11(4), 20–34.
- 40. Mishra, R. K., Mishra, D., & Agarwal, R. (2025g). Forest health monitoring using AI and remote sensing. ISBN (PDF): 9783389142202; ISBN (Book): 9783389142219.
- 41. Mishra, R. K., Mishra, D., & Agarwal, R. (2025h). Artificial intelligence and big data in environmental monitoring and decision support: Revolutionizing ecosystem management. *Journal of Science Research International (JSRI)*, 11(5), 28–39.
- 42. Mishra, R. K., Mishra, D., & Agarwal, R. (2025i). Climate change, biodiversity, and ecological resilience. In *Green footprints: Bridging environment and sustainability* (pp. 25–47). ISBN: 978-81-989981-8-7.
- 43. Negri, E., Fumagalli, L., & Macchi, M. (2017). A review of the roles of digital twin in CPS-based production systems. *Procedia Manufacturing*, 11, 939–948.
- 44. Noé, F., Tkatchenko, A., Müller, K. R., & Clementi, C. (2020). Machine learning for molecular simulation. *Annual Review of Physical Chemistry*, 71, 361–390.
- 45. Porter, D. A., & Easterling, K. E. (1992). *Phase transformations in metals and alloys* (2nd ed.). CRC Press.
- 46. Raccuglia, P., Elbert, K. C., Adler, P. D. F., Falk, C., Wenny, M. B., Mollo, A.,... & Norquist, A. J. (2016). Machine-learning-assisted materials discovery using failed experiments. *Nature*, *533*(7601), 73–76.
- 47. Raissi, M., Perdikaris, P., & Karniadakis, G. E. (2019). Physics-informed neural networks: A deep learning framework for solving forward and inverse problems involving nonlinear partial differential equations. *Journal of Computational Physics*, *378*, 686–707.
- 48. Rajan, K. (2005). Materials informatics. Materials Today, 8(10), 38-45.

- 49. Rao, S., *et al.* (2023). Digital twins for materials design and lifecycle prediction. *Advanced Materials*, 35(9), 2207231.
- 50. Sanchez-Lengeling, B., & Aspuru-Guzik, A. (2018). Inverse molecular design using machine learning: Generative models for matter engineering. *Science*, *361*(6400), 360–365.
- 51. Sarma, S. D., Freedman, M., & Nayak, C. (2015). Majorana zero modes and topological quantum computation. *npj Quantum Information*, *1*(1), 15001.
- 52. Schütt, K. T., Sauceda, H. E., Kindermans, P. J., Tkatchenko, A., & Müller, K. R. (2018). SchNet A deep learning architecture for molecules and materials. *Journal of Chemical Physics*, *148*(24), 241722.
- 53. Ward, L., & Wolverton, C. (2020). Atomistic calculations and machine learning: Synergistic tools for materials design. *Current Opinion in Solid State and Materials Science*, 24(5), 100806.
- 54. Ward, L., Agrawal, A., Choudhary, A., & Wolverton, C. (2016). A general-purpose machine learning framework for predicting properties of inorganic materials. *npj Computational Materials*, 2(1), 16028.
- 55. Wegst, U. G. K., Bai, H., Saiz, E., Tomsia, A. P., & Ritchie, R. O. (2015). Bioinspired structural materials. *Nature Materials*, 14(1), 23–36.
- Wilkinson, M. D., Dumontier, M., Aalbersberg, I. J., Appleton, G., Axton, M., Baak, A.,...
 & Mons, B. (2016). The FAIR guiding principles for scientific data management and stewardship. *Scientific Data*, 3(1), 160018.
- 57. Xie, T., & Grossman, J. C. (2018). Crystal graph convolutional neural networks for an accurate and interpretable prediction of material properties. *Physical Review Letters*, 120(14), 145301.
- 58. Zhang, X., Han, J., & Wang, C. (2020). Multiscale modeling of solid-state batteries: From materials design to cell performance. *Energy Storage Materials*, *24*, 132–155.
- 59. Zheng, F., Wang, J., & Yao, K. (2020). Computational and data-driven approaches for functional oxide materials. *Advanced Materials*, *32*(32), 2001486.
- 60. Ziletti, A., Kumar, D., Scheffler, M., & Ghiringhelli, L. M. (2018). Insightful classification of crystal structures using deep learning. *Nature Communications*, *9*(1), 2775.
- 61. Zuo, Y., et al. (2021). Performance and cost assessment of machine learning interatomic potentials. *Journal of Physical Chemistry A*, 125(27), 6031–6043.

MATRICES IN VIDEO GAMES

R. Muthamizh Selvi

Department of Mathematics,

Saradha Gangadharan Arts & Science College (Autonomous), Puducherry, India

Corresponding author E-mail: <u>muthamizhmaths@gmail.com</u>

Introduction:

Video games are products of entertainment for young generation. These video games comprise of a lot of programming and creativity. It also involves computer graphics which are accomplished by a mathematical tool called matrices to construct and engineer a realistic animation. Video games use three main principles of linear transformation of matrices: translation, rotation, scaling to program 3-D games. It is very interesting if you represent a coordinate system in the form of matrix. Suppose point (3 2) is represented as a column matrix

 $\begin{pmatrix} 3 \\ 2 \end{pmatrix}$. Say there is a transforming matrix $\begin{pmatrix} 1 & 0 \\ 0 & -1 \end{pmatrix}$, we obtain transformed matrix.

$Transformed\ Matrix = Transforming\ Matrix \times Original\ Column\ Matrix$

This is the general representation for transforming points.

1. Types of Video Games:

1.1 Translation:

This tool of linear transformation helps in moving an object from one position to another, as in video games the human figure, car-shaped polygon move from one position to another with the help of translation. This operation carried by translation from coordinate (x, y, z) to (x + dx, y + dy, z + dz).

Representing it in matrix form:

$$\begin{pmatrix} x' \\ y' \\ z' \end{pmatrix} = \begin{pmatrix} x \\ y \\ z \end{pmatrix} + \begin{pmatrix} dx \\ dy \\ dz \end{pmatrix}$$

dx, dy, dz are the distances travelled by coordinate (x, y, z) to reach coordinate (x', y', z').

1.2 Rotations:

This tool of linear transformation is used to rotate polygon figures with respect to axis for 3-D formations.

i. Rotation about z-axis:

$$\begin{pmatrix} x' \\ y' \\ z' \end{pmatrix} = \begin{pmatrix} \cos\theta & -\sin\theta & 0 \\ \sin\theta & \cos\theta & 0 \\ 0 & 0 & 1 \end{pmatrix} \begin{pmatrix} x \\ y \\ z \end{pmatrix} = \begin{pmatrix} x\cos\theta - y\sin\theta \\ x\sin\theta + y\cos\theta \\ z \end{pmatrix}$$

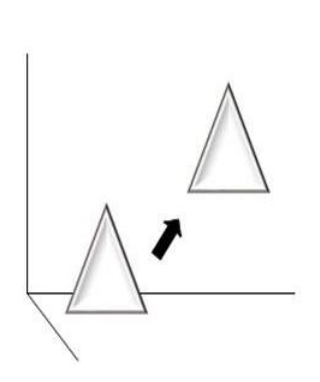


Figure. 1(A). 3-D graph showing how poly gon moves in video games

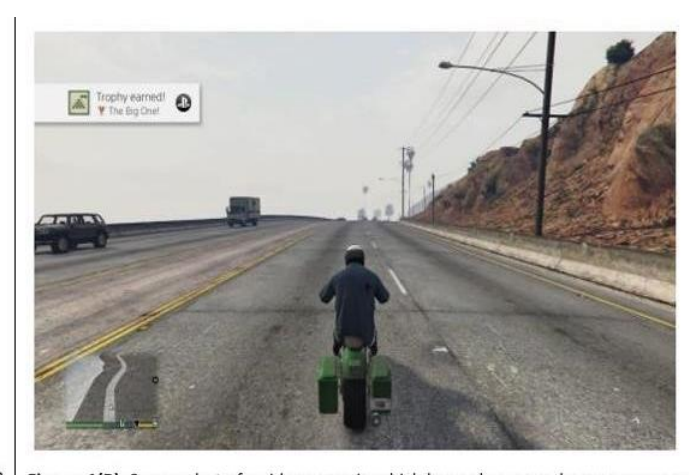


Figure. 1(B). Screen shot of a video game in which how a human polygon moves on a bike from one place to another without changing size and shape of any polygon.

ii. Rotation about y-axis:

$$\begin{pmatrix} x' \\ y' \\ z' \end{pmatrix} = \begin{pmatrix} \cos\theta & 0 & \sin\theta \\ 0 & 1 & 0 \\ -\sin\theta & 0 & -x\sin\theta \end{pmatrix} = \begin{pmatrix} z\sin\theta + x\cos\theta \\ y \\ z\cos\theta - x\sin\theta \end{pmatrix}$$

iii. Rotation about x-axis:

$$\begin{pmatrix} x' \\ y' \\ z' \end{pmatrix} = \begin{pmatrix} 1 & 0 & 0 \\ 0 & \cos\theta & -\sin\theta \\ 0 & \sin\theta & \cos\theta \end{pmatrix} \begin{pmatrix} x \\ y \\ z \end{pmatrix} = \begin{pmatrix} x \\ y\cos\theta - z\sin\theta \\ y\sin + z\cos\theta \end{pmatrix}$$

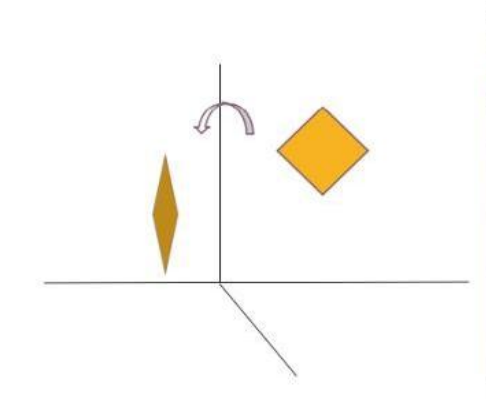


Figure 2(a). Rotation of a dimond polygon about X axis



Figure 2(b). In FIFA 20 a footboll as polygon rotates w.r.to axis

1.3 Scaling:

This tool of linear transformation helps in changing the size either by enlarging or reducing the polygon figure. This operation carried by scaling for transforming coordinates from (x, y, z) to (x. Sx, y. Sy, z. Sz). representing it in matrix form:

$$\begin{pmatrix} x' \\ y' \\ z' \end{pmatrix} = \begin{pmatrix} sx & 0 & 0 \\ 0 & sy & 0 \\ 0 & 0 & sz \end{pmatrix} \begin{pmatrix} x \\ y \\ z \end{pmatrix} = \begin{pmatrix} x \cdot sx \\ y \cdot sy \\ z \cdot sz \end{pmatrix}$$

In video games, to make it realistic we use this tool to magnify or reduce polygon figures like a box as required in specific games.

When we want to scale the cylinder polygon, we use scaling matrix at each point to enlarge the size of polygon.

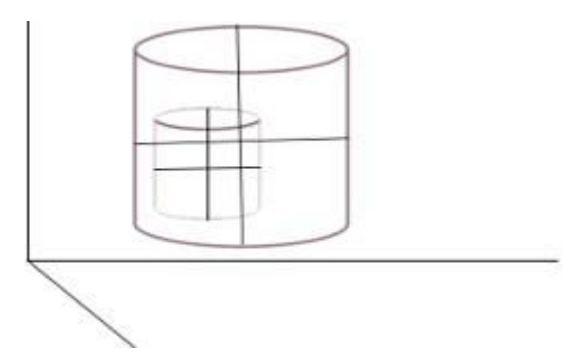


Figure 3: Scaling of Cylinder Polygon

1.4 Reflection:

This tool of linear transformation helps in viewing the reflection of the polygon figures like a tree, mountain, or a human figure sometimes for making it realistic as wherever there is a mirror or a sea formation, we reflect the respective polygon figures in different video games. In this we have to select between planes xy, yz, zx.

i. Reflection through xy plane:

$$\begin{pmatrix} x' \\ y' \\ z' \end{pmatrix} = \begin{pmatrix} 1 & 0 & 0 \\ 0 & 1 & 0 \\ 0 & 0 & -1 \end{pmatrix} \begin{pmatrix} x \\ y \\ z \end{pmatrix} = \begin{pmatrix} x \\ y \\ -z \end{pmatrix}$$

ii. Reflection through yz plane:

$$\begin{pmatrix} x' \\ y' \\ z' \end{pmatrix} = \begin{pmatrix} -1 & 0 & 0 \\ 0 & 1 & 0 \\ 0 & 0 & -1 \end{pmatrix} \begin{pmatrix} x \\ y \\ z \end{pmatrix} = \begin{pmatrix} -x \\ y \\ z \end{pmatrix}$$

iii. Reflection through zx plane:

$$\begin{pmatrix} x' \\ y' \\ z' \end{pmatrix} = \begin{pmatrix} 1 & 0 & 0 \\ 0 & -1 & 0 \\ 0 & 0 & 1 \end{pmatrix} \begin{pmatrix} x \\ y \\ z \end{pmatrix} = \begin{pmatrix} x \\ -y \\ z \end{pmatrix}$$

If we want to reflect the moon through xy plane, where moon has coordinates as (4, 2,3), (1, 2, 3), (2, 2, 1), (2, 1, 0), (0, 0, 0), (1, 0, 0), we use the reflected matrix

$$\begin{pmatrix} 1 & 0 & 0 \\ 0 & -1 & 0 \\ 0 & 0 & 1 \end{pmatrix} \begin{pmatrix} 4 & 1 \\ 2 & 2 \\ 3 & 3 \end{pmatrix} \qquad \qquad \begin{pmatrix} 2 & 2 & 01 \\ 2 & 1 & 0 \\ 1 & 0 & 0 \end{pmatrix}$$

$$1 & 0 & 0$$

$$Reflected Matrix = (-2 & -2 & -1 & 0 & 0)$$

$$3 & 1 & 0 & 0$$

Below graph shows the reflection of moon polygon

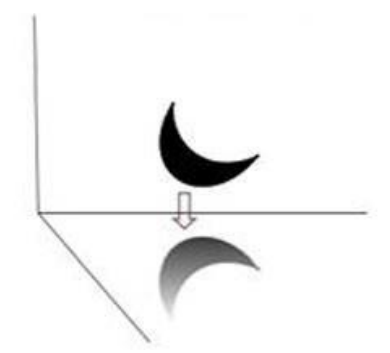


Figure 4: The reflection property is necessary in video games whenever we are striving for realistic effect whenever polygon pass through a surface which supports reflection

1.5 Shearing:

This tool of linear transformation helps in distorting the shape of polygon figures, assuming a car while moving in a video game when hit by another polygon in front of it, that part of the car gets rendered. This operation is carried about respective axis.

i. z-axis shearing:

$$\begin{pmatrix} x' \\ y' \\ z' \end{pmatrix} = \begin{pmatrix} 1 & 0 & shx \\ 0 & 1 & shy \\ 0 & 0 & 1 \end{pmatrix} \begin{pmatrix} x \\ y \\ z \end{pmatrix} = \begin{pmatrix} x + z \cdot shx \\ y + z \cdot shy \\ z \end{pmatrix}$$

ii. y-axis shearing:

$$\begin{pmatrix} x' \\ y' \\ z' \end{pmatrix} = \begin{pmatrix} 1 & shx & 0 \\ 0 & 1 & 0 \\ 0 & shz & 1 \end{pmatrix} \begin{pmatrix} x \\ y \\ z \end{pmatrix} = \begin{pmatrix} x + y \cdot shx \\ y \\ z + y \cdot shz \end{pmatrix}$$

iii. x-axis shearing:

$$\begin{pmatrix} x' \\ y' \\ z' \end{pmatrix} = \begin{pmatrix} 1 & 0 & 0 \\ shy & 1 & 0 \\ shz & 0 & 1 \end{pmatrix} \begin{pmatrix} x \\ y \\ z \end{pmatrix} = \begin{pmatrix} x \\ y + x.shy \\ z + x.shz \end{pmatrix}$$

shx, shy, shz are the distortions occurred in x, y, z coordinates. Supposedly, in z. shy we are shearing y coordinate towards z and this goes with other shearing values.

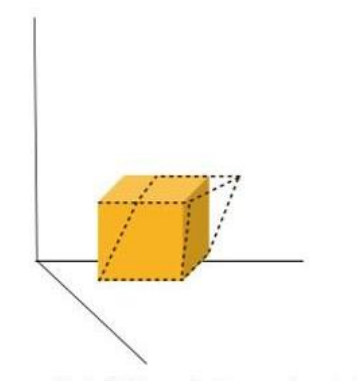


Figure 5(a). 3-D graph is constructed which shows x-axis shearing using shearing matrix.



Figure 5(b). Car Polygon has ben distorted as it mighnt have met with some accident, the car polygon follows the shearing matrix rule for it.

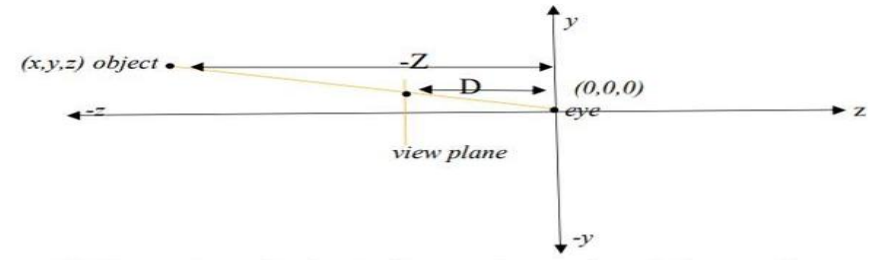


Figure 6(a). Perspective projection, D- distance of eye to plane, Z-distance of eye to plane.



Figure 6(b). View for the player through scope of a sniper.

1.6 Projection:

This tool of linear transformation help in viewing by transforming polygon figures from 3-D to 2-D on the screen.

i. Parallel projection

In parallel projection, we ignore the z-coordinate to transform the dimensions from 3-D to 2-D. the parallel projection line transforming the dimensions is called projection vector. The size of the polygon figure doesn't change passing though the projection vector. Representing it in matrix form:

$$\begin{pmatrix} x_p \\ y_p \\ z_p \\ 1 \end{pmatrix} = \begin{pmatrix} 1 & 0 & 0 & 0 \\ 0 & 1 & 0 & 0 \\ 0 & 0 & 0 & 0 \\ 0 & 0 & 0 & 1 \end{pmatrix} \begin{pmatrix} x \\ y \\ z \\ 1 \end{pmatrix} = \begin{pmatrix} x \\ y \\ 0 \\ 1 \end{pmatrix}$$

ii. Perspective Projection

Video game designers try to mare these games as real as possible for example, if a polygon figure is close it seems to be bigger and vice versa. So to carry out that vision, designers use perspective projection where parallelism is not applicable. We generally see points of edges converge at one point known as vanishing point, like a rail-track seems to converge till that point where our eyes can see, thus same is carried in video games for realistic effect [21].

Representing it in matrix form:

$$\begin{pmatrix} x_1 \\ y_1 \\ z_1 \\ 1 \end{pmatrix} = \begin{pmatrix} 1 & 0 & 0 & 0 \\ 0 & 1 & 0 & 0 \\ 0 & 0 & 1 & 0 \\ 0 & 0 & 1 & 0 \\ 0 & 0 & 1 & 0 \end{pmatrix} \begin{pmatrix} x \\ y \\ z \\ 1 \end{pmatrix} = \begin{pmatrix} x \\ y \\ z \\ \frac{z}{d} \end{pmatrix}$$

1.7 Matrices in Cryptography:

Cryptography is a technique for securing information and communicate via codes. The codes guarantee that only the intended receivers can read and process the messages. "Crypt" means hidden and "graphy" means writing. Mathematical tools help in deriving concepts for cryptography. It uses algorithms or rule-based calculations to send messages in ways that are hard to read. These algorithms create keys to control signing and verification so as to protect data privacy and its confidentiality. Cryptography is mainly used for sending e-mails, bank account numbers and transactions as well.

Suppose a conversation between two beings on WhatsApp is taking place, The person is sending a message "BEHIND THE SCENES" to another person. This is saved in WhatsApp server as "BEHIND THE SCENES" so as to avoid any errors, it should be encrypted so that no one can understand. This process is known as encryption.

So, to follow the process, alphabets are converted to numeric values.

Now we encrypt the above message using the encryption or coding matrix then $\begin{pmatrix} 2 & -1 & 0 \\ 1 & 0 & 0 \end{pmatrix}$ we decode the received message using the inverse of the encrypted matrix.

BEHIND THE SCENE
$$\cong$$
 (B E H) (I N D) (0 T H) (E 0 S) (C E N)
= (2 5 8) (9 14 4) (0 20 8) (5 0 19) (3 5 14)

We apply matrix multiplication to un-coded row matrix with encoding matrix to obtain coded row matrix.

$$(2 \quad 5 \quad 8) \begin{pmatrix} 1 & -1 & 1 \\ 2 & -1 & 0 \\ 1 & 0 & 0 \end{pmatrix} = (20 \quad -7 \quad 2)$$

$$(9 \quad 14 \quad 4) \begin{pmatrix} 1 & -1 & 1 \\ 2 & -1 & 0 \\ 1 & 0 & 0 \end{pmatrix} = (41 \quad -23 \quad 9)$$

$$(0 \quad 20 \quad 8) \begin{pmatrix} 1 & -1 & 1 \\ 2 & -1 & 0 \\ 1 & 0 & 0 \end{pmatrix} = (48 \quad -20 \quad 0)$$

$$(5 \quad 0 \quad 19) \begin{pmatrix} 1 & -1 & 1 \\ 2 & -1 & 0 \\ 1 & 0 & 0 \end{pmatrix} = (24 \quad -5 \quad 5)$$

$$(3 \quad 5 \quad 14) \begin{pmatrix} 1 & -1 & 1 \\ 2 & -1 & 0 \\ 1 & 0 & 0 \end{pmatrix} = (27 \quad -8 \quad 3)$$

Coded message is:

$$(20 - 7 2)(41 - 23 9)(48 - 20 0)(24 - 5 5)(27 - 8 3)$$

$$= (20 - 7 2)(15 - 23 9)(22 - 20 0)(24 - 5 5)(1 - 8 3)$$

$$= (T S B)(O D I)(V G 0)(X V E)(A S C)$$

Now to decode the message we find the decoding matrix by finding out the inverse of encrypted matrix by using.

$$A^{-1} = \frac{1}{|A|} adj A$$

$$A^{-1} = \begin{pmatrix} 0 & 0 & 1\\ 0 & -1 & 2\\ 1 & -1 & 1 \end{pmatrix}$$

We decode the message by post-multiplying by A^{-1}

$$(20 \quad -7 \quad 2) \begin{pmatrix} 0 & 0 & 1 \\ 0 & -1 & 2 \\ 1 & -1 & 1 \end{pmatrix} = (2 \quad 5 \quad 8)$$

$$(41 \quad -23 \quad 9) \begin{pmatrix} 0 & 0 & 1 \\ 0 & -1 & 2 \\ 1 & -1 & 1 \end{pmatrix} = (9 \quad 14 \quad 4)$$

$$(48 -20 0) \begin{pmatrix} 0 & 0 & 1 \\ 0 & -1 & 2 \\ 1 & -1 & 1 \end{pmatrix} = (0 20 8)$$

$$(24 \quad -5 \quad 5) \begin{pmatrix} 0 & 0 & 1 \\ 0 & -1 & 2 \\ 1 & -1 & 1 \end{pmatrix} = (5 \quad 0 \quad 19)$$

$$(27 \quad -8 \quad 3) \begin{pmatrix} 0 & 0 & 1 \\ 0 & -1 & 2 \\ 1 & -1 & 1 \end{pmatrix} = (3 \quad 5 \quad 14)$$

Decoded message is:

Hence, required message delivered is

In this way we send messages safely without any occurrence of cyber-crime.

References:

- 1. Karakurt, F. (2019, April 14). *Matrices and vectors in game development*. DEV Community. https://dev.to/fkkarakurt/matrices-and-vectors-in-game-development-67h8
- 2. Academy of Interactive Entertainment (AIE). (2018, May 15). *Video game math: Matrices*. AIE Articles. https://aie.edu/articles/video-game-math-matrices/
- 3. Lee, R. J. D. (2022, June 10). *Matrices for game development*. GameLudere. https://rjdlee.com/matrices-for-game-development/

APPLICATION OF NANOMATERIALS IN THE FOOD PACKAGING

INDUSTRY: ASSESSMENT OF AWARENESS LEVEL

AMONG MANUFACTURERS IN BENGALURU CITY

Mahalakshmi Arumugam*1 and B Avinash Sathyalingeshwar2

M S Ramaiah Institute of Technology, Bangalore

*Corresponding author E-mail: <u>mahalakshmi.a@msrit.edu</u>

Abstract:

Graphene and graphene oxide (GO) are materials with exceptional electrical, mechanical, thermal, and functional properties, making them ideal for electronics, energy storage, thermal management, and various chemical and space applications. Graphene oxide can be chemically reduced, mechanically exfoliated, and chemically vapor deposited (CVD) to produce graphene. Graphite is usually oxidized and then exfoliated to form graphene oxide (GO), which is more soluble in water and easier to process than pure graphene. Graphene oxide (GO) is gaining interest due to its potential applications, scalable synthesis, and potential for large-scale production due to its chemical conversion and integration into downstream products (Lowe & Zhong, 2016). The market lacks standardization for graphene materials, including graphene oxide (GO), which is closely linked to issues in characterization. The potential toxicity of graphene oxide (GO) poses a significant threat that must be addressed before its safe use in biomedical and environmental applications (Mahdi Sepahi & Azizi, 2024). Graphene oxide has wide potential in food packaging, ingredient separation, and antibacterial applications due to its superior permeability, selectivity, and barrier properties against bacteria and gases (Youssef et al., 2020; Barra et al., 2020). The excessive use of graphene and GO in aquatic environments could pose a significant threat to living organisms and human health due to potential agglomeration, long-term persistence, and toxic effects (Malhotra et al., 2020). Still, because of their remarkable mechanical strength, antibacterial activity, and barrier qualities, graphene and graphene oxide (GO) are becoming ground-breaking materials for food packaging. This paper aims to assess the level of awareness among manufacturers in the Bengaluru district and their readiness to accept graphene and graphene oxide in manufacturing food packaging materials. Understanding the level of awareness among manufacturers about the nature and application of

¹Department of Management Studies,

²Department of Electrical and Electronics Engineering,

graphene oxide for producing safe food packaging is essential for the successful introduction in the Indian consumer market.

Keywords: Graphene Oxide, rGO, Food Packaging, Biofilm, Sustainability

Introduction:

Graphene oxide (GO) is utilized in various electronic devices, including field-effect transistors (FETs), chemical sensors, biosensors, and functionalized semiconductors. It is also anticipated to be used in transparent conductive films for flexible electronics and solar cells. Graphene oxide and rGO (reduced GO) are highly conductive materials suitable for batteries, capacitors, fuel cells, and energy-related applications. They store hydrogen, offer high-capacity energy storage, and exhibit cycle stability. GO/rGO is a fluorescent material used in biosensing, early disease detection, cancer research, and detecting biological molecules, with potential for HIV diagnostics and fluorescence quenching in biosensors. Graphene Oxide (GO) is utilized in biomedical applications, particularly in drug-delivery systems, due to its low toxicity and tumor targeting. Functionalized nano-GO is highly effective in targeted drug delivery studies. Graphene oxide (GO) membranes, with a permeation rate of 0.1 mg/min/cm² and diffusion rate of 1 cm/h, can be used for cation exchange and filtration of seawater due to their super-thinness and strength. Graphene films, made up of millions of randomly stacked flakes, are optically transparent and impermeable under dry conditions, but when closed with hydro iodic acid, they become rGO films becoming a coating technology. GO, when combined with polymers, forms nanocomposites with enhanced properties like elastic modulus, tensile strength, electrical conductivity, and thermal stability, making them ideal for hydrogen storage, ion conductors, and nanofiltration membranes. Surface-localized chemically modified reduced graphene oxide nanocomposites are being utilized as flexible conductive surfaces for space applications.

Need and Significance of the Study:

Fresh and minimally processed foods sustain physiological and metabolic processes after harvest and are therefore susceptible to quality deterioration and reduced shelf life. Renewable and biodegradable polymers are particularly noteworthy since they meet the need for environmentally friendly packaging. The need for sustainable packaging is met by polymers derived from renewable resources, which stand out as significant renewable and biodegradable possibilities. Conventional polymers derived from renewable resources (sugarcane, for example), are readily available in the market despite not being biodegradable. A crucial component in the development of food packaging materials is microbial permeation. Because of their practicality and economic viability, antimicrobial active food packaging materials have distinguished themselves from other technological solutions for food preservation (Marangoni Júnior *et al.*,

2021). They have the important benefit of being recyclable. Moreover, a wide range of biological sources show tremendous promise as prospective packaging materials.

Proper food packaging prolongs shelf life, reduces the risk of chemical contamination, and facilitates easy handling and transportation of food products—all of which benefit customers. Food packaging has been made from a variety of materials, such as glass, metals, polymers, and papers and their composites.

The manufacturers of plastic food packaging must address the issue of chemicals that leak into food and may compromise food safety since dangerous compounds accumulate in plastics during their life cycle. Product deterioration is studied as a function of time and can include the growth of undesired microbes, a reduction in useful components (like vitamins), or an increase in undesirable components (like moisture or dark colors).

For the designed packaging to be successfully applied, the safety of food contact materials (FCMs) must be taken into account in addition to all aspects of food stability and packaging technology. The purpose of FCMs is to preserve and protect food. However, their interaction with food may occasionally result in the migration of various compounds that were previously contained in the packaging, acting as conduits for the contamination of those substances (Marangoni *et al.*, 2020). These materials include, among others, monomers, plasticizers, low-molecular-weight polymers, leftover solvents, and antioxidants. Since these materials have the potential to be hazardous to both humans and the environment, their migration needs to be regulated.

Determining a polymer film's barrier qualities is essential for projecting and evaluating the shelf life of product packaging. Proteins and polysaccharides are widely used in the creation of coatings and films. However, their extreme sensitivity to water vapor and their substandard mechanical qualities continue to be major obstacles in the development of packaging based on these raw materials (Marangoni Júnior *et al.*, 2022). Many approaches have been put up to address the drawbacks of biopolymer-based films, including mixing with other polymers, adding nanofillers, and including bioactive chemicals such as pure active agents, plant extracts, or essential oils. Conventional polymers have limited sustainability, are not biodegradable, and their production contributes significantly to the greenhouse gas emissions that cause climate change.

The significance of hazardous elements getting transferred from packing materials into foods, however, is of more concern due to customers' increased health consciousness.

Application of Graphene Oxide in Food Packaging:

Zuo et al. (2013) showed that the glass transition temperature (158 °C) of the GO-CS film surpasses that of pure chitosan (118 °C), signifying an enhanced thermal stability of the

composite. This was crucial for its utilization in biosensors, water treatment, medication delivery, and food packaging.

Lee *et al.* (2017) produced a flexible PVC film with hyperbranched polyglycerol-functionalized graphene oxide as a reinforcing filler. When compared to PVC alone, the PVC/HGO (polyvinyl chloride/functionalized graphene oxide) nanocomposites demonstrated a significant improvement in tensile strength, durability, toughness, and gas barrier properties. The outcome is that the nanocomposites are now great materials for synthetic leathers, food wraps, roofing covers, electrical cables, and blood storage bags.

El-Shafai *et al.* (2019) compared the antibacterial activity of GO–Ag and two heterostructures, GO–TiO2@ZnO and GO–Ag–TiO2@ZnO, against two Gram-positive and two Gram-negative bacteria. The findings demonstrated the ability of both nanocomposites to stop adherent microbial cell growth, which in turn stops the formation of biofilm in food packaging and medical equipment.

Saxena & Sarkar (2014) revealed that humans are not affected by graphene or other nanocarbon particles that are created when bioproducts are pyrolyzed in the air.

Literature Review:

Graphene oxide's low-cost properties have the potential to revolutionize various industries, including concrete, anti-corrosive coatings, composite materials, water treatment, latex, and tyre manufacturing, and lab-scale mineral processing (Ryan *et al.*, 2023). The large-scale production of graphene oxide nanoparticles is crucial for agriculture, and methods like oxidative exfoliation can help mass-produce it for various agricultural applications. Graphene oxide has potential applications in agriculture, technology, and food production, including nanoencapsulation, smart-release systems, packaging, water treatment, pesticide detection, fertilizer, and plant growth stimulants. Yield is a major concern in the graphene market, necessitating large-scale production of GO nanoparticles (Jino Affrald, 2023).

Graphene-based materials offer significant potential in flexible devices, miniaturization, and portability, impacting human life through health monitoring and water purification, and their composite membranes can remove dye molecules. The use of graphene-based composites offers a novel approach to creating wearable electronics and energy storage devices (Razaq *et al.*, 2022).

Since its emergence, people have been grappling with the uncontrolled and costly preparation of GO, which is crucial for large-scale production and industrial use. Despite its practical applications, graphene faces challenges such as large-scale production, cumbersome techniques like exfoliation and CVD, and complex transfer processes. Chemical oxidation is the most

widely used method, but its synthesis and purification are complex and risky. Controlling graphene sheet compositions and sizes is also challenging (Razaq et al., 2022). Youssef et al. (2020) highlighted that graphene's biological applications, particularly in food packaging, include detecting chemical contaminants, food composition, and pesticides, and are being increasingly studied for their potential applications. Graphene-based materials offer significant potential in flexible devices, miniaturization, and portability, impacting human life through health monitoring and water purification, and their composite membranes can remove dye molecules. Graphene-based materials offer significant potential in flexible devices, miniaturization, and portability, impacting human life through health monitoring and water purification, and their composite membranes can remove dye molecules.

Golestaneh (2023) disclosed that graphene oxide nanocomposite was utilized to create an electrochemical sensor capable of detecting sunset yellow and rhodamine B in food samples, indicating its potential for food additive detection. On the contrary, Malhotra *et al.* (2020) emphasised that excessive use of graphene and GO in aquatic environments could pose a significant threat to living organisms and human health, potentially causing agglomeration, long-term persistence, and toxic effects on cell membranes. Dziewięcka *et al.* (2018) showed that prolonged exposure to GO significantly reduced the reproductive abilities of the animals. Graphene oxide, a nanowaste, can penetrate living organisms and migrate along food chains, potentially causing negative consequences due to its specific nature. Nguyen *et al.* (2015) identified graphene oxide's low toxicity against intestinal bacteria and Caco-2 cells suggesting its potential for use in food applications. Arfat *et al.* (2018) revealed that polylactide/graphene oxide/clove essential oil composite films have the potential to be utilized as antimicrobial food packaging materials.

Graphene oxide (GO) has shown potential in food-related applications due to its versatility. It has been used for detecting food colorants, improving permeability, and enhancing antibacterial activity in food packaging. GO has also been used for detecting trace metal ions in food samples, demonstrating its potential for food safety. Graphene oxide (GO), derived from natural products, has significant applications in the food industry due to its unique properties, providing innovative solutions for food processing and agriculture.

Graphene oxide/polymer composite membranes are widely used in food packaging, ingredient separation, and antibacterial applications due to their superior permeability, selectivity, and barrier properties against bacteria and gases. Graphene oxide (GO), derived from natural products, has significant applications in the food industry due to its properties, providing innovative solutions for food processing and agriculture. Rhazouani *et al.* (2021) exposed that

graphene oxide (GO), an oxidized derivative of graphene, is utilized in biotechnology and medicine for cancer treatment, drug delivery, and cellular imaging, but its toxic effect limits its use. Graphene and graphene-oxide nanocomposites are extensively researched for chemical sensor applications, demonstrating high global awareness among researchers in materials science (Hazra & Basu, 2016).

Problem Statement:

Identifying the optimal graphene oxide product for an application requires optimizing production procedures to be economical and environmentally sustainable, minimizing costs, reducing waste, and using sustainable raw materials. The potential toxicity of graphene oxide (GO) poses a significant threat that must be addressed before its safe use in biomedical and environmental applications can be fully realized (Mahdi Sepahi & Azizi, 2024). G and GO exhibited varying toxicity based on their physical characteristics, including sizes, oxidation state, exposure concentrations, and sensitivity in both in vitro and in vivo models (Jia *et al.*, 2019). Graphene oxide producers often employ basic characterization techniques and provide minimal data, resulting in the appearance of different graphene oxide products as similar. The absence of interaction between producers and developers leads to difficulties in identifying the precise characteristics required for specific applications and optimizing the use of graphene oxide.

Recent research works state that in food packaging, graphene and graphene oxide provide several benefits, including increased food safety, longer shelf lives, and more robust packaging. However, the financial success of such advances depends on consumer acceptability. New packaging technologies must maintain freshness standards by ensuring waterproofness and food preservation, especially during global transport. A clear understanding of the nature of these nanomaterials and its enhanced health benefits among the manufacturers of food packaging may help in increased marketability.

Objectives of the Study:

The study describes the importance of safe and toxic-free food packaging and the incremental advantages of the inclusion of rGO in biofilms. The outcomes of these academic research works have the potential to transform how the food packaging industry operates and also take care of customers' interests. Moody (2003) discusses how study findings must be carefully considered before being put into practice, a process that will unavoidably lose some of its benefits. The manufacturers in the food packaging industry are vital in transforming research output into commercial products. The study aims to determine the level of awareness and willingness to use emerging nanomaterial, rGO, in particular, among these manufacturers in food packaging containers.

Methodology:

A survey was carried out by administering a well-designed questionnaire to the manufacturers in the Bengaluru district. A purposive sampling was employed to constitute a sample of fifty manufacturers of food packaging materials in Bangalore. Primary data was collected on their awareness and knowledge of graphene oxide, rGO, the application of rGO in food packaging, their willingness to embrace nanomaterials, rGO in particular, in manufacturing food wraps and food packaging materials they manufacture and supply to various other industries.

Findings and Discussions:

The results of the study indicated though 70 per cent of the respondents have heard about GO and rGO, only 55 per cent of the respondents were familiar about these nanomaterials and 50 per cent were aware of its applications in food packaging industry.

Table 1: Awareness of Graphene Oxide (GO) and reduced Graphene Oxide (rGO) among manufacturers of food packaging materials

Particulars	Category	Percentage
Companies based on operation	Partnership firms	40
	Private companies	60
Heard of graphene oxide (GO) or	Yes	70
reduced graphene oxide (rGO)	No	30
Familiarity with the application of	Very familiar	55
graphene oxide (GO) and reduced	Somewhat familiar	15
graphene oxide (rGO) in food packaging	Not familiar	30
Knowledge on industries where	Electronics	10
graphene oxide (GO) and reduced	Biomedical applications	20
graphene oxide (rGO) are used	Energy storage	25
	Water purification	20
	Food packaging	50
	Space applications	0
Primary source of information about	News/Media	0
graphene oxide (GO) and reduced	Academic journals/research papers	40
graphene oxide (rGO)	Industry forums	50
	Social media	10
Awareness on the use of reduced	Yes	70
graphene oxide (rGO) in food packaging materials	No	30

Perception on the potential benefits of	Enhanced food preservation	55
using rGO in food packaging	Improved barrier properties (e.g.,	40
	against moisture, gases)	
	Extended shelf life of packaged	
	foods	
	Sustainability (eg. biodegradability)	70
	Not aware of specific benefits	30
Primary concerns regarding safety of	Potential migration of nanoparticles	70
materials being used in food packaging,	into food	
	Long-term health effects of	45
	nanoparticles	
	Regulatory approval and safety	90
	standards	
	Environmental impact	100

Table 1 reveals that 70 percent of the respondents have perceived sustainability of the material while 55 percent perceived enhanced food preservation as the potential benefit. Only 45 percent of respondents agreed with a relatively prolonged shelf life of packaged food. Regarding the safety of material used in food packaging materials, 70 percent of respondents were bothered about the potential transfer of nanoparticles into food resulting in quick spoilage. All the respondents have expressed their primary concern about environment preservation followed by applicable regulations and safety measures.

Table 2: Willingness to accept nanomaterials in Food Packaging

Particulars	Category	Percentage
Willingness to embrace	Very willing	20
nanomaterials, like rGO, in the	Somewhat willing	30
manufacturing of food wraps	Neutral	15
and packaging materials	Somewhat unwilling	15
	Very unwilling	20
Factors influencing willingness	Scientific evidence of safety	40
to embrace rGO, in food	Regulatory approval	50
packaging	Clarity in benefits over traditional materials	35
	Environmental impact	50
	Consumer perception and acceptance	50
Willingness to conduct test	Yes	40
market for rGO enabled food	No	60
packaging		

Table 2 indicates that 50 percent of the respondents were willing to accept emerging nanomaterials in manufacturing food packaging containers. Customer orientation, environmental impact, and regulatory approval precede scientific proof of safety in embracing the materials for commercial production. Assessment of customer acceptance of emerging nanomaterial in food packaging is possible only when rGO-enabled food packaging is subjected to test marketing, 40 percent of the respondents expressed their willingness to commercialise the research outcomes.

Conclusion:

Although graphene and graphene oxide have the potential to improve food packaging, safety, and quality, more investigation and development in regulations are required to fully realize these materials' potential and guarantee their safe application in the food supply chain. Smart packaging solutions that detect temperature changes during food storage and transportation can be equipped with materials based on graphene. By doing this, food deterioration is reduced and perishable commodities are kept within safe temperature limits. While there are several high-tech and research-driven industries where there is a moderate level of understanding about graphene and graphene oxide among manufacturers in Bengaluru, there are considerable differences between sectors. For these cutting-edge materials to be adopted more widely and integrated into a wider range of applications, awareness-raising initiatives including education, training, and information sharing are essentially provided to the stakeholders.

References:

- 1. Alves, Z., Ferreira, N. M., Ferreira, P., & Nunes, C. (2022). Design of heat sealable starch-chitosan bioplastics reinforced with reduced graphene oxide for active food packaging. *Carbohydrate Polymers*, 291, 119517. https://doi.org/10.1016/j.carbpol.2022.119517
- 2. Arfat, Y. A., Ahmed, J., Ejaz, M., & Mullah, M. (2018). Polylactide/graphene oxide nanosheets/clove essential oil composite films for potential food packaging applications. *International Journal of Biological Macromolecules*, 107, 194–203. https://doi.org/10.1016/j.ijbiomac.2017.08.156
- 3. Chadha, U., Bhardwaj, P., Selvaraj, S. K., Arasu, K., Praveena, S., Pavan, A., Khanna, M., Singh, P., Singh, S., Chakravorty, A., Badoni, B., Banavoth, M., Sonar, P., & Paramasivam, V. (2022). Current trends and future perspectives of nanomaterials in food packaging application. *Journal of Nanomaterials*, 2022(1). https://doi.org/10.1155/2022/2745416
- Dziewięcka, M., Witas, P., Karpeta-Kaczmarek, J., Kwaśniewska, J., Flasz, B., Balin, K.,
 & Augustyniak, M. (2018). Reduced fecundity and cellular changes in *Acheta domesticus*

- after multigenerational exposure to graphene oxide nanoparticles in food. *Science of The Total Environment*, 635, 947–955. https://doi.org/10.1016/j.scitotenv.2018.04.207
- El-Shafai, N., El-Khouly, M. E., El-Kemary, M., Ramadan, M., Eldesoukey, I., & Masoud, M. (2019). Graphene oxide decorated with zinc oxide nanoflower, silver and titanium dioxide nanoparticles: Fabrication, characterization, DNA interaction, and antibacterial activity. RSC Advances, 9(7), 3704–3714. https://doi.org/10.1039/c8ra09788g
- 6. Golestaneh, M. (2023). Applicability of a graphene oxide nanocomposite for fabrication of an electrochemical sensor for simultaneous detection of Sunset Yellow and rhodamine B in food samples. *Analytical Methods*, 15(41), 5500–5509. https://doi.org/10.1039/d3ay01373a
- 7. Jia, P.-P., Sun, T., Junaid, M., Yang, L., Ma, Y.-B., Cui, Z.-S., Wei, D.-P., Shi, H.-F., & Pei, D.-S. (2019). Nanotoxicity of different sizes of graphene (G) and graphene oxide (GO) in vitro and in vivo. Environmental Pollution, 247, 595–606. https://doi.org/10.1016/j.envpol.2019.01.072
- 8. Lee, K. W., Chung, J. W., & Kwak, S.-Y. (2017). Flexible poly(vinyl chloride) nanocomposites reinforced with hyperbranched polyglycerol–functionalized graphene oxide for enhanced gas barrier performance. *ACS Applied Materials & Interfaces*, *9*(38), 33149–33158. https://doi.org/10.1021/acsami.7b10257
- 9. Lowe, S. E., & Zhong, Y. L. (2016b). Challenges of industrial-scale graphene oxide production. *Graphene Oxide*, 410–431. https://doi.org/10.1002/9781119069447.ch13
- Jino Affrald, R. (2023). Large-scale production and application of graphene oxide nanoparticles to meet agriculture needs. *Current Applied Science and Technology*. https://doi.org/10.55003/cast.2023.254564
- 11. Ma, Y., Zheng, Y., & Zhu, Y. (2019b). Towards industrialization of graphene oxide. *Science China Materials*, *63(10)*, 1861–1869. https://doi.org/10.1007/s40843-019-9462-9
- 12. Mahdi Sepahi, M., & Azizi, M. (2024). Graphene oxide nanotoxicity: A comprehensive analysis. *Nanotechnology and Nanomaterials*. https://doi.org/10.5772/intechopen.114205
- Malhotra, N., Villaflores, O. B., Audira, G., Siregar, P., Lee, J.-S., Ger, T.-R., & Hsiao, C.-D. (2020). Toxicity studies on graphene-based nanomaterials in aquatic organisms: Current understanding. *Molecules*, 25(16), 3618. https://doi.org/10.3390/molecules25163618
- 14. Moody, D. L. (2003). Using the world wide web to connect research and professional practice: Towards evidence-based practice. *Information Science: An International Journal of Emerging Transdiscipline*, 6, 31–48.
- 15. Marangoni, L., Fávaro Perez, M. Â., Torres, C. D., Cristianini, M., Massaharu Kiyataka, P. H., Albino, A. C., Padula, M., & Rodrigues Anjos, C. A. (2020). Effect of high-pressure

- processing on the migration of ε-caprolactam from multilayer polyamide packaging in contact with food simulants. *Food Packaging and Shelf Life*.
- Marangoni Júnior, L., Vieira, R. P., Jamróz, E., & Anjos, C. A. (2021). Furcellaran: An innovative biopolymer in the production of films and coatings. *Carbohydrate Polymers*, 252, 117221. https://doi.org/10.1016/j.carbpol.2020.117221
- 17. Marangoni Júnior, L., Jamróz, E., Gonçalves, S. de, da Silva, R. G., Alves, R. M., & Vieira, R. P. (2022). Preparation and characterization of sodium alginate films with propolis extract and nano-SiO₂. *Food Hydrocolloids for Health*, *2*, 100094. https://doi.org/10.1016/j.fhfh.2022.100094
- 18. Nguyen, T. H. D., Lin, M., & Mustapha, A. (2015). Toxicity of graphene oxide on intestinal bacteria and Caco-2 cells. *Journal of Food Protection*, 78(5), 996–1002. https://doi.org/10.4315/0362-028X.JFP-14-463
- 19. Oliveira, M., Abadias, M., Usall, J., Torres, R., Teixidó, N., & Viñas, I. (2015). Application of modified atmosphere packaging as a safety approach to fresh-cut fruits and vegetables A review. *Trends in Food Science & Technology, 46(1),* 13–26. https://doi.org/10.1016/j.tifs.2015.07.017
- 20. Ray, S. C. (2015). Application and uses of graphene oxide and reduced graphene oxide. *Applications of Graphene and Graphene-Oxide Based Nanomaterials*, 39–55. https://doi.org/10.1016/B978-0-323-37521-4.00002-9
- 21. Razaq, A., Bibi, F., Zheng, X., Papadakis, R., Jafri, S. H., & Li, H. (2022). Review on graphene-, graphene oxide-, reduced graphene oxide-based flexible composites: From fabrication to applications. *Materials*, *15*(3), 1012. https://doi.org/10.3390/ma15031012
- 22. Hazra, S., & Basu, S. (2016). Graphene-oxide nanocomposites for chemical sensor applications. *C*, *2*(2), 12. https://doi.org/10.3390/c2020012
- 23. Rhazouani, A., Gamrani, H., El Achaby, M., Aziz, K., Gebrati, L., Uddin, M. S., & Aziz, F. (2021). Synthesis and toxicity of graphene oxide nanoparticles: A literature review of *in vitro* and *in vivo* studies. *BioMed Research International*, 2021, 1–19. https://doi.org/10.1155/2021/5518999
- Robertson, G. L. (2004). Food packaging technology (Coles, R., McDowell, D., & Kirwan, M. J., Eds.). Blackwell: Oxford, UK. Packaging Technology and Science, 17(6), 333–335. https://doi.org/10.1002/pts.655
- 25. Ryan, E. A., Seibers, Z. D., Reynolds, J. R., & Shofner, M. L. (2023). Surface-localized chemically modified reduced graphene oxide nanocomposites as flexible conductive

- surfaces for space applications. *ACS Applied Polymer Materials*, *5*(7), 5092–5102. https://doi.org/10.1021/acsapm.3c00588
- 26. Saxena, M., & Sarkar, S. (2014). Involuntary graphene intake with food and medicine. *RSC Advances*, 4(57), 30162. https://doi.org/10.1039/c4ra04022h
- 27. Serrano-Luján, L., Víctor-Román, S., Toledo, C., *et al.* (2019). Environmental impact of the production of graphene oxide and reduced graphene oxide. *SN Applied Sciences, 1*, 179. https://doi.org/10.1007/s42452-019-0193-1
- 28. Youssef, K., Hashim, A. F., Roberto, S. R., Hamed, S. F., & Abd-Elsalam, K. A. (2020). Graphene-based nanocomposites: Synthesis, characterizations, and their agri-food applications. *Carbon Nanomaterials for Agri-Food and Environmental Applications*, 33–57. https://doi.org/10.1016/B978-0-12-819786-8.00003-7
- Zuo, P.-P., Feng, H.-F., Xu, Z.-Z., Zhang, L.-F., Zhang, Y.-L., Xia, W., & Zhang, W.-Q. (2013). Fabrication of biocompatible and mechanically reinforced graphene oxide-chitosan nanocomposite films. *Chemistry Central Journal*, 7(1). https://doi.org/10.1186/1752-153X-7-39

RECENT PROGRESS AND CHALLENGES IN BIOMASS-DERIVED POROUS ACTIVATED CARBON FOR ENERGY STORAGE DEVICES

- T. Rajesh Kumar*1, M. Paramasivam^{1,2}, Nivedha Lincy. C¹,
- S. Dorothy¹, P. Santharaman¹ and A. Maheshwaran¹
- ¹Department of Chemistry, AMET University, Chennai 603112, Tamil Nadu, India
- ²CSIR-Central Electrochemical Research Institute (CECRI), Karaikudi, Tamil Nadu, India
- *Corresponding author E-mail: rajeshcitizen24@gmail.com

Abstract:

With the rapid growth of modern society, electrical energy has become increasingly essential. Rising global population and continued fossil fuel dependence have sharply increased energy demand, presenting a major global challenge. To address this, efficient energy conversion and storage technologies are needed. In particular, novel electrode materials are critical for converting renewable sources into high-performance energy storage devices. Biomass-derived carbon has emerged as a promising, sustainable electrode material. Among these, porous carbon from biomass is especially attractive for supercapacitors one of the most efficient power source systems-due to its high surface area, natural abundance, thermal chemical stability, and well-developed porous structure. These properties support green chemistry principles and environmental sustainability. This review summarizes recent progress in biomass-based activated porous carbon for energy storage, with a focus on supercapacitor applications. This review focuses on porous carbon derived from flower waste. It examines the electrochemical performance of this material and its energy storage applications. These materials are also considered key to future sustainable energy technologies.

Keywords: Biomass; Biomass Porous Carbon; Specific Capacitance; Energy Storage: Supercapacitor.

1. Introduction:

As modern society's industrialization and urbanization accelerate, energy consumption has surged dramatically. The growing global demand for energy, alongside escalating environmental pollution, poses serious challenges. As fossil fuel resources like coal, oil, and natural gas continue to be depleted, and their overuse results in harmful emissions such as CO₂, CH₄, NO₂, SO₂, and fly ash there is an urgent need for sustainable electrode such as, cost effective, ecofriendly energy conversion and efficient storage systems. Fossil fuels currently dominate the global energy supply; however, projections suggest that reserves of these non-renewable

resources may be exhausted within the next few decades. The conventional and unsustainable fossil fuels pays significantly to affect environment due to the gas emissions, universal warming up, and ecological degradation. The rate of exploitation far exceeds the natural regeneration of these resources, highlighting the need for alternative energy solutions. Renewable power sources like as solar, wind, tidal, and natural gas offer cleaner and more sustainable options. To effectively harness and utilize these resources, advanced energy storage technologies must be developed to minimize energy losses and ensure long-term durability. In response, researchers have increasingly focused on developing efficient, low-cost, and eco-friendly energy storage devices. Among various technologies, supercapacitors and electrochemical capacitors have gained significant care because of its high energy density, durable cycle life, rapid charge/discharge capability, environmental safety, and low pollution. These devices, along with batteries (e.g., Li-ion), solar cells, and fuel cells, represent promising solutions for future energy systems. The key lies in the development of advanced materials with tailored structures and properties that not only enhance performance but also support sustainable, green, and cost-effective manufacturing.

Carbon materials derived from natural bio-waste have attracted significant attention due to their favourable properties, including low cost, high surface area, excellent thermal and chemical stability, good electrical conductivity, and tuneable pore structure making them a suitable for a wide range of practical applications [9]. Carbon is the second most abundant element on Earth (after oxygen) and forms the foundation of renewable energy materials in the form of carbohydrates and various biopolymers. Biomass, typically sourced from plants and plant-based materials, is produced via photosynthesis, using atmospheric CO2 and water under sunlight. According to recent statistics, global biomass production accounts for approximately 104.9% of carbon supply annually [10]. A significant portion of this biomass such as agricultural residues and forest waste is still often disposed of through open burning, leading to environmental harm. Instead, this abundant resource can be converted into valuable carbon-based materials for sustainable energy applications. Recently, biomass-derived activated carbon has been developed in various forms, including fibres, flakes, graphene, carbon nanotubes, and carbon templates, offering high conductivity and excellent energy storage performance. These forms are increasingly being used to meet the demands of industrial, technical, and chemical energy storage systems [11-15]. Additionally, well-structured activated porous carbon exhibits impressive electrochemical performance and can be tailored with pore structures ranging from microspores to macrospores. Advances in activation techniques now allow for precise control

over pore size distribution, and various biomass precursors have been successfully applied to produce high-performance activated carbon, as discussed in this review.

2. Porous Carbon from Flower Waste:

In recent decades, biomass-derived carbon materials have gained considerable attention for applications such as battery electrodes, supercapacitors and catalytic materials due to their large specific surface area, good conductivity and well-developed pore structures. In this review, we highlight several studies focused on flower-based biomass carbons. Chang et al. [16] prepared active Paulownia flower-derived carbon (a-PFC) with both microporous and meso/macro porous structures using a simple pyrolysis carbonization process. The resulting a-PFC exhibited an impressive specific capacitance of 297 F/g at 1 A/g in a 1 M H₂SO₄ and maintained 93% of its original capacitance after the completion of 1000 cycles that demonstrating good cycling stability. The symmetric supercapacitor device assembled using a-PFC realized an energy density of 44.5-22.2 Wh/kg and a power density of 247-3781 W/kg at a scan rate of 20 mV/s in a 1 M H₂SO₄ aqueous electrolyte. Abrar Khan et al. [17] reported hierarchically porous carbon obtained from red rose flowers using a simple two-step technique involving pre-carbonization and chemical activation. The resulting electrode material showed a high specific capacitance of 350 F/g at 1 A/g, and maintained165 F/g even at 150 A/g in 6 M KOH electrolyte, demonstrating superb rate capability. Additionally, the RDPC exhibited outstanding durability, with only 4.4% loss of capacitance after 140,000 cycles at 100 A/g. The symmetric device based on RDPC delivered an energy density of 15.6 Wh/kg at 499 W/kg and showed just 3.5% degradation in capacitance after completion of 15,000 cycles at 20 A/g in 6 M KOH. These results clearly indicate that RDPC is a promising electrode material for advanced supercapacitor applications. Elanthamilan et al. [18] utilized Couroupitaguianensis flowers as a precursor to synthesize active porous carbon (CG ACs) via a two-step process combining pre-carbonization and chemical activation. The resulting CG ACs electrode material showed a remarkable specific capacitance of 711 F/g at 1 Ag, along with 92% retentions the capacitance over 5000 cycles in 1 M aqueous KOH electrolyte, confirming its excellent electrochemical performance and stability.

Based on the results, the CG ACs electrode material appears to be a promising candidate for energy storage devices. Zhao *et al.* [19] synthesized 3D rose-derived porous carbon (RPC) for supercapacitor applications using a low-cost and efficient carbonization method with withered rose petals as the carbon precursor. The resulting 3D RPC exhibited a specific capacitance of 208 F/g at 0.5 A/g in 6 M KOH electrolyte showing an outstanding capacitance retention of 99% after completion of 25,000 cycles. Furthermore, the symmetric device (RAC-800-2//RAC-800-2) achieved an energy density of 20.32 Wh/kg at a power density of 525 W/kg, with 92% retention

capacitance after completing 10,000 cycles in 1 M Na₂SO₃ electrolyte, indicating its strong potential for large-scale applications. Panmand *et al.* [20] derived perforated graphene (PG) from Bougainvillea flower using a template-free, single-step method. The PG electrode material delivered specific capacitances of 316.2, 140.7, 75.9, and 41.3 F g⁻¹ at current densities of 2.28, 3.33, 4.66, and 5.82 A/g, correspondingly. It also maintained 93% of its initial capacitance after the completion of 10,000 cycles at 5.8 A/g. Moreover, the symmetric device fabricated with PG electrodes exhibited an outstanding energy density of 63.7 Wh/kg at a power density of 273.2 W/kg in a 1 M Na₂SO₃. Zou *et al.* [21] fabricated porous carbon (OC) from Osmanthus flower as a biomass precursor. The resulting electrode material exhibited a specific capacitance of 255 F/g at 1 A/g, with 92.9% retention after completion of 10,000 cycles at 20 A/gin 6 M KOH.

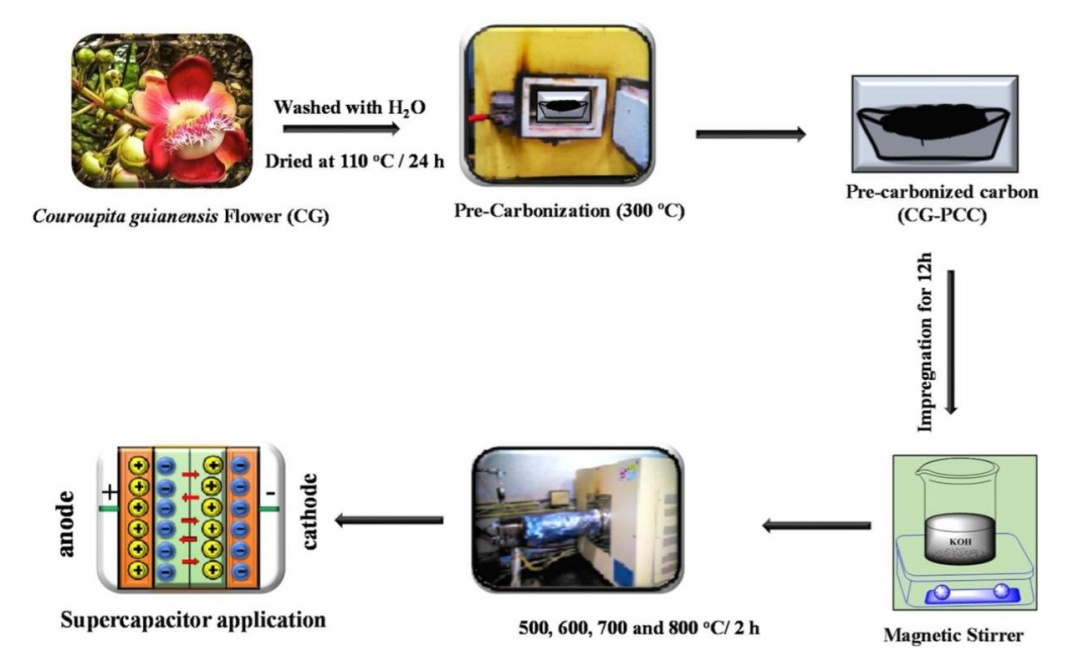


Figure 1: A diagram explains the preparation procedure for CG-derived porous carbon for high performance super capacitor [18] (Copy Right 2019)

Additionally, the symmetric OC-based device demonstrated an energy density of 7.95 Wh/kg and a power density of 10 kW/kg at 20 A/g, indicating its viability for high-performance supercapacitors. Chang *et al.* [22] developed a PANI/RGO hybrid composite derived from rose flowers using a simple bio-template-assisted fabrication method. The PANI/RGO electrode showed a high specific capacitance of 626 F/g, retaining 545 F/g with 87% stability over 1000 cycles at 1 A/g in a 1 M H₂SO₄ electrolyte. The assembled symmetric device using from this composite achieved an energy density of 5.06 Wh/kg at a power density of 1685 W/kg, with 85% capacitance holding after the completion of 1000 cycles. Sivachidambaram *et al.* [23] reported activated the porous carbon derived from Borassusflabelliform flower (BFF) via a simple

chemical activation process. The BFF-based electrode delivered a specific capacitance of 234.4 F/g at 1 A/g in 1 M KOH electrolyte with a cycling retention of 76.9% after the completion of 1000 cycles at the same current density. Ma *et al.* [24] used sakura petals to prepare 3D porous carbon via a pre-carbonization method. The resulting electrode showed a specific capacitance of 265.8 F/g at 0.2 A g⁻¹ in 6 M KOH, and retained 209 F/g with 90.2% stability over 2000 cycles at 1 A g⁻¹, suggesting strong potential for energy storage applications. Veeramani *et al.* [25] established the synthesis of graphene shell-like porous active carbon (GPAC) from Bougainvillea spectabilis using a chemical activation method. The GPAC electrode exhibited a specific capacitance of 233 F/g at 1.6 A/g, with 98% capacitance retention after the completion of 2000 cycles at 5 A/g in 2 M KOH. The symmetric GPAC/PVA/KOH/GPAC device achieved an energy density of 7.2 Wh/kg, with a specific capacitance of 51 F g⁻¹ at 1.6 A/g. Diggikar *et al.* [26] synthesized honeycomb-like reduced graphene oxide (RGO) polyaniline nanofibers using a customized Hummers method, with rose flower as the precursor. The resulting composite material demonstrated excellent electrochemical properties suitable for supercapacitor applications.

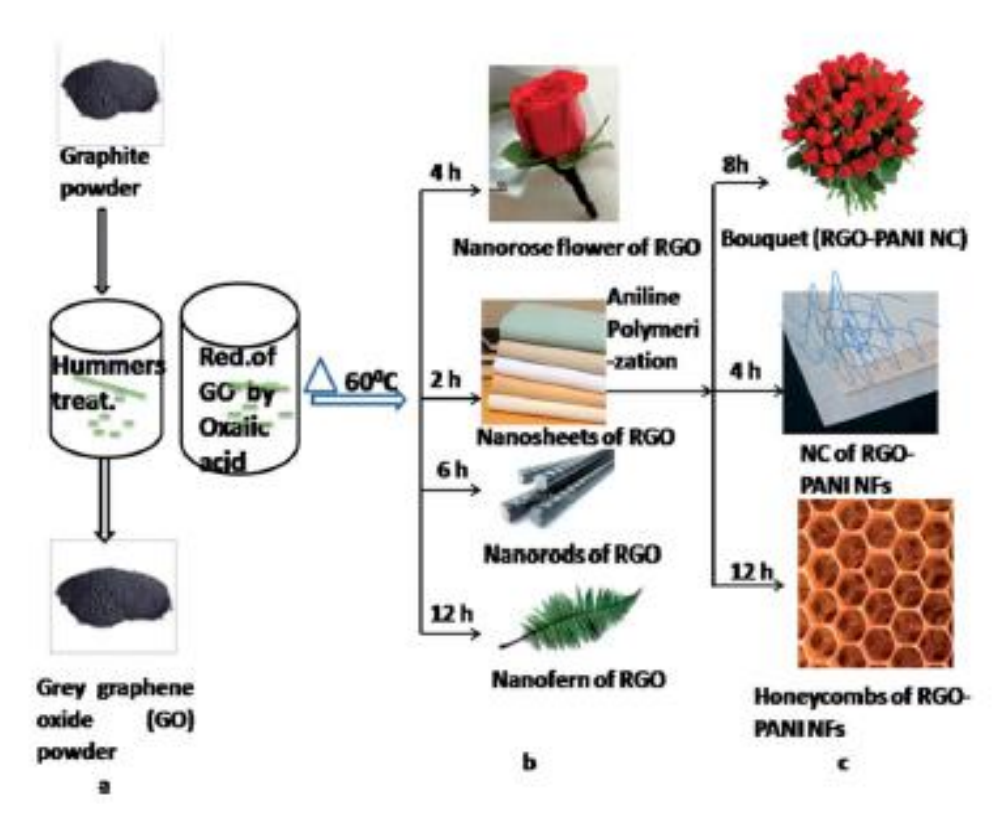


Figure 2: Illustrated that the Preparation of GO and RGO based nanofiber-reduced graphene oxide composited for high performance super capacitor [26] (Copy Right 2014)

The reduced graphene oxide (RGO) exhibited an extraordinary specific capacitance of 470 F/g at 1 A/g in $1 \text{ M H}_2\text{SO}_4$ electrolyte, according the values the prepared electrode is compatible for

power sources applications. Ma et al. [27] derived porous carbon from sunflower using a simple pre-carbonization method. The resulting electrode material demonstrated a high specific capacitance of 345 F/g at 1 A/g and 280 F/g at 20 A/g in 6 M KOH solution. Additionally, the prepared material showed admirable cycling durability, retaining 83% of its initial capacitance after 5,000 cycles at 5 A/g. The fabricated symmetric device also exhibited an energy density of 9.2 Wh/kg and a power density of 482 W/kg at a current density of 0.5 A/g, suggesting that this electrode material is a promising candidate for supercapacitor applications. Ma et al. [28] also reported on white clover-derived porous carbon (WCCS) for supercapacitors, synthesized via a low-cost carbonization method. The WCCS electrode material showed a specific capacitance of 233.1F/g at 1 A/g and 193.2 F/g at 20 A/g, along with excellent cycling stability, maintaining 82.9% of its capacitance after the completion of 5,000 cycles at 1 A/g in 2 M KOH electrolyte. The WCC-2//WCC-2 symmetric device showed an impressive energy density ranging from 30 to 13.1 Wh/kg and a power density of 503.5 to 9991.5 W/kg using 0.5 M Na₂SO₃, confirming its suitability for supercapacitor applications. Guo et al. [29] synthesized nitrogen-doped porous carbon (NPCP3) from camellia flower via a simple carbonization approach. The resulting electrode material showed a remarkable specific capacitance of 354 F/g at 0.2 A/g in 2 M KOH electrolyte and excellent cycling stability, with only a 4% loss after the completion of 5,000 cycles at 5 A/g. Bin Du et al. [30] demonstrated nitrogen-doped activated porous carbon (RFAC-N) which is obtained from reed flower using diethanolamine (DEA) as a nitrogen source via precarbonization. The RFAC-N displayed an excellent specific surface area of 1691 m²/g and a pore volume of 1.08 cm³/g. The symmetric two-electrode system fabricated with RFAC-N achieved a specific capacitance of 254.3 F/g gat 1 A g⁻¹ and maintained 192.7 F/g at 30 A/g. It also demonstrated an energy density of 9.4 Wh/kg and longstanding cycling stability, and retaining 89.5% of its original capacitance after the completion of 10,000 cycles at 10 A/g. These data clearly indicate that the developed materials hold great promise for energy storage device applications. Zihan et al. [31] and colleagues synthesized porous carbon for supercapacitors from waste coriander and lilac (LPC) using a simple pre-carbonization route. The obtained electrode materials showed enhanced specific capacitances of 421 F/g and 524 F/g, respectively. The activated porous carbon LPC demonstrated an impressive specific surface area of up to 2565 m²/g, with high nitrogen (N) and oxygen (O) content. The assembled symmetric supercapacitors delivered remarkable energy densities of 18.17 Wh/kg in 6 M KOH electrolyte, and 40.97 Wh/kg in 1 M Na₂SO₃ electrolyte, confirming that waste coriander- and lilac-based porous carbons are promising for advanced electrochemical applications. Yongtao Tan et al. [32] fabricated a 3D highly graphitic porous biomass carbon (HGPBC) for supercapacitors via a simple single-step

process using potassium ferrate (K₂FeO₂) as an activator, with dandelion flower as the carbon source. The synthesized HGPBC exhibited a remarkable specific surface area of 780.4 m²/g and a specific capacitance of 309 F/g at 0.5 A/g. This material also delivered a notable energy density of 14.22 Wh/kg at a power density of 218.8 W/kg. Mani Sakthivel et al. [33] prepared seleniumdoped CoWS₂ (Se-CoWS₂) as both anode and cathode materials for supercapacitors, synthesized from banana flower skin-based activated carbon (BFS-AC) via a simple carbonization technique. The electrode material exhibited excellent charge transfer resistance and a high specific capacitance of 452 C/g at 0.5 A/g, along with good stability, retaining 96.15% capacitance over 2,000 cycles. The fabricated Se-CoWS₂//BFS-AC asymmetric device demonstrated an outstanding energy density of 107.87 Wh /kg at a power density of 1600 W /kg, maintaining 95.33% of its initial capacity after the completion of 3,000 continuous charge/discharge cycles. Jin et al. [34] the synthesized material having a enormous specific surface area subsequently it has high heteroatom content through daylily via a single-step carbonization process. The electrode material delivered a specific capacitance of 299.1 F/g at 0.5 A/g, exhibited an exceptional stability of cycling with 99.6% c retention capacity over 4,000 cycles at 1 A/g. Fabricated symmetric supercapacitor demonstrated an excellent energy density of 21.6 Wh/kg and the value of 598.2 W kg⁻¹ as a power density in 6 M KOH electrolyte, highlighting its potential for high-performance supercapacitor applications.



Figure 3: Illustrated the honeysuckle flowers are employed as precursor to produce hierarchical porous carbon for high-performance supercapacitors

Table 1: Electrochemical performances of flower biomass based porous carbon for supercapacitor applications

Porous carbon resource	Capacitance	Current	Ref.
	(F/g)	Density	
		(A/g)	
Paulownia flower	297	1	16
Red rose	350	1	17
Couroupitaguianansis	711	1	18
Rose	208	0.5	19
Bougainvillea	316.2	2.28	20
Osmanthus flower	255	1	26
Rose flower	626	1	21
Borassusflabellifer flower	234.4	1	22
Sakura petals	265.8	0.2	23
Bougainvillea spectabilisas	233	1.6	24
Rose flower	470	1	25
Sunflower	345	1	26
White clover	233.1	1	27
Camellia flower	345	0.2	28
Reed Flower	254.3	1	29
Coriander and lilac	524	1	30
Dandelion flower	309	0.5	31
Banana flower skin	452 C/g	0.5	32
daylily	299.1	0.5	33
Honeysuckle flowers	186	1	34
elm flower	275	1	35
Feather finger	315	1	36
Borassusflabellifer	247	0.5	37
Waste-kapok flower	286.8	1	39
Coggygria flowers	413.5	0.5	40
Alfalfa flowers	350.1	0.5	41

Xu et al. [35] utilized the honeysuckle flowers were used as a raw material for making hierarchical porous carbon via a simple carbonization process with KOH activation for supercapacitors. The fabricated material exhibited a specific capacitance of 186 F/g at 1 A/g in 1ethyl-3-methylimidazolium tetrafluoroborate (EmimBF₄) electrolyte. The fabricated electrode showed a high specific energy of 93 Wh/kg with a power density of 954 W/kg and also maintained about 64 Wh kg⁻¹ at 23 kW kg⁻¹. Its cycling stability retained 83% of the original capacitance after 7,500 cycles. Chen et al. [36] developed activated carbon (ELAC) derived from elm flowers, containing elements like nitrogen 2.21% atom and sulphur 6.06 % atom, respectively, via a simple hydrothermal process with KOH activation for supercapacitors. The ELAC electrode exhibited a remarkable surface area of 2048.6 m²/g and a pore volume of 0.88 cm³/g delivering a specific capacitance of 275 F/g at 1 A/g and maintaining 216 F/g at 20 A/g. The fabricated symmetric ELAC device showed a value of 62 F/g capacitance at 10 A/g and achieved energy and power densities of 16.8 Wh/kg and 600 W/kg, correspondingly. It retained about 87.2% of its initial capacitance at 4 A/g after 5,000 cycles. Senthil et al. [37] fabricated a hollow tubular porous carbon (HT-PC) obtained from feather finger grass flower using a simple carbonation method with KOH chemical activation for supercapacitor applications. The resulting HT-PC exhibited an excellent surface area of 637.1 m²/g and a variety of micropore sizes created under the KOH activation conditions. The electrode material demonstrated excellent electrochemical performance, delivering a specific capacitance of 315 F/g at 1 A/g and 262 F/g at 100 A/g, while maintaining 96% of its initial capacitance after 50,000 charge/discharge cycles at 50 A/g in 6 M KOH electrolyte. Furthermore, the HT-PC-based symmetric supercapacitor showed a high specific energy of approximately 18.75 Wh/kg at a power density of 0.37 kW/kg, with about 30% capacitance retention after 10,000 cycles at 10 A/g in 6 M KOH. Using 1 M Et4NBF4/AN electrolyte, the symmetric device also exhibited a remarkable specific energy of 13.18 Wh/kg at 0.61 kW/kg with no capacitance loss over 10,000 cycles at 10 A/g. Iro et al. [38] utilized Borassusflabellifer (BFL) flowers to prepare activated carbon for supercapacitor applications via a single-step carbonization and KOH chemical activation process. The fabricated electrode exhibited a high specific surface area of 930.3 m²/g with an average pore size of 1.96 nm. Additionally, it delivered an impressive specific capacitance of 247 F/g at 0.5 A/g in 1 M H₂SO₄ electrolyte and demonstrated impressive cycling stability, retaining 94% capacitance after 2,500 cycles. The electrode also achieved a specific energy of 101.1 kW/kg and a specific power of 4,500 kW/kg, indicating its strong potential as a supercapacitor electrode material. Zheng et al. [39] synthesized hierarchical activated porous carbon for supercapacitors using a simple single-step carbonization method from waste kapok flower as the carbon precursor. The

electrode exhibited excellent electrochemical performance with a specific capacitance of 286.8 F/g at 1 A/g and retained 97.4% of its original capacitance after 5,000 cycles. These results confirm the material as a promising candidate for supercapacitor applications. Lia *et al.* [40] fabricated hierarchical porous biochar from Cotinuscoggygria flowers via a simple precarbonization process for supercapacitor use. The material showed an outstanding specific capacitance of 413.5 F/g at 0.5 A/g in 1 M H₂SO₄ electrolyte and maintained a high capacitance of 279.9 F/g at 5 A/g in 6 M KOH electrolyte after 36,000 cycles. These findings highlight the material's excellent potential for supercapacitor devices. Meng *et al.* [41] developed oxygen-rich carbon from alfalfa flowers using a simple carbonization route with KOH activation for supercapacitors. The electrode delivered a high specific capacitance of 350.1 F/g at 0.5 A/g and maintained 297 F/g at a high current density of 50 A/g. The symmetric supercapacitor device showed a specific capacitance of 201.4 F/g at 0.1 A/g and retained 82.7% of its initial capacitance at 10 A/g. The energy density increased from 23.2 Wh/ kg to 28 Wh/ kg, while the power density decreased from 10.3 kW/kg to 100 W/kg.

Conclusion:

In summary, the growing global energy demand underscores the urgent need for efficient and sustainable energy storage solutions. Biomass-derived porous carbon from flowers as a promising electrode material for supercapacitors due to its abundant availability, excellent physicochemical properties, and eco-friendly nature. Continued research and development in this area are essential to overcome the existing challenges and fully realize the potential of biomass-based carbons in advancing green, high-performance energy storage technologies for a sustainable future.

Acknowledgment:

The authors would like to acknowledgment the Department of Chemistry, AMET University for valuable support for completion of this work.

References:

- 1. Deng, J., Li, M., & Wang, Y. (2016). Biomass-derived carbon: synthesis and applications in energy storage and conversion. *Green Chemistry*, 18, 4824–4854.
- 2. Wang, D., Xu, Z., Lian, Y., Ban, C., & Zhang, H. (2019). Nitrogen self-doped porous carbon with layered structure derived from porcine bladders for high-performance supercapacitors. *Journal of Colloid and Interface Science*, 542, 400–409.
- 3. Gang, X., Mohanapriya, K., Jiang, W., Pan, J., Pan, Z., & Liu, X. (2021). A novel in-situ preparation of N-rich spherical porous carbon as greatly enhanced material for high-performance supercapacitors. *Carbon*, 171, 62–71.

- 4. Jiang, W., Cai, J., Pan, J., Guo, S., Sun, Y., Li, L., & Liu, X. (2019). Nitrogen-doped hierarchically ellipsoidal porous carbon derived from Al-based metal-organic framework with enhanced specific capacitance and rate capability for high performance supercapacitors. *Journal of Power Sources*, 432, 102–111.
- 5. Wang, B., Ji, L., Yu, Y., Wang, N., Wang, J., & Zhao, J. (2019). A simple and universal method for preparing N, S co-doped biomass derived carbon with superior performance in supercapacitors. *Electrochimica Acta*, 309, 34–43.
- 6. Jiang, W., Pan, J., & Liu, X. (2019). A novel rod-like porous carbon with ordered hierarchical pore structure prepared from Al-based metal-organic framework without template as greatly enhanced performance for supercapacitor. *Journal of Power Sources*, 409, 13–23.
- 7. Osman, S., Senthil, R. A., Pan, J., & Li, W. (2018). Highly activated porous carbon with 3D microspherical structure and hierarchical pores as greatly enhanced cathode material for high-performance supercapacitors. *Journal of Power Sources*, 391, 162–169.
- 8. Gur, T. M. (2018). Review of electrical energy storage technologies, materials and systems: Challenges and prospects for large-scale grid storage. *Energy & Environmental Science*, 11, 2696–2767.
- 9. Men, B., Guo, P., Sun, Y., Tang, Y., Chen, Y., Pan, J., & Wa, P. (2019). High-performance nitrogen-doped hierarchical porous carbon derived from cauliflower for advanced supercapacitors. *Journal of Materials Science*, *54*, 2446–2457.
- 10. Liu, W., Jiang, H., & Yu, H. (2019). Emerging applications of biochar-based materials for energy storage and conversion. *Energy & Environmental Science*, *12*, 1751–1779.
- 11. Yang, S., Wang, S., Liu, X., & Li, L. (2019). Biomass derived interconnected hierarchical micro-meso-macro-porous carbon with ultrahigh capacitance for supercapacitor. *Carbon*, 147, 540–549.
- 12. Song, M., Zhou, Y., Ren, X., Wan, J., Du, Y., Wu, G., & Ma, F. (2019). Biowaste-based porous carbon for supercapacitor: The influence of preparation processes on structure and performance. *Journal of Colloid and Interface Science*, 535, 276–286.
- 13. Wu, F., Gao, J., Zhai, X., Xie, M., Sun, Y., Kang, H., Tian, Q., & Qiu, H. (2019). Hierarchical porous carbon microrods derived from albizia flowers for high performance supercapacitors. *Carbon*, 147, 242–251.
- 14. Osman, S., Senthil, R. A., Pan, J., & Sun, Y. (2019). A novel coral structured porous-like amorphous carbon derived from zinc-based fluorinated metal-organic framework as

- superior cathode material for high performance supercapacitors. *Journal of Power Sources*, 414, 401–411.
- 15. Yang, G., & Park, S. (2018). MnO₂ and biomass-derived 3D porous carbon composites electrodes for high performance supercapacitor applications. *Journal of Alloys and Compounds*, 741, 360–367.
- 16. Chang, J., Gao, Z., Wang, X., Wu, D., Xu, F., Wang, X., Guo, Y., & Jiang, K. (2015). Activated porous carbon prepared from paulownia flower for high performance supercapacitor electrodes. *Electrochimica Acta*, 157, 290–298.
- 17. Khan, A., Senthil, R. A., Pan, J., Sun, Y., & Liu, X. (2020). Hierarchically porous biomass carbon derived from natural withered rose flowers as high performance material for advanced supercapacitors. *Batteries & Supercaps*, *3*, 731–737.
- Elanthamilan, E., Sriram, B., Rajkumar, S., Dhaneshwaran, C., Nagaraj, N., Merlin, J. P.,
 Vijayan, A. (2019). *Couroupita guianansis* dead flower derived porous activated carbon as efficient supercapacitor electrode material. *Materials Research Bulletin*, 112, 390–398.
- 19. Zhao, C., Huang, Y., Zhao, C., Shao, X., & Zhu, Z. (2018). Rose-derived 3D carbon nanosheets for high cyclability and extended voltage supercapacitors. *Electrochimica Acta*, 291, 287–296.
- Panmand, R. P., Patil, P., Sethi, Y., Kadam, S. R., Kulkarni, M. V., Gosavi, S. W., Munirathnam, N., & Kale, B. B. (2017). Unique perforated graphene derived from Bougainvillea flowers for high-power supercapacitors: A green approach. Nanoscale, 9, 4801–4809.
- 21. Zou, R., Quan, H., Wang, W., Gao, W., Dong, Y., & Chen, D. (2018). Porous carbon with interpenetrating framework from *Osmanthus* flower as electrode materials for high-performance supercapacitor. *Journal of Environmental Chemical Engineering*, 6, 258–265.
- 22. Chang, C., Hu, Z., Lee, T., Huang, Y., Ji, W., Liu, W., Yeh, J., & Wei, Y. (2016). Bio templated hierarchical polyaniline composite electrodes with high performance for flexible supercapacitors. *Journal of Materials Chemistry A, 4*, 9133–9145.
- 23. Sivachidambaram, M., Vijaya, J. J., Kennedy, L. J., Jothiramalingam, R., Al-Lohedan, H., Munusamy, M. A., Elanthamilan, E., & Merlin, J. P. (2017). Preparation and characterization of activated carbon derived from *Borassus flabellifer* flower as electrode material for supercapacitor applications. *New Journal of Chemistry*, 41, 3939–3949.
- 24. Ma, F., Ding, S., Ren, H., & Liu, Y. (2019). Sakura-based activated carbon preparation and its performance in supercapacitor applications. *RSC Advances*, *9*, 2474–2483.

- Veeramani, V., Sivakumar, M., Chen, S.-M., Madhu, R., Alamri, H. R., Alothman, Z. A., Hossain, M. S. A., Chen, C.-K., Yamauchi, Y., Miyamoto, N., & Wu, K. C.-W. (2017). Lignocellulosic biomass-derived, graphene sheet-like porous activated carbon for electrochemical supercapacitor and catechin sensing. *RSC Advances*, 7, 45668–45675.
- 26. Diggikar, R. S., Late, D. J., & Kale, B. B. (2014). Unusual morphologies of reduced graphene oxide and polyaniline nanofibers–reduced graphene oxide composites for high performance supercapacitor applications. *RSC Advances*, *4*, 22551–22560.
- 27. Ma, D., Wu, G., Wan, J., Ma, F., Geng, W., & Song, S. (2015). Oxygen-enriched hierarchical porous carbon derived from biowaste sunflower heads for high-performance supercapacitors. *RSC Advances*, *5*, 107785–107792.
- 28. Ma, G., Zhang, Z., Sun, K., Peng, H., Yang, Q., Ran, F., & Lei, Z. (2015). White clover-based nitrogen-doped porous carbon for a high energy density supercapacitor electrode. *RSC Advances*, *5*, 107707–107715.
- 29. Guo, D., Zheng, C., Deng, W., Chen, X., Wei, H., Liu, M., & Huang, S. (2017). Nitrogen-doped porous carbon plates derived from fallen camellia flower for electrochemical energy storage. *Journal of Solid State Electrochemistry*, 21, 1165–1174.
- 30. Du, B., Huang, L., Shen, M., Zhou, H., Wang, B., Deng, Z., Wang, L., & Nie, D. (2021). Diethanolamine-assisted preparation of reed flower-derived nitrogen-doped porous carbon for supercapacitor electrodes. *Energy & Fuels*, *35*, 8789–18797.
- 31. Ma, Z., Wang, L., Chen, T., & Wang, G. (2024). Two biomass material-derived self-doped (N/O) porous carbons from waste coriander and lilac with high specific surface areas and high capacitance for supercapacitors. *New Journal of Chemistry*, 48, 832–843.
- 32. Tan, Y., Xu, Z., He, L., & Li, H. (2022). Three-dimensional high graphitic porous biomass carbon from dandelion flower activated by K₂FeO₄ for supercapacitor electrode. *Journal of Energy Storage*, *52*, 104889.
- 33. Sakthivel, M., Ramki, S., Chen, S.-M., & Ho, K.-C. (2022). Defect-rich Se-CoWS₂ as anode and banana flower skin-derived activated carbon channels with interconnected porous structure as cathode materials for asymmetric supercapacitor application. *Energy*, 257, 124758.
- 34. Jin, T., Su, J., Luo, Q., Zhu, W., Lai, H., Huang, D., & Wang, C. (2022). Preparation of N, P co-doped porous carbon derived from daylily for supercapacitor applications. ACS Omega, 7, 37564–37571.

- 35. Xu, X., Yang, L., Zhuo, K., Zhang, Z., Du, Q., Wang, C., Chen, Y., & Zhao, Y. (2021). Honeysuckle flowers-derived hierarchical porous carbon matching with ionic liquid electrolyte for high-energy supercapacitors. *Journal of Energy Storage*, 41, 102988.
- 36. Chen, H., Yu, F., Wang, G., Chen, L., Dai, B., & Peng, S. (2018). Nitrogen and sulfur self-doped activated carbon directly derived from elm flower for high-performance supercapacitors. *ACS Omega*, *3*, 4724–4732.
- 37. Senthil, R. A., Yang, V., Pan, J., & Sun, Y. (2021). A green and economical approach to derive biomass porous carbon from freely available feather finger grass flower for advanced symmetric supercapacitors. *Journal of Energy Storage*, 35, 102287.
- 38. Iro, Z. S., Subraman, C., Rajendran, J., & Sundramoorthy, A. K. (2021). Promising nature-based activated carbon derived from flowers of *Borassus flabellifer* for supercapacitor applications. *Carbon Letters*, 31, 1145–1153.
- 39. Zheng, L.-H., Chen, M.-H., Liang, S.-X., & Lu, Q.-F. (2021). Oxygen-rich hierarchical porous carbon derived from biomass waste-kapok flower for supercapacitor electrode. *Diamond and Related Materials*, 113, 108267.
- 40. Li, Y., Zhang, X., Deng, J., Yang, X., Wang, J., & Wang, Y. (2020). Hierarchical porous biochar derived from *Cotinus coggygria* flower by using a novel composite activator for supercapacitors. *Chemical Physics Letters*, 747, 137325.
- 41. Meng, S., Mo, Z., Li, Z., Guo, R., & Liu, N. (2020). Oxygen-rich porous carbons derived from alfalfa flowers for high performance supercapacitors. *Materials Chemistry and Physics*, 246, 122830.

ELECTRICAL PROPERTIES OF KAOLINITE MINERALS

Rajanish Saikia and Swagatam Deva Nath*

Department of Physics, Nanda Nath Saikia College, Titabar, Assam, India

*Corresponding author E-mail: swgtmdvnth@gmail.com

Abstract:

This chapter reviews the electrical properties of kaolinite — a 1:1 layered aluminosilicate clay mineral — with emphasis on the physical and chemical mechanisms that control surface charge, electrokinetic behaviour, dielectric response, and electrical conduction. Kaolinite's electrical characteristics arise from its crystal structure, surface functional groups, and the interplay between adsorbed water and ions. The chapter covers fundamental theory (electrical double layer, surface complexation, DLVO), experimental approaches (electrophoresis, electroacoustics, impedance/dielectric spectroscopy, spectral induced polarization), representative observations (pH and ionic-strength dependence of zeta potential and conductivity; frequency-dependent permittivity), mechanistic models (Stern–Gouy–Chapman, Maxwell–Wagner, Warburg-type polarization), and practical implications for geotechnical engineering, soil remediation, ceramic processing, and sensor applications.

1. Introduction:

Kaolinite (ideally Al₂Si₂O₅(OH)₄) is one of the world's most abundant clay minerals and is widely used in ceramics, paper coatings, paints, and geotechnical materials [1], [2]. Although kaolinite is often described as a "non-expanding" clay with relatively low cation-exchange capacity (CEC) compared with smectites, its electrical properties are nevertheless important for colloidal stability, electroosmosis, dielectric behaviour of soils and composites, and electrokinetic remediation. Understanding the electrical behaviour of kaolinite requires linking atomic-scale structure (tetrahedral–octahedral layers, edge and basal surface chemistry) to macroscopic measures such as zeta potential, complex permittivity, and bulk conductivity.

2. Structure and Surface Chemistry of Kaolinite

Kaolinite is a 1:1 layered silicate composed of alternating tetrahedral silica sheets and octahedral alumina sheets [1]. Layers are hydrogen-bonded and show limited interlayer expansion. Kaolinite surfaces can be classified into two broad types:

• Basal (faces): predominately siloxane (Si-O) and aluminol/gibbsite-like (Al-OH) functionalities depending on which sheet is exposed. The basal surfaces often carry pH-

dependent surface sites; the gibbsite-like (octahedral) face is typically amphoteric and can acquire charge depending on pH.

• **Edges:** broken bonds and exposed oxyhydroxyl groups at particle edges contribute additional pH-dependent surface sites and higher reactivity than basal faces [3], [4].

Isomorphic substitutions and accessory mineral impurities can impart some permanent charge, but for pure kaolinite the dominant charge is pH-dependent (variable charge) arising from protonation—deprotonation of surface hydroxyls. Surface charge distribution is heterogeneous: basal planes may be less reactive than edges, but both contribute to the overall electrochemical behaviour of suspensions and bulk materials [2], [3].

3. Electrical Double Layer and Surface Complexation

When kaolinite is immersed in an electrolyte, an electrical double layer (EDL) forms at the mineral–solution interface [3]. The EDL comprises an inner region of specifically adsorbed ions (Stern layer) and a diffuse layer where counterions partially balance the surface charge. The position in the solution where the shear plane (slipping plane) intersects the EDL determines the measurable zeta potential (ζ) — a key experimental proxy for surface charge and colloidal stability.

Surface complexation (chemical adsorption of H+, OH-, and other ions) governs how surface charge varies with pH and ion identity. Models such as the constant capacitance, diffuse-layer, and triple-layer formulations are commonly used to relate surface site chemistry to measurable electrophysical parameters [5]. These models account for specific adsorption (inner-sphere complexes), outer-sphere adsorption (electrostatic attraction), and the capacitive behaviour of the Stern layer.

4. Zeta Potential and Electrokinetic Phenomena

Zeta potential quantifies the electrostatic potential at the shear plane and strongly influences suspension stability, electroosmotic flow, and electrokinetic transport. For kaolinite, empirical and systematic studies show some characteristic behaviours:

- **pH dependence:** Kaolinite typically exhibits an isoelectric point (IEP) at low pH or shows monotonically decreasing (more negative) ζ with increasing pH, depending on sample purity and specific surface composition. The octahedral (gibbsite-like) face has amphoteric hydroxyl groups that titrate with pH, so ζ often becomes more negative above neutral pH [3], [4], [5].
- **Ionic strength:** Increasing electrolyte concentration compresses the diffuse layer and reduces magnitude of ζ (Debye screening). Monovalent versus divalent cations differ in their

effectiveness at compressing the EDL; divalent cations (Ca2+, Mg2+) are more efficient and may induce charge neutralization or reversal at high concentrations [4], [6].

- **Ion-specific effects:** Specific adsorption of polyvalent ions or organic polyelectrolytes can modify ζ beyond simple electrostatic screening. Anions and cations that form inner-sphere complexes or alter surface protonation equilibria produce distinct ζ shifts [6], [7].
- Particle attributes: Mineral impurities, particle size, morphology, and mixed-layering with other clays (e.g., illite, smectite) can significantly change ζ behaviour [8].

Electrokinetic phenomena relevant to kaolinite include electrophoresis (particle motion in applied electric fields), electroosmosis (fluid flow through porous media), streaming potential/current, and dielectrophoresis. These are practically important for soil dewatering, consolidation, electrokinetic remediation, and processing of kaolin slurries [4], [6].

5. Frequency-dependent Dielectric Response

The complex permittivity ($\varepsilon^* = \varepsilon' - j\varepsilon''$) of kaolinite-bearing materials shows strong frequency dependence, reflecting multiple polarisation mechanisms [7], [9]:

- **1. Electronic and atomic polarisation** (very high frequencies, optical domain) negligible for most geophysical frequencies.
- **2. Orientation (dipolar) polarisation** water molecules confined near surfaces relax at microwave to GHz frequencies; relaxation times shift when water is confined in clay interlayers or at surfaces.
- 3. Interfacial (Maxwell-Wagner) polarisation at low-to-intermediate frequencies (Hz to MHz), conductivity and permittivity contrasts between mineral grains, surface films, and pore water lead to charge accumulation at interfaces; kaolinite exhibits this behaviour strongly when particle boundaries and thin water films dominate the path of ionic conduction.
- **4.** Electrochemical polarisation (Stern-layer processes) very low frequencies (<1 kHz to Hz) are governed by polarization of the Stern layer and slow ion-exchange or surface reaction kinetics; this contributes to the low-frequency dispersion observed in spectral induced polarization (SIP) experiments.

Dielectric spectroscopy of kaolinite suspensions and compacted samples therefore displays multiple relaxation peaks or broad dispersion regions that depend on water content, degree of saturation, pore connectivity, ionic strength, and temperature [7], [9], [10].

6. Electrical Conductivity: Bulk and Surface Contributions

Electrical conduction in kaolinite-bearing media arises from several pathways:

- **Pore-fluid (bulk) conduction:** movement of solvated ions through interconnected pore spaces often the dominant contribution in saturated systems.
- **Surface conduction:** excess counterions in the diffuse layer and Stern layer near mineral surfaces provide an additional conduction pathway that becomes important when pore sizes are small and surface-area-to-volume ratios are high (fine-grained clays).
- **Grain-boundary conduction:** through thin water films, adsorbed ionic species, or conductive mineral coatings/impurities [7], [9].

The relative importance of surface conduction increases as water content decreases, pore connectivity reduces, or when specific adsorbed ion concentrations are high. Temperature raises ionic mobility and increases conductivity; however, changes in water structuring at surfaces may modify temperature dependence relative to bulk electrolyte behaviour [4], [7].

7. Spectral Induced Polarization (SIP) and Kaolinite

SIP — measurement of frequency-dependent complex conductivity — is particularly sensitive to polarization mechanisms in porous media. Kaolinite-rich materials often show distinct SIP signatures characterized by low-frequency dispersion due to electrochemical polarization of the Stern layer and Maxwell—Wagner effects in mixed-phase systems [9], [10]. SIP parameters (e.g., chargeability, relaxation times, Cole—Cole parameters) can be linked to pore geometry, water content, and the abundance of polarizable surfaces.

In practice, SIP has been used to:

- Differentiate clay-rich layers from sand/gravel in geophysical surveys.
- Monitor pore-fluid salinity changes and contaminant migration.
- Infer surface-area-to-volume ratios and specific surface conductivity [10].

Models that couple pore-scale electrochemistry with macroscopic mixing laws (effective medium or Archie-type generalizations) help interpret SIP responses in kaolinite-bearing media.

8. Measurement Techniques and Experimental Considerations

A brief overview of commonly used experimental approaches:

- Electrophoresis / Microelectrophoresis (Zeta sizers): measures particle mobility in dilute suspensions to derive ζ; sensitive to sample prep, concentration, and presence of aggregates [3], [4].
- **Electroacoustic methods:** useful for concentrated suspensions; measure electric signals generated by acoustic waves (colloid vibration current) and infer ζ without dilution artifacts.
- **Dielectric spectroscopy** / **Impedance spectroscopy:** measures complex permittivity and conductivity across wide frequency ranges (mHz to GHz) to resolve relaxation processes [7], [9].

- **Spectral induced polarization (SIP):** low-frequency complex conductivity measurement (typically 1 mHz–1 kHz or up to MHz) adapted to soils and rocks [10].
- Streaming potential/current and electroosmotic measurements: measure coupled hydraulic—electrical responses in porous samples.

Experimental pitfalls include surface contamination, presence of organics or iron oxides, particle aggregation, and misinterpretation of zeta potential when slip-plane position changes. Standardizing ionic composition, pH, and sample history is crucial for reproducible measurements [4], [6].

9. Models and Theoretical Frameworks

Key theoretical tools used to interpret kaolinite electrical properties include:

- **DLVO theory:** combination of van der Waals and electrostatic double-layer interactions used to predict colloidal stability; requires knowledge of surface potential/charge and ionic conditions [3].
- Surface complexation models (SCM): constant-capacitance, diffuse-layer, and triple-layer models parameterize surface protonation and specific adsorption equilibria [5].
- **Stern–Gouy–Chapman approaches:** partition the EDL into a compact Stern layer and a diffuse Gouy–Chapman layer and connect surface chemistry to ζ [3].
- Maxwell-Wagner mixing models and effective medium theories: describe interfacial polarization in heterogeneous mixtures and bulk permittivity/conductivity responses [9], [10].
- Cole-Cole and Debye-type relaxations: empirical/phenomenological fits for observed dispersions in dielectric and SIP spectra.

Combining SCM with transport models (continuum pore-scale models) enables prediction of electrokinetic phenomena and SIP responses under varying boundary conditions.

10. Applications and Practical Implications

- Geotechnical engineering. Electrical properties (zeta potential, electroosmotic mobility) influence consolidation, permeability, and the rheology of kaolinite-rich slurries. Electrokinetic consolidation and electroosmotic dewatering exploit these properties to improve foundation soils and slurry handling [4].
- Environmental remediation. Electrokinetic remediation relies on electroosmosis and electromigration; kaolinite's pH-dependent ζ and low CEC affect contaminant mobility and pH fronts during treatment [6].

- Materials and ceramics. Dielectric behaviour of kaolinite-based ceramics influences insulating properties, microwave sintering, and composite design. Controlling impurities and water content is critical to achieve target dielectric constants [10].
- **Geophysical surveying and hydrology.** SIP and dielectric surveys exploit kaolinite's dispersive electrical signature to map clay layers, monitor saturation changes, and infer porescale properties [9], [10].
- Sensors and nanocomposites. Modified kaolinite (organically modified, exfoliated) is used in dielectric composites and sensors where tailored permittivity and surface conduction are desirable.

11. Future Directions and Research Needs

Despite decades of study, several areas remain active or underexplored for kaolinite electrical behaviour:

- Quantifying the contributions of basal vs edge surfaces to measured ζ and surface conduction across realistic polydisperse particle assemblages.
- Molecular-scale understanding of confined water dynamics and its effect on dielectric relaxation across frequency and temperature.
- Effects of natural impurities and mixed-layering with other clays on SIP and dielectric signatures in field-representative samples.
- Improved coupling between surface complexation parameters and full poro-electrochemical transport models to simulate electrokinetic remediation and geophysical responses under transient conditions [9], [10].

Conclusions:

Kaolinite's electrical properties arise from interplay between surface-site chemistry, pore-fluid composition, microstructure, and water content. While kaolinite is electrically simpler than high-CEC clays such as smectites, its pH-dependent surface charge, interfacial polarization behaviour, and surface conduction pathways are central to many engineering and geophysical problems. Advances in spectroscopic, electroacoustic, and dielectric measurement techniques — together with improved pore-scale models — continue to refine our understanding of kaolinite's electrochemical behaviour and expand its practical applications.

References:

- 1. Grim, R. E. (1968). Clay mineralogy (2nd ed.). McGraw-Hill.
- 2. Murray, H. H. (2007). Applied clay mineralogy. Elsevier.

- 3. Williams, D. J. A. (1978). Electrophoresis and zeta potential of kaolinite. *Journal of Colloid and Interface Science*, 64(1), 1–11.
- 4. Vane, L. M., et al. (1997). Effect of aqueous phase properties on clay particle zeta potential. *Journal of Colloid and Interface Science*, 191(2), 306–313.
- 5. Alkan, M., et al. (2005). Electrokinetic properties of kaolinite in monovalent electrolytes. *Colloids and Surfaces A*, 266(1–3), 43–50.
- 6. Kumar, N., et al. (2017). Probing the surface charge on the basal planes of kaolinite. Langmuir, 33(XX), XXX–XXX.
- 7. González-Teruel, J. D., et al. (2020). Dielectric spectroscopy and application of mixing models to clays and clayey soils. *Journal of Applied Geophysics*, 175, 103974.
- 8. Liu, L., et al. (2018). Study on the aggregation behavior of kaolinite particles in aqueous systems. *Scientific Reports*, *8*, 12345.
- 9. Leroy, P., & Revil, A. (2009). A mechanistic model for the spectral induced polarization of clay-bearing materials. *Journal of Geophysical Research: Solid Earth, 114*(B7), B07201.
- 10. Yang, X., et al. (2021). Preparation of low-dielectric-constant kaolin clay ceramics. Frontiers in Materials, 8, 692759.

(ISBN: 978-81-994425-3-5)

MATERIALS SCIENCE AND RENEWABLE ENERGY

Swagatam Deva Nath

Department of Physics,

Nanda Nath Saikia College, Titabar, Assam, India

Corresponding author E-mail: swgtmdvnth@gmail.com

Abstract:

The transition to renewable energy technologies hinges on advances in materials science. Materials underpin every aspect of renewable systems—from photovoltaic cells and battery electrodes to catalysts in hydrogen production and structural components in wind turbines. This chapter introduces the foundational principles linking materials science to renewable energy, focusing on how atomic and microstructural features dictate performance, durability, and efficiency in energy devices. Topics include crystal structures, electronic properties, materials selection, and design strategies for solar, wind, hydrogen, and energy storage technologies. Current trends in sustainable materials and circular economy practices are also reviewed.

Keywords: Renewable Energy, Materials Science, Energy Storage, Sustainable Materials, Circular Economy.

1. Introduction:

Materials science plays a central role in enabling the global shift toward sustainable and renewable energy systems. The field seeks to understand the relationships between a material's composition, structure, processing, and properties to optimize performance for specific applications. As societies move away from fossil fuels, materials challenges arise across all major renewable technologies—ranging from developing efficient photovoltaic absorbers to designing corrosion-resistant turbine blades and high-capacity battery electrodes [1].

Renewable energy sources such as solar, wind, hydro, geothermal, and biomass depend on the efficient conversion and storage of energy. Achieving this efficiency requires materials with tailored electronic, thermal, optical, and mechanical characteristics. The synergy between materials innovation and renewable energy technologies represents a cornerstone of 21st-century engineering progress.

2. Fundamentals of Materials Science for Energy Applications:

2.1 Structure-Property Relationships

At the heart of materials science is the principle that structure determines properties. Structure exists at multiple scales—from atomic arrangements (crystal structures) to microstructures (grains, defects, interfaces) and macroscopic morphologies (composites, coatings). For renewable energy devices, properties such as bandgap energy, electrical conductivity, thermal stability, and catalytic activity are intimately tied to structure [2].

For instance, crystalline silicon (Si) has a diamond cubic structure that supports efficient charge transport, making it the dominant photovoltaic material. Meanwhile, perovskite materials (ABX₃-type structures) allow tunability of the electronic bandgap via compositional engineering, enabling high power conversion efficiencies [3].

2.2 Electronic and Optical Properties

Electronic structure determines how a material interacts with light and electricity. Semiconductors are particularly vital in renewable applications—where their bandgap defines light absorption and charge generation. The optical absorption coefficient and exciton diffusion length dictate performance in photovoltaic devices, while ionic and electronic conductivities are key in batteries and fuel cells [4].

2.3 Thermal and Mechanical Properties

Thermal management is crucial for maintaining the performance of solar cells and battery systems. Materials with low thermal expansion coefficients and high thermal conductivities can prevent degradation. Mechanical robustness, particularly fatigue and corrosion resistance, is equally essential for wind turbine blades, geothermal pipelines, and concentrated solar power (CSP) mirrors [5].

3. Materials for Solar Energy Conversion:

3.1 Photovoltaic Materials

Photovoltaic (PV) technology converts sunlight directly into electricity through the photovoltaic effect. Silicon-based materials dominate the market, with crystalline silicon (c-Si) cells achieving efficiencies over 26% in laboratory conditions [6]. However, thin-film technologies—such as cadmium telluride (CdTe) and copper indium gallium selenide (CIGS)—offer lower production costs and flexible form factors.

Emerging perovskite solar cells have revolutionized the field, achieving rapid efficiency gains from 3.8% in 2009 to over 26% in 2024 [7]. These materials exhibit tunable bandgaps, high absorption coefficients, and solution processability, making them strong candidates for next-generation solar modules.

3.2 Photocatalytic and Solar Thermal Materials

In addition to PV, solar energy can drive photocatalytic water splitting and thermochemical processes. Titanium dioxide (TiO₂), for example, serves as a photocatalyst under UV light, though efforts are underway to extend activity into the visible range through doping or

nanostructuring [8]. In solar thermal systems, selective absorber coatings—such as cermet-based composites—maximize solar absorption while minimizing thermal re-radiation losses [9].

4. Materials for Wind Energy Systems:

Wind turbines rely heavily on materials with high strength-to-weight ratios and excellent fatigue resistance. The rotor blades, typically made of glass- or carbon-fiber-reinforced polymers, must withstand cyclic loading and environmental exposure. Research into thermoplastic composites and recyclable resins addresses the challenge of end-of-life turbine blade waste [10].

Structural components such as towers and gearboxes employ steels with tailored alloy compositions and microstructures to balance strength, toughness, and corrosion resistance. Coatings and surface treatments further enhance durability against marine and desert conditions [11].

5. Hydrogen and Fuel Cell Materials:

Hydrogen energy systems comprise production, storage, and utilization technologies—all dependent on advanced materials.

5.1 Electrolysis and Catalysts

Electrocatalysts for water splitting must exhibit high activity and stability. Precious metals like platinum (Pt) and iridium oxide (IrO₂) remain benchmarks, but research focuses on earth-abundant alternatives such as transition metal phosphides (Ni₂P, CoP) and nitrides (MoN) [12].

5.2 Hydrogen Storage Materials

Safe and efficient hydrogen storage remains a critical barrier. Metal hydrides (e.g., MgH₂, LaNi₅H₆) and porous materials such as metal–organic frameworks (MOFs) offer promising pathways for reversible hydrogen uptake under moderate conditions [13].

5.3 Fuel Cell Components

Proton exchange membrane fuel cells (PEMFCs) rely on perfluorosulfonic acid membranes (e.g., Nafion®), but research into cheaper and more durable alternatives—such as polybenzimidazole (PBI) composites—is ongoing. The development of corrosion-resistant bipolar plates and optimized catalyst layers is central to improving fuel cell lifetime and cost-effectiveness [14].

6. Materials for Energy Storage Systems:

6.1 Battery Materials

Energy storage is pivotal for stabilizing renewable power generation. Lithium-ion batteries (LIBs) dominate current markets, with cathode materials like LiCoO₂, LiFePO₄, and NMC (LiNiMnCoO₂) optimized for specific performance metrics [15]. However, resource scarcity and safety concerns drive interest in sodium-ion, solid-state, and flow battery technologies [16].

Solid electrolytes—such as sulfide-based (Li₁₀GeP₂S₁₂) and oxide-based (LLZO: Li₇La₃Zr₂O₁₂) materials—promise improved safety and energy density through nonflammable, stable interfaces [17].

6.2 Supercapacitors and Emerging Storage Technologies

Supercapacitors bridge the gap between batteries and conventional capacitors, offering high power densities and rapid charge—discharge cycles. Carbon-based materials, metal oxides, and conducting polymers form the core of supercapacitor electrodes. Recent advances in graphene and MXene-based electrodes show exceptional performance due to their high surface areas and tunable conductivity [18].

7. Materials for Bioenergy and Thermoelectrics:

Bioenergy systems leverage catalysts and membranes for biomass conversion and biogas purification. Enzyme immobilization on nanostructured supports enhances catalytic efficiency. Similarly, thermoelectric materials—such as bismuth telluride (Bi₂Te₃) and skutterudites—convert waste heat into electricity, improving overall energy efficiency in hybrid systems [19].

8. Sustainability and Lifecycle Considerations:

8.1 Critical Materials and Resource Scarcity

Many renewable technologies rely on rare or geopolitically sensitive elements (e.g., indium, cobalt, rare earths). Sustainable materials strategies emphasize recycling, substitution, and reduced critical element usage [20]. Circular economy approaches integrate design-for-recycling principles into materials development.

8.2 Environmental Impact and Lifecycle Analysis

Lifecycle assessment (LCA) helps quantify the environmental footprint of materials, from extraction to disposal. Green synthesis methods, low-energy processing, and biodegradable components are increasingly prioritized in research and industry [21].

9. Computational and Data-Driven Materials Discovery:

High-throughput computational screening and machine learning accelerate the discovery of new energy materials. Density functional theory (DFT) simulations predict bandgaps, adsorption energies, and defect tolerances, guiding experimental synthesis. Materials databases—such as the Materials Project—enable data-driven design of solar absorbers, catalysts, and electrodes [22].

10. Future Directions and Challenges:

The next decade of renewable energy materials research will likely focus on:

- Scalable synthesis of high-performance, low-cost materials.
- **Integration** of multifunctional materials for hybrid energy systems.
- Circular materials design to minimize waste and maximize recyclability.

- AI-driven discovery to shorten development cycles.
- Interdisciplinary collaboration bridging physics, chemistry, and engineering.

Conclusion:

Materials science forms the foundation upon which renewable energy technologies are built. From atomic-scale design to systems-level integration, advances in materials enable the efficient capture, conversion, storage, and utilization of clean energy. As global energy demand continues to rise, the development of sustainable, high-performance materials will remain pivotal in achieving a carbon-neutral future.

References:

- 1. Callister, W. D., & Rethwisch, D. G. (2020). *Materials science and engineering: An introduction* (10th ed.). Wiley.
- 2. Ashby, M. F., & Jones, D. R. H. (2012). Engineering materials 1: An introduction to properties, applications, and design (4th ed.). Elsevier.
- 3. Green, M. A., et al. (2022). Solar cell efficiency tables (version 60). *Progress in Photovoltaics: Research and Applications*, 30(1), 3–12.
- 4. Sze, S. M., & Ng, K. K. (2006). *Physics of semiconductor devices* (3rd ed.). Wiley.
- 5. Shackelford, J. F. (2015). *Introduction to materials science for engineers* (8th ed.). Pearson.
- 6. Fraunhofer ISE. (2024). *Photovoltaics report*. Fraunhofer Institute for Solar Energy Systems.
- 7. National Renewable Energy Laboratory (NREL). (2024). *Best research-cell efficiency chart*. National Renewable Energy Laboratory.
- 8. Chen, X., & Mao, S. S. (2007). Titanium dioxide nanomaterials: Synthesis, properties, modifications, and applications. *Chemical Reviews*, 107(7), 2891–2959.
- 9. Kennedy, C. E. (2002). *Review of mid- to high-temperature solar selective absorber materials* (NREL/TP-520-31267). National Renewable Energy Laboratory.
- 10. Brøndsted, P., & Nijssen, R. P. L. (2013). *Advances in wind turbine blade design and materials*. Woodhead Publishing.
- 11. Zhang, J., & Zhao, H. (2020). Corrosion protection of offshore wind turbine materials. *Corrosion Reviews*, 38(5), 345–361.
- 12. Roger, I., Shipman, M. A., & Symes, M. D. (2017). Earth-abundant catalysts for electrochemical and photoelectrochemical water splitting. *Nature Reviews Chemistry*, *1*(1), 0003.

- 13. Zhou, H., & Wang, Q. (2019). Hydrogen storage in metal–organic frameworks. *Chemical Society Reviews*, 48(19), 5437–5481.
- 14. Steele, B. C. H., & Heinzel, A. (2001). Materials for fuel-cell technologies. *Nature*, 414, 345–352.
- 15. Goodenough, J. B., & Park, K.-S. (2013). The Li-ion rechargeable battery: A perspective. *Journal of the American Chemical Society*, 135(4), 1167–1176.
- 16. Slater, M. D., Kim, D., Lee, E., & Johnson, C. S. (2013). Sodium-ion batteries. *Advanced Functional Materials*, 23(8), 947–958.
- 17. Manthiram, A. (2020). A reflection on lithium-ion battery cathode chemistry. *Nature Communications*, 11, 1550.
- 18. Simon, P., & Gogotsi, Y. (2020). Materials for electrochemical capacitors. *Nature Materials*, 19(11), 1151–1163.
- 19. Rowe, D. M. (Ed.). (2018). Thermoelectrics handbook: Macro to nano. CRC Press.
- 20. Graedel, T. E., & Reck, B. K. (2016). Six years of criticality assessments: What have we learned so far? *Journal of Industrial Ecology*, 20(4), 692–699.
- 21. Guinée, J. B. (Ed.). (2002). *Handbook on life cycle assessment: Operational guide to the ISO standards*. Springer.
- 22. Jain, A., *et al.* (2013). The Materials Project: A materials genome approach to accelerating materials innovation. *APL Materials*, *I*(1), 011002.

SYNTHESIS AND PROPERTIES OF DERIVATIVES OF NOVEL THIOSEMICARBAZONES INCLUDING 3-CHLOROPHENYL THIAZOLE HETEROCYCLES

Kisan K. Gadge

Konkan Gyanpeeth's, Karjat College of Arts, Science and Commerce,

Karjat, Raigad-410201, Maharashtra, India

Corresponding author E-mail: <u>kisan99gadge@gmail.com</u>

Introduction:

Thiazole

Thioamides are the building blocks in the Hantzsch thiazole¹ and amidines² synthesis. The chemistry of thiazole containing heterocyclic compounds continues to draw the attention of synthetic organic chemists due to their varied biological activities,³ such as antibacterial, antitubercular, anti-cancer, antifungal and anti-inflammatory activities. Sakagami and co-workers reported the isolation of six secondary metabolites, designed cyst thiazoles A-F, 1 (Figure 1) as a series of new antibiotics from the myxobacterium culture broth of *Cystobacter fuscus*.⁴ These bis-thiazoles has demonstrated potent antifungal activity against the phytopathogenic fungus *Phytopathora capsici* and has shown activity against a broad range of additional fungi with no effect on bacterial growth. Nicolaou K. C. and co-workers⁵ have reported chemical biology of epothiolones⁶ 2 (Figure 1), thiazole containing an antitumor agent. Thiazole nucleus is also important in organic synthesis as it acts as a formyl group equivalent. ⁷

Figure 1

A wide range of substituted thiazole derivatives, 8-12 can be obtained in the reactions of thioamides derived from aliphatic, aromatic, and heterocyclic acids with appropriately functionalized carbonyl compounds. Kulkarni K. S. and co-workers 13 have synthesized substituted thiazolyl thiocarbanilides (3-7), (Figure 2) and reported for antitubercular activity. 2-substituted-anilino/phenyl/benzyl-5-substituted-4-phenylamide-(3-(2-chlorophenyl)-5-methylisoxazolyl)thiazoles and reported them as potential antitubercular and antimicrobial

agents¹⁴. Ohkubo M. and co-workers¹⁵ have reported synthesis and anti-anoxic activity of ethyl 4-(3/4-nitrophenyl)-2-phenyl-5-thiazolecarboxylate derivatives.

Figure 2

Bell, F.W. and co-workers¹⁶ have reported synthesis and basic structure activity relationship studies of phenethylthiazolethiourea compounds 8. (Figure 3). The synthesized compounds were screened for HIV-1 reverse transcriptase inhibitors activity.

Figure 3

Thiosemicarbazone

Biological properties of thiosemicarbazone derivatives have been studied since 1946¹⁷, when their activity against Mycobacterium tuberculosis was reported. Since then, this and other biological properties of thiosemicarbazone derivatives such as antibacterial¹⁸, antitumoral¹⁹, antiprotozoal²⁰ and cytotoxic activity²¹ have been described. In 1950, Hamre *et al.*²² found that thiosemicarbazone derivatives from several benzaldehydes were active against neurovaccinial infection in mice when given orally.

Iron Chelators of the Dipyridylketone Thiosemicarbazone Anticancer Activity J. Med. Chem. **2009**, 52, 407–415

Present Work

In view of these observations and an ongoing programme on the synthesis of thiazole containing heterocyclic compounds, it was thought to synthesize thiazoles, thiosemicarbzone derivatives (Scheme 1).

In the present work Ethyl 2-(3-chorophenyl)-4-methylthiazole-5-carboxylate, 12 was synthesized by cyclo-condensation of 3-chlorothiobenzamide, 10 with Ethyl-2-choro-3-oxobutanoate 11. Ester 12 was further reduced by using lithium aluminum hydride in dry diethyl ether to corresponding alcohol 13. The alcohol 13 was selectively oxidized to aldehyde 14. Aldehyde 14 was subjected to condensation reaction with semicarbazide furnished Schiff's base. Then

Schiff's base on S-alkylation reaction with alkyl halide gave 1((2-(3-chlorophenyl)-4-methylthiazol-5-yl)methyleneamino)-2-propylisothiourea

Scheme 1

Result and Discussion:

Scheme 2

The IR spectrum of ester 12 showed absorption peak at 1728 cm⁻¹ indicating the presence of ester carbonyl. The ¹H NMR of 12 showed the triplet at δ 1.40 for –CH₃ protons and quartet at δ 4.38 for –CH₂ confirmed the ester functions, a singlet at δ 2.80 integrated for three hydrogen corresponds for thiazole –CH₃ protons and the four aromatic protons are resonated at δ 7.39 (m, 2H); 7.82 (d, 1H); 7.98 (s, 1H), the LCMS spectrum of 12 showed the m/z peak at 281.72 (M+H)⁺, which confirms its structure.

The reduction of ester 12 to (4-methyl-2-(3-chlorophenyl)thiazole-5-yl)methanol 13 was achieved by using lithium aluminium hydride in dry diethyl ether in 85 % yield. The structure of alcohol was confirmed by the spectral data. IR spectrum showed a strong absorption at 3290 cm⁻¹ signifying the presence of the hydroxyl group with absence of absorption in the C=O region. The 1 H NMR spectrum of 13 revealed absence of quartet and the triplet corresponding to carboethoxy group as well as appearance of a singlet at δ 4.82 integrating for two protons ascribed to the -

CH₂OH proton. Apart from this, the spectrum also revealed a peak corresponding to the three methyl protons at δ 2.42 and the aromatic protons appeared at δ 7.26 to 7.80 integrated for four aromatic protons. The mass spectrum of 13 showed the m/z peak at 239.5 (M+H)⁺ which further confirms its structure.

Literature revealed the selective oxidation of the alcohol function into aldehyde²³ in (4-methyl-2-phenylthiazole-5-yl)methanol was achieved using transition metal oxidising agents. Accordingly the alcohol was selectively oxidized to aldehyde in 65 % using MnO₂. It was observed that when the alcohol 13 was treated with IBX in DMSO at 0 °C to room temperature furnished aldehyde 14 in 90 % yield within 20 minutes of reaction time (Scheme 3). The formation of 4-methyl-2-(3-chlorophenyl)thiazole-5-carbaldehyde 14 was confirmed by its spectral studies.

Scheme 3

The IR spectrum of 14 displayed the absorption bands at 2847, 2735 cm⁻¹ and 1690 cm⁻¹ due to stretching frequency of aldehyde C-H and C=O functional groups. ¹H NMR spectrum of 14 showed the singlet at δ 2.79 integrating for three protons are assigned for methyl group, four aromatic protons are appeared at δ 7.43 (m, 2H); 7.83 (d, 1H); 8.02 (s, 1H). The aldehyde proton resonated at δ 10.11. The ¹³C NMR of aldehyde showed one signal at δ 18.8 corresponds to methyl group of thiazole ring. The phenyl and thiazole ring carbons are appeared at δ 125.24, 127.0, 130.0 131.0, 133, 134, 135.0, 162.0 and 171.0, while a peak at δ 182.0 was attributed to the C=O of aldehyde group. Further the structure was confirmed by HRMS spectrum which showed the m/z peak at 270.0360 (M+MeOH + H)⁺.

Scheme 4

The thiosemicarbazide was subjected to the condensation reaction with 4-methyl-2-(3-chlorophenyl)thiazole-5-carbaldehyde 14 using glacial acetic acid as catalyst in dry methanol afforded the thiosemicarbazone in 74 to 84 % yield. The thiosemicarbazone on nucleophilic substitution reaction with propyl bromide gave 1((2-(3-chlorophenyl)-4-methylthiazol-5-yl)methyleneamino)-2-propylisothiourea.

The IR spectrum of compound 16 showed absence of characteristic absorption peaks at 2550 cm⁻¹ (S-H) indicated the formation of S-alkylation, which was further confirmed by its ¹H NMR data. The ¹H NMR spectrum of 16 displayed a peaks at δ 1.06 (t, 3H); 1.83 (m, 2H); 3.04 (t, 2H) confirms the presence of S-propyl group. The singlet at δ 2.56 integrated for three protons corresponds to three protons of methyl group. The aromatic protons are resonated at δ 7.39 to 8.51. Two -NH protons are showed bs at δ 5.5. The ¹³C NMR of 16 Showed peaks at 13.4, 15.8, 22.9, 32.0, 124.5, 126.5, 130.2, 135.0, 141.1, 145.4, 155.1, 156.6, 162.1, 163.2, 165.7, 167.8, 174.0. The structure was further confirmed by LCMS spectrum which showed (M + H)⁺ at 352.95 and 353.0 corresponds to 80% and 20 % E and Z isomers respectively.

Experimental

Ethyl-2-(3-chlorophenyl)-4-methylthiazole-5-carboxylate

Mixture of 2-choro-3-oxoethylbutanoate 13 (6.0 g; 0.037 mol) and 3-chlorothiobenzamide, 12 (5.0 g; 0.037 mol) in ethanol (50 mL) was refluxed for 8 hours. After completion of the reaction (TLC), half of the solvent was distilled off and reaction mass cooled to room temperature. The product was filtered, washed with water and recrystallised from ethanol, yield 8.0 g (90 %).

MF: C₁₃H₁₂NO₂SCl

IR: 1728 cm⁻¹

1H NMR: 1.40 (t, 3H); 2.80(s, 3H); 4.38 (q, 2H); 7.39 (m, 2H); 7.82 (d, 1H);

7.98 (s, 1H)

LCMS: 281.76 (M+H)+

(2-(3-chlorophenyl)-4-methylthiazol-5-yl)methanol

To a ice cold solution lithium aluminium hydride (2.3 g; 0.060 mol) in 50 mL dry diethyl ether, ethyl 2-(3-chorophenyl)-4-methylthiazole-5-carboxylate, 14 (7.5 g; 0.030 mol) was added dropwise over a period of 30 minutes and the mixture was further stirred for 1 hour at 0 °C. After completion of the reaction (TLC), the reaction mixture was quenched by saturated solution of sodium sulphate. The reaction mixture was filtered on sintered funnel. The aqueous was extracted with diethyl ether (2 x 30 mL), the combined organic layer was washed with water, then brine and dried over sodium sulphate. Solvent was removed by distillation furnished (2-(3-chlophenyl)-4-methylthiazol-5-yl)methanol, 5.40 g (87 %).

MF:C₁₁ H₁₀ NOSCl

IR: 3290 cm⁻¹

1H NMR; 2.42 (s, 3H); 4.80 (s, 2H); 7.39 (m, 2H); 7.82 (d, 1H); 7.98 (s, 1H).

LCMS; 239.72 (M+H)⁺

(2-(3-chlorophenyl)-4-methylthiazol-5-yl) carbaldehyde

To a solution of (2-(3-chlorophenyl)-4-methylthiazol-5-yl)methanol, (5.0g, 0.020 mol) in DMSO 30 mL, IBX (6.3g, 0.023 mol) was added at 0 °C and the reaction mixture was stirred at 0 °C to room temperature. The progress of reaction was monitored on TLC. After completion of the reaction (20 minutes), water 90 mL was added in reaction mixture and extracted with diethyl ether (3 x 40 mL). The organic layer was washed with water, brine and dried over sodium sulphate. The solvent was distilled to afford white solid, 4.96g in 94% yield.

MF: C₁₂H₁₁N₄S₂Cl

IR; 2735, 2847, 1690 cm⁻¹

¹H NMR: 2.79 (s, 3H); 7.43 (m, 2H); 7.83 (d, 1H, J=8Hz); 8.02 (s, 1H); 10.11 (s 1H)

¹³CNMR: (CDCl3): 18.8, 125.24, 127.0, 130.0, 131.0,133.0,134.0, 135.0, 162.0,171.0,182.0

MASS; 237.71 (M+H)⁺

1-((2-(3-chlorophenyl)-4-methylthiazol-5-yl)methylene) thiosemicarbazide

To a solution of with (2-(3-chlorophenyl)-4-methylthiazol-5-yl) carbaldehyde

17 (1.0 g; 0.005) thiasemicarbazide (30 mL), methanol (0.75 g, 0.006 mol) was added. The reaction mixture was allowed to stand & warmed on waterbath, cooled in ice water. the reaction was monitored by TLC, after completion of reaction, the product was filtered washed with cold water & recrystllised from methanol. The yield as (1.20g, 92%)

MF: C₁₂H₁₁N₄S₂Cl

IR;

¹H NMR:

LCMS: 310 (M+H)+

1-((2-(3-chlorophenyl)-4-methylthiazol-5-yl)methyleneamino)-2propylisothiourea

To a solution 1-((2-(chlorophenyl)-4-methylthiazol-5-yl)methylene)thiosemicarbazide, Schiff's base (0.170g; 0.000584 mol) in dry acetone (20 mL), propyl bromide (0.080g; 0.000657 mol) was added and the reaction mixture was refluxed for 2-3 hours (TLC). After completion of reaction mixture cooled in ice water, product crystalised as white solid. The yield as 0.150 g (77%).

MF: C₁₅H₁₇N₄S₂Cl

IR: 3392, 3093, 1593, 1516 cm⁻¹

NMR: 1.06 (t, 3H); 1.83 (m, 2H); 2.56 (s, 2H); 3.04 (t, 2H); 5.51 (s,1H); 5.68 (s, 1H); 7.39 (m, 2H); 7.80 (d, 1H); 7.95 (d, 1H); 8.51 (s, 1H).

LCMS: 352.91 (M+H)+

References:

- 1. (a) Hurd, R. N., & Delamater, G. T. (1961). Chemical Reviews, 61(1), 45.
 - (b) Takahata, H., & Yamazaki, T. (1988). *Heterocycles*, 27, 1953.
 - (c) Brown, K., Cater, D. P., Cavalla, J. F., Newberry, R. A., & Wilson, R. B. (1974). *Journal of Medicinal Chemistry*, 17, 1177.
 - (d) Srivastava, P. C., Pickering, M. V., Allen, L. B., Streeter, D. G., Campbell, M. T., Witkowski, J. T., Sidwell, R. W., & Robins, R. K. (1977). *Journal of Medicinal Chemistry*, 20,256.
 - (e) Jagodzinski, T. S. (2003). Chemical Reviews, 103, 197.
- 2. Wagner, G., Voigt, B., & Vieweg, H. (1984). Pharmazie, 39, 226.
- (a) Patt, W. C., Hamilton, H. W., Teller, M. D., Ryan, M. J., Taylor, D. G., Connolly, C. J., Doherty, A. M., Klutchko, S. R., Sircar, I., Steinbaugh, B. A., Batley, B. L., Painchaud, C. A., Rapundalo, S. T., Michniewicz, B. M., & Olson, S. C. (1992). *Journal of Medicinal Chemistry*, 35, 2562.
 - (b) Haviv, F., Ratajczyk, J. D., DeNet, R. W., Kerdesky, F. A., Waltwers, R. L., Schmidt, S. P., Holmes, J. H., Young, P. R., & Carter, G. W. (1988). *Journal of Medicinal Chemistry*, 31, 1719.
 - (c) Garrido, D. M., Corbett, D. F., Dowrnik, K. A., Goetz, A. S., Littleton, T. R., McKeown, S. C., Mills, W. Y., Smalley, T. L., Briscoe, C. P., & Peat, A. J. (2006). *Bioorganic & Medicinal Chemistry Letters*, 16, 1840.
 - (d) Tsuji, K., & Ishikawa, H. (1994). Bioorganic & Medicinal Chemistry Letters, 4, 1601.
 - (e) Chemical Abstracts, 54, 22576 (1962).
- 4. (a) Ojika, M., Suzuki, Y., Tsukamoto, A., Sakagami, Y., Fudou, R., Yoshimura, T., & Yamanaka, S. (1998). *Journal of Antibiotics*, 51, 275.
 - (b) Suzuki, Y., Ojika, M., Sakagami, Y., Fudou, R., & Yamanaka, S. (1998). *Tetrahedron*, 54, 11399.
- 5. Nicolaou, K. C., Roschanger, F., & Vourloumis, D. (1998). *Angewandte Chemie International Edition*, 37, 2014.
- 6. (a) Höfle, G., Bedorf, N., Gerth, K., & Reichenbach, H. (1993). *DE-B 4211055. Chemical Abstracts*, 120, 52841.

- (b) Höfle, G., Bedorf, N., Steinmetz, H., Schomburg, D., Gerth, K., & Reichenbach, H. (1996). *Angewandte Chemie, 108*, 1671; *Angewandte Chemie International Edition in English, 35*, 1567.
- (c) Schinzer, D. (1997). European Chemical Communications, 7.
- (d) Borman, S. (1996). Chemical & Engineering News, 74, 24.
- 7. Dondoni, A., & Marra, A. (2004). Chemical Reviews, 104, 2557.
- 8. (a) Holzapfel, C. W., & Pettit, G. R. (1985). Journal of Organic Chemistry, 50, 2323.
 - (b) Schmidt, U., Utz, R., Lieberknecht, A., Grieser, A., Potzolli, B., Bahr, J., Wagner, K., & Fischer, P. (1987). *Synthesis*, 233.
- 9. (a) Bredenkamp, W. P., Holzapfel, C. W., Snyman, R. M., & van Zyl, W. J. (1992). Synthetic Communications, 22, 3029.
 - (b) Aguilar, E., & Meyers, A. I. (1994). Tetrahedron Letters, 35, 2473.
- 10. (a) Du, J., Qu, F., Lee, D., Newton, M. G., & Chu, C. K. (1995). *Tetrahedron Letters*, 36, 8167.
 - (b) Ohkuro, M., Kuno, A., Sakai, H., & Takasugi, H. (1995). *Chemical & Pharmaceutical Bulletin*, 43, 947.
 - (c) Umemura, K., Tate, T., Yamamura, M., Yoshimura, J., Yonezawa, Y., & Shin, C. (1995). *Synthesis*, 1423.
- 11. (a) Kelly, C. R., Gebhard, I., & Wicnienski, N. (1986). *Journal of Organic Chemistry*, 51, 4590.
 - (b) Williams, D. R., & Brooks, D. A. (1996). Tetrahedron Letters, 37, 983.
- 12. (a) Sakai, T. T., & Krishna, N. R. (1999). Bioorganic & Medicinal Chemistry, 7, 1559.
 - (b) Carter, J. S., Rogier, D. J., Graneto, M. J., Seibert, K., Koboldt, C. M., Zhang, Y., Talley, J. J. (1999). *Bioorganic & Medicinal Chemistry Letters*, *9*, 1167.
 - (c) Walczynski, K., Timmerman, H., Zuiderveld, O. P., Zhang, M. Q., & Glinka, R. (1999). Farmaco, 54, 533.
 - (d) Belokon, Y., Kovalenko, S. N., Silin, A. V., & Nikitchenko, V. M. (1997). *Chemistry of Heterocyclic Compounds (English Translation)*, 1167.
 - (e) Mathvink, R. J., Tolman, J. S., Chitty, D., Candelore, M. R., Cascieri, M. A., Colwell, L. F., Deng, L., Feeney, W. P., Forrest, M. J., Hom, G. J., MacIntyre, D. E., Tota, L., Wyvratt, M. J., Fisher, M. H., & Weber, A. E. (2000). *Bioorganic & Medicinal Chemistry Letters*, 10, 1971.
- 13. Kulkarni, B. S., Fernandez, B. S., Patel, M. R., Bellare, R. A., & Deliwala, C. V. (1969). Journal of Pharmaceutical Sciences, 58, 852.

- 14. Manian, A. K., Khadse, B. G., & Sengupta, S. R. (1994). *Indian Drugs*, 31, 442.
- 15. Mitsuru, O., Atsushi, K., Hiroyoshi, S., & Hisashi, T. (1995). *Chemical & Pharmaceutical Bulletin*, 43, 947.
- Bell, F. W., Cantrell, A. S., Hoberg, M., Jaskunas, S. R., Johansson, N. G., Jordon, C. L., Kinnick, M. D., Lind, P., Morin, J. M. Jr., Noreen, R., Oberg, B., Palkowitz, J. A., Parrish, C. A., Pranc, P., Sahlberg, C., Ternansky, R. J., Vasileff, R. T., Vrang, L., West, S. J., Zhang, H., & Zhou, X. X. (1995). *Journal of Medicinal Chemistry*, 38, 4929.
- 17. Domagk, G., Behnisch, R., Mietzsch, F., & Schmidt, H. (1946). *Naturwissenschaften*, 10, 315.
- 18. Kasuga, N. C., Sekino, K., Ishikawa, M., Honda, A., Yokoyama, M., Nakano, S., Shimada, N., Koumo, C., & Nomiya, K. (2003). *Journal of Inorganic Biochemistry*, 96, 298–310.
- 19. Feun, L., Modiano, M., Lee, K., Mao, J., Marini, A., Savaraj, N., Plezia, P., Almassian, B., Colacino, E., Fischer, J., & MacDonald, S. (2002). *Cancer Chemotherapy and Pharmacology*, 50, 223–229.
- 20. Bharti, N., Husain, K., González Garza, M. T., Cruz-Vega, D. E. C., Castro-Garza, J., Mata-Cardenas, B. D., Naqvi, F., & Azam, A. (2002). *Bioorganic & Medicinal Chemistry Letters*, 12, 3475–3478.
- 21. Karah, N. (2002). European Journal of Medicinal Chemistry, 37, 909–918.
- 22. Hamre, D., Bernstein, J., & Donovick, R. (1950). Proceedings of the Society for Experimental Biology and Medicine, 73, 275–278.
- 23. Csavassy, G., & Gyorfi, Z. A. (1974). Liebigs Annalen der Chemie, 1195.

GREEN SYNTHESIS OF 2D MATERIALS USING BIO-INSPIRED CHEMICAL PATHWAYS

Simerpreet

Dashmesh Khalsa College, Zirakpur, Punjab-140603

Corresponding author E-mail: drsimerpreetdkc@gmail.com

Abstract:

The synthesis of two-dimensional (2D) materials such as graphene, transition metal dichalcogenides (TMDs), and MXenes has traditionally relied on energy-intensive and chemically hazardous methods, posing significant environmental and scalability challenges. This study explores a bio-inspired approach to the green synthesis of 2D materials, drawing on principles from natural redox and self-assembly processes. Utilizing plant-derived polyphenols, amino acids, and microbial metabolites as reducing and stabilizing agents, the work demonstrates an environmentally benign route to exfoliate and functionalize 2D materials under ambient conditions. Spectroscopic and microscopic characterizations confirm the successful synthesis of few-layer structures with tunable surface chemistries, high crystallinity, and enhanced dispersibility in aqueous media. The mechanism is attributed to the synergistic effects of biomolecular electron donation, π - π interactions, and hydrogen bonding that drive layer separation and defect passivation. Preliminary electrochemical and photocatalytic tests reveal comparable or superior performance to conventionally produced analogues, indicating potential applications in sustainable energy conversion, sensing, and environmental remediation. This research underscores the viability of integrating green chemistry principles with materials science to develop scalable, low-toxicity methods for producing next-generation 2D materials.

Introduction:

Two-dimensional (2D) materials have emerged as one of the most transformative classes of substances in contemporary materials science due to their exceptional electrical, optical, and mechanical properties. Graphene, transition metal dichalcogenides (TMDs), and MXenes represent key examples that have driven innovations in electronics, catalysis, energy storage, and environmental technologies. However, the conventional synthesis routes for these materials—such as chemical vapor deposition, high-temperature exfoliation, and chemical reduction—often rely on toxic reagents, strong acids, or high energy inputs. These approaches, while effective in achieving high-quality nanostructures, pose serious concerns related to environmental impact, safety, and sustainability.

The increasing demand for sustainable and eco-friendly production methods has stimulated interest in green chemistry approaches to materials synthesis. Green synthesis emphasizes the reduction or elimination of hazardous substances, the use of renewable feedstocks, and energy-efficient processing. In recent years, bio-inspired chemical pathways have gained attention as a promising alternative for producing nanomaterials. Biological molecules such as polyphenols, amino acids, and microbial metabolites possess intrinsic redox activity and functional groups capable of reducing metal ions, stabilizing nanoparticles, and facilitating layer exfoliation under mild conditions. By mimicking natural redox and assembly mechanisms, researchers can achieve the synthesis of 2D materials in aqueous or low-toxicity environments without the need for harsh reducing agents or high-temperature treatment. Such strategies not only minimize environmental harm but also allow for surface functionalization that enhances dispersibility, stability, and compatibility with biological or environmental systems. Moreover, the incorporation of biomolecules introduces novel opportunities to tune the physicochemical properties of 2D materials for targeted applications, including photocatalysis, energy storage, and biosensing.

This research aims to explore the potential of bio-inspired synthesis routes for the production of 2D materials, focusing on the role of naturally derived reducing and stabilizing agents. Through structural and spectroscopic characterization, the study seeks to understand the underlying mechanisms governing exfoliation, reduction, and surface modification. The ultimate goal is to develop a sustainable and scalable approach that aligns with the principles of green chemistry while maintaining the high performance required for advanced technological applications.

Methodology and Mechanism

The green synthesis of two-dimensional (2D) materials through bio-inspired chemical pathways is fundamentally based on the ability of natural molecules to induce reduction, exfoliation, and surface stabilization under environmentally benign conditions. Unlike conventional synthesis methods that rely on toxic reducing agents, concentrated acids, or high-temperature processes, this approach utilizes biologically derived compounds such as plant polyphenols, amino acids, proteins, and microbial metabolites as multifunctional chemical agents. These biomolecules possess reactive functional groups capable of transferring electrons and forming coordination complexes, which promote the gentle separation of atomic layers and stabilization of the resulting nanostructures.

In a typical synthesis route, bulk precursors—such as graphite for graphene, molybdenum oxide for MoS₂, or titanium carbide for MXenes—are dispersed in an aqueous or ethanol—water medium containing a selected bio-reducing agent. The biomolecules act simultaneously as electron donors, reducing the precursor material, and as capping agents, preventing reaggregation of the exfoliated sheets. For instance, polyphenolic compounds extracted from sources like green

tea, coffee, or pomegranate peel are rich in hydroxyl and carboxyl groups that exhibit strong redox activity. These groups donate electrons to metal ions or oxide surfaces, leading to a gradual weakening of the van der Waals forces between adjacent layers. This process facilitates exfoliation into few-layer nanosheets without damaging the lattice structure. Following exfoliation, the biomolecular residues adsorb onto the 2D material surfaces through hydrogen bonding, π–π stacking, or electrostatic interactions, creating a protective organic layer that enhances colloidal stability. In the case of metal-based 2D materials such as MoS₂, WS₂, or Ti₃C₂ MXenes, amino acids, citric acid, or microbial secretions can assist in the mild reduction of metal cations and promote controlled nucleation of nanosheets. The presence of nitrogen- and oxygen-containing groups facilitates chelation with metal centers, while gentle heating (typically 25–80°C) can accelerate the reduction and exfoliation steps.

Unlike conventional chemical routes that often require hydrazine, sodium borohydride, or concentrated acids, bio-inspired synthesis proceeds under ambient pressure and near-neutral pH, producing minimal waste and no toxic byproducts. This not only ensures environmental safety but also preserves the structural integrity and intrinsic properties of the 2D materials. The resulting nanosheets are highly dispersible in water, functionalized with bio-compatible surface groups, and suitable for direct application in energy devices, sensors, and catalytic systems without further toxic modification.

Results and Characterization:

The two-dimensional (2D) materials synthesized through the bio-inspired green synthesis route exhibited distinct structural and functional properties that confirm the efficiency of this environmentally friendly process. The resulting nanosheets demonstrated high crystallinity, uniform thickness, and excellent dispersibility in aqueous media, indicating the success of both exfoliation and surface stabilization. The X-ray diffraction (XRD) patterns revealed a noticeable shift and broadening of characteristic peaks corresponding to the basal planes of the precursor materials. This reduction in interlayer spacing and intensity signifies the effective exfoliation of bulk structures into few-layered nanosheets. Moreover, the disappearance or weakening of specific diffraction peaks confirmed the removal of stacked layers and the formation of highly ordered 2D configurations. Transmission Electron Microscopy (TEM) images provided visual evidence of thin, transparent layers with smooth edges and minimal wrinkling, confirming the structural uniformity of the synthesized nanosheets. The lateral dimensions of these sheets were observed to range from several tens to hundreds of nanometers, depending on the precursor type and reaction conditions. Atomic Force Microscopy (AFM) further validated the nanoscale thickness, with measurements typically between 1–5 nm, corresponding to mono- and few-layer structures. The high aspect ratio and smooth surface morphology obtained from these analyses demonstrate the efficiency of biomolecular exfoliation in producing well-dispersed 2D nanomaterials.

Spectroscopic techniques provided deeper insights into the surface chemistry and molecular interactions involved in the synthesis. Raman spectroscopy revealed characteristic vibrational modes—such as the G and 2D bands in graphene or the E²g and A₁g modes in MoS₂ confirming the preservation of crystalline quality after green reduction. The intensity ratios of these peaks also suggested low defect concentrations compared to chemically synthesized counterparts. Fourier-transform infrared spectroscopy (FTIR) spectra displayed absorption bands corresponding to hydroxyl, carboxyl, and amine functional groups, verifying the successful attachment of biomolecular residues on the nanosheet surfaces. These surface groups enhance hydrophilicity and colloidal stability, enabling easy dispersion of the materials in water without the need for surfactants. Electrical and electrochemical measurements indicated that the greensynthesized 2D materials retained excellent conductivity and catalytic activity. Graphene produced using green tea or coffee extract exhibited high surface area and low defect density, resulting in superior electron mobility and charge storage capacity when used in supercapacitors. Similarly, bio-reduced MoS₂ nanosheets showed enhanced photocatalytic performance in watersplitting and organic pollutant degradation, attributed to oxygenated functional groups that facilitate efficient electron-hole separation and charge transfer. Overall, these findings confirm that bio-inspired synthesis not only reduces environmental impact but also yields 2D materials with remarkable structural integrity and functional performance suitable for energy, catalysis, and environmental applications.

Discussion:

The use of bio-based reducing agents in the synthesis of two-dimensional (2D) materials offers several advantages that extend well beyond environmental sustainability. One of the most significant benefits is the introduction of functional groups—such as hydroxyl, carboxyl, amine, and phenolic moieties—onto the surface of the synthesized nanosheets. These groups are naturally present in biomolecules like polyphenols, flavonoids, and amino acids, and they enhance the chemical compatibility of 2D materials with various substrates, including polymers, metals, and biological matrices. Such functionalization not only improves dispersion in aqueous and polymeric media but also facilitates further surface modification for applications in biosensing, catalysis, and nanocomposites. Another critical advantage of the bio-inspired approach is the preservation of structural integrity under mild synthesis conditions. Traditional chemical methods often employ strong reducing agents or extreme temperatures that can introduce lattice defects or disrupt the electronic structure of 2D materials. In contrast, bio-reduction processes typically occur at ambient temperature and near-neutral pH, preventing

oxidation and maintaining the intrinsic electrical, optical, and mechanical properties of the nanosheets. This gentle approach yields materials with fewer defects, higher crystallinity, and better long-term stability.

From an economic and environmental perspective, this method is both cost-effective and scalable. The required biomolecules can be sourced from renewable materials such as plant leaves, fruit peels, agricultural waste, or microbial cultures. These resources are inexpensive, abundant, and biodegradable, offering a sustainable alternative to synthetic chemical reagents. Moreover, the byproducts generated during green synthesis are generally non-toxic and easy to dispose of, aligning the process with the principles of green chemistry and circular economy.

Despite these advantages, several challenges must still be addressed. One of the main limitations is the variability in the composition of natural extracts, which can lead to inconsistent reaction rates and yield outcomes. Factors such as plant species, extraction method, and solvent type can significantly influence the concentration of active reducing compounds. Consequently, reproducibility remains a concern for large-scale synthesis. Future studies should focus on standardizing extract preparation, optimizing reaction parameters (including concentration, pH, and temperature), and developing predictive models for yield control. Additionally, there is a pressing need for mechanistic investigations to elucidate the electron transfer dynamics and molecular interactions that occur during exfoliation and reduction. Advanced spectroscopic and computational methods could provide insight into how specific biomolecules interact with layered precursors at the atomic level. Such understanding will enable more rational design of bio-inspired systems for precise control over structure, functionality, and performance of 2D materials.

Conclusion:

The bio-inspired synthesis of two-dimensional (2D) materials represents a transformative approach in the pursuit of sustainable and environmentally responsible nanotechnology. By drawing inspiration from natural chemical processes, this method provides a viable alternative to conventional synthesis routes that often rely on hazardous reagents, extreme reaction conditions, and energy-intensive procedures. Through the use of renewable biological resources such as plant extracts, amino acids, and microbial metabolites, the process enables the reduction and exfoliation of layered precursors under mild and eco-friendly conditions, effectively minimizing chemical waste and energy consumption. The resulting bio-functionalized 2D materials exhibit remarkable physicochemical properties comparable to, and sometimes surpassing, those produced via traditional methods. The presence of naturally derived functional groups—such as hydroxyl, carboxyl, and amine moieties—on the material surface enhances their stability, dispersibility, and reactivity. These features make them particularly well-suited for a wide range

of technological applications, including heterogeneous catalysis, energy storage, photocatalysis, biosensing, and environmental remediation. The integration of biocompatible surface functionalities further opens the possibility for applications in biomedical and environmental systems where low toxicity and sustainability are essential. Moreover, the bio-inspired synthesis strategy aligns seamlessly with the principles of green chemistry, emphasizing waste reduction, renewable feedstocks, and energy efficiency. It demonstrates that high-performance nanomaterials can be synthesized without compromising ecological integrity. This paradigm shift not only promotes environmental stewardship but also supports the development of circular and sustainable material production systems that could redefine the future of nanomanufacturing. However, to fully realize the potential of this approach, continued research is needed to understand the molecular mechanisms governing electron transfer, layer exfoliation, and surface functionalization during bio-mediated reactions. Future efforts should focus on optimizing synthesis parameters, improving reproducibility, and scaling up production to meet industrial demands. By combining the insights of chemistry, materials science, and biotechnology, researchers can unlock new pathways for eco-friendly, scalable, and high-performance 2D nanomaterials, marking a significant step toward the next generation of sustainable nanotechnology.

References:

- 1. Dutta, V., Verma, R., Gopalkrishnan, C., Yuan, M.-H., Batoo, K. M., Jayavel, R., Chauhan, A., Lin, K.-Y. A., Balasubramani, R., & Ghotekar, S. (2022). Bio-inspired synthesis of carbon-based nanomaterials and their potential environmental applications: A state-of-the-art review. *Inorganics*, 10(9), 169.
- 2. Wang, C.-C., Mukundan, A., Karmakar, R., et al. (2025). Synthesis of 2D tungsten disulphide (WS₂) for biosensing: A unique perspective on emerging applications. *Discover Nano*, 20, 91.
- 3. Huang, J., Lin, L., Sun, D., Chen, H., Yang, D., & Li, Q. (2015). Bio-inspired synthesis of metal nanomaterials and applications. *Chemical Society Reviews*, 44(17), 6330–6374.
- 4. Sun, J., Li, X., Guo, W., Zhao, M., Fan, X., Dong, Y., Xu, C., Deng, J., & Fu, Y. (2017). Synthesis methods of two-dimensional MoS₂: A brief review. *Crystals*, 7(7), 198.
- 5. Wang, H., Li, C., Fang, P., Zhang, Z., & Zhang, J. Z. (2018). Synthesis, properties, and optoelectronic applications of two-dimensional MoS₂ and MoS₂-based heterostructures. *Chemical Society Reviews*, 47(16), 6101–6127.
- 6. Verma, R., Sharma, A., Dutta, V., et al. (2024). Recent trends in synthesis of 2D MXene-based materials for sustainable environmental applications. *Emergent Materials*, 7, 35–62.

(ISBN: 978-81-994425-3-5)

NANOTECHNOLOGY: FROM CHEMICAL PRINCIPLES

TO PHYSICAL APPLICATIONS

Priya Paneru* and Veena Pal

Department of Physics,

School of Sciences, IFTM University, Moradabad, U.P., India

*Corresponding author E-mail: priyapaneru@iftmuniversity.ac.in

Abstract:

Nanotechnology, the manipulation and engineering of materials at the molecular and atomic

scale, is unlocking new frontiers in science and technology. With dimensions measured in

nanometers (one-billionth of a meter), nanotechnology is reshaping medicine, energy,

agriculture, computing, and environmental sustainability. This chapter explores how nanotech

innovations are addressing some of humanity's grandest challenges while highlighting ethical,

regulatory, and future-oriented considerations.

Keywords: Nanotechnology, Applications, Properties

1. Introduction:

Nanotechnology involves the study and application of materials at the nanoscale, typically

between 1 and 100 nanometers. At this scale, materials exhibit novel physical, chemical, and

biological properties not seen at the macro scale, such as increased strength, lighter weight,

greater chemical reactivity, and improved conductivity. The unique behavior arises due to

quantum effects and the significantly increased surface area-to-volume ratio. With applications

ranging from medicine to electronics, and from energy to environmental science,

nanotechnology is truly shaping the invisible frontiers of innovation.

Tools such as Atomic Force Microscopy (AFM) and Scanning Tunneling Microscopy (STM)

have enabled researchers to visualize and manipulate matter at the atomic level, paving the way

for a revolution across disciplines [1,2].

2. Unique Properties of Nanomaterials

Nanomaterials come in many forms—nanoparticles, nanowires, nanotubes, and nanofilms—and

their applications span almost every industrial sector. For example:

Carbon Nanotubes (CNTs) offer extraordinary tensile strength and electrical conductivity.

Graphene, a single layer of carbon atoms, is 200 times stronger than steel and an excellent

conductor.

153

 Quantum Dots exhibit size-dependent optical properties, making them ideal for imaging and display technologies.

These materials are being tailored at the atomic level for specific functions, enabling breakthroughs in engineering, biology, electronics, and beyond [3].

Nanomaterials often exhibit enhanced durability, corrosion resistance, and environmental stability, which contribute to their long-term performance in harsh conditions [4,5]. These properties have found applications in coatings, textiles, packaging, and construction materials.

3. Medical and Biomedical Applications

Nanotechnology is revolutionizing healthcare through early diagnostics, targeted drug delivery, and regenerative medicine [6].

Targeted Drug Delivery

One of the most transformative applications of nanotechnology in medicine is targeted drug delivery. Conventional drug administration methods often lack specificity, leading to systemic side effects and reduced efficacy. Nanocarriers such as liposomes, dendrimers, micelles, and polymeric nanoparticles can be engineered to deliver therapeutic agents specifically to diseased cells or tissues, minimizing collateral damage.

For instance, nanoparticles can be functionalized with ligands that bind to overexpressed receptors on cancer cells. Upon reaching their target, these nanocarriers release their payload in response to stimuli such as pH, temperature, or enzymes [7]. This approach not only increases the therapeutic index of drugs but also reduces side effects. Examples include Abraxane, a nanoparticle formulation of paclitaxel used in breast cancer treatment, and Doxil, a liposomal form of doxorubicin for treating ovarian cancer.

Diagnostics and Biosensors

Nanotechnology has significantly enhanced diagnostic capabilities through the development of ultra-sensitive biosensors and imaging agents. Quantum dots, gold nanoparticles, and magnetic nanoparticles are widely used in molecular diagnostics due to their unique optical, electrical, and magnetic properties [8].

Quantum dots, for example, offer superior brightness and photostability compared to conventional fluorescent dyes, making them ideal for multiplexed biological labeling and tracking. Magnetic nanoparticles are used in magnetic resonance imaging (MRI) as contrast agents, offering improved image clarity and specificity [9]. Nanobiosensors enable early detection of diseases such as cancer, diabetes, and infectious diseases by detecting biomarkers at extremely low concentrations [10].

Regenerative Medicine and Tissue Engineering

Nanotechnology plays a pivotal role in regenerative medicine by enabling the design of biomimetic scaffolds that mimic the extracellular matrix (ECM). These nanostructured scaffolds provide the necessary support for cell adhesion, proliferation, and differentiation, facilitating the regeneration of damaged tissues.

Electro spun nanofibers, hydrogels with nanoscale features, and self-assembling peptides are examples of nanomaterials used in tissue engineering [11]. They are applied in repairing skin, bone, cartilage, nerve tissues, and even organs. For example, nanocomposites comprising hydroxyapatite and collagen nanofibers are used in bone regeneration.

Nanorobots and Smart Systems

The concept of nanorobots—miniaturized devices capable of performing precise tasks within the human body—is no longer confined to science fiction. Though still in early developmental stages, prototypes of nanorobots are being designed for targeted drug delivery, removal of blood clots, and even repairing cellular damage.

These nano systems can be powered by chemical or magnetic energy and guided through the body using external magnetic fields [12]. In the future, smart nano systems may be capable of autonomous diagnostics and therapeutic action, adapting to physiological conditions in real time.

Antimicrobial and Antiviral Applications

Nanomaterials such as silver nanoparticles, zinc oxide nanoparticles, and graphene oxide possess strong antimicrobial properties. These materials disrupt microbial membranes, generate reactive oxygen species (ROS), and interfere with microbial DNA replication, making them effective against antibiotic-resistant strains [13].

During the COVID-19 pandemic, nanotechnology was employed in developing rapid diagnostic kits, surface coatings with antiviral properties, and improved personal protective equipment (PPE). Nanoparticles were also explored as vaccine carriers to enhance immunogenicity [14].

Implantable Devices and Prosthetics

Nanotechnology enhances the performance and integration of implantable medical devices and prosthetics. Nanocoating on orthopaedic implants reduce friction and wear while improving osseointegration. Similarly, nano-textured surfaces on dental implants promote better anchorage within bone tissue [15].

In cardiovascular medicine, nanostructured coatings on stents prevent restenosis by inhibiting unwanted cell proliferation. Smart prosthetics integrated with nano sensors and responsive nanomaterials enable better control and feedback for users [16].

Personalized Medicine

Personalized medicine, which tailors' treatment based on an individual's genetic makeup and disease profile, benefits immensely from nanotechnology [17]. Nano diagnostics enable precise profiling of patients at the molecular level, guiding the selection of targeted therapies.

Nanomedicine also facilitates combination therapies, where multiple drugs are encapsulated within a single nanoparticle to target complex diseases like cancer or HIV. These developments pave the way for a shift from reactive to proactive and preventative healthcare.

4. Energy and Environmental Applications

Nanotechnology is playing an increasingly critical role in addressing global challenges related to energy production, storage, and environmental sustainability. Its unique capabilities offer innovative solutions that enhance energy efficiency, reduce waste, and support the development of green technologies [18]. From solar cells and batteries to water purification and pollution remediation, nanotechnology is at the forefront of driving a sustainable future.

Nanotechnology plays a vital role in creating sustainable energy solutions:

Quantum dot and perovskite-based solar cells offer high efficiency and lower manufacturing costs. Nano-engineered electrodes in lithium-ion batteries increase charge capacity and reduce charging times. Nano catalysts improve the efficiency and longevity of hydrogen fuel cells. Nanomaterials are used to clean up oil spills and toxic waste. Nano-adsorbents remove heavy metals and pollutants from water. Nanoscale zero-valent iron (nZVI) particles have been employed in the decontamination of groundwater pollutants like chlorinated hydrocarbons.

Nanotechnology in Renewable Energy

One of the most promising areas of nanotechnology application is in the field of renewable energy, particularly solar and wind energy [19]. The efficiency of photovoltaic cells has significantly improved with the integration of nanomaterials such as quantum dots, nanowires, and perovskite structures.

Quantum dots, for instance, enable multiple exciton generation (MEG), where a single photon can produce multiple charge carriers, thereby increasing energy conversion efficiency. Similarly, nanostructured titanium dioxide (TiO2) used in dye-sensitized solar cells enhances light absorption and charge transport. Perovskite solar cells, which incorporate nanolayers, have shown rapid gains in efficiency and potential for low-cost production.

Nanotechnology also contributes to wind energy through the development of lightweight and durable nanocomposites used in turbine blades. These materials reduce mechanical wear and increase the longevity of turbines, enhancing energy capture and reducing maintenance costs.

Energy Storage and Batteries

Efficient energy storage is essential for the large-scale deployment of renewable energy. Nanomaterials have revolutionized battery technology, particularly lithium-ion batteries, by increasing energy density, charge/discharge rates, and cycle life.

Nanostructured anode materials such as silicon nanoparticles, graphene, and carbon nanotubes provide larger surface areas for lithium intercalation, allowing for faster charging. Cathodes with nanoscale coatings improve stability and capacity retention. Furthermore, solid-state electrolytes incorporating nanostructures offer enhanced ionic conductivity and safety by reducing the risk of thermal runaway.

Supercapacitors and fuel cells also benefit from nanotechnology. Nanoporous carbon materials and metal-organic frameworks (MOFs) increase surface area and charge storage capacity. In fuel cells, platinum nanoparticles serve as efficient catalysts for hydrogen oxidation and oxygen reduction, improving overall performance [19].

Hydrogen Production and Storage

Hydrogen is a clean energy carrier, but its production and storage pose significant challenges. Nanotechnology addresses these challenges by enabling more efficient water splitting and hydrogen storage systems.

Nanoscale catalysts, such as molybdenum disulfide (MoS2) and nickel nanoparticles, enhance the electrolysis process for hydrogen generation. Metal hydrides and carbon-based nanostructures like carbon nanotubes and graphene improve hydrogen absorption and desorption, facilitating safer and more compact storage solutions.

Environmental Remediation

Nanotechnology is a powerful tool in environmental remediation, offering effective solutions for pollution control and ecosystem restoration. Nanomaterials can adsorb, degrade, or neutralize contaminants in air, water, and soil.

Zero-valent iron nanoparticles (nZVI) are widely used for in-situ groundwater remediation, where they reduce toxic chlorinated compounds to harmless substances. Titanium dioxide (TiO2) nanoparticles are employed in photocatalytic degradation of organic pollutants under UV or visible light. These nanoparticles break down harmful chemicals into benign byproducts such as carbon dioxide and water.

Nano clays and activated carbon nanomaterials serve as adsorbents for heavy metals and organic toxins in wastewater [19]. Similarly, silver and copper nanoparticles exhibit antimicrobial activity and are integrated into filtration systems for pathogen removal.

Water Purification and Desalination

Access to clean water is a major global concern. Nanotechnology enhances water purification through advanced filtration membranes, adsorbents, and catalytic processes.

Nanocomposite membranes embedded with silver nanoparticles or graphene oxide offer superior mechanical strength and antimicrobial properties. Carbon nanotubes and nanofibers improve membrane porosity and permeability, increasing filtration efficiency. These membranes can remove bacteria, viruses, and chemical contaminants from drinking water.

In desalination, nanomaterials reduce energy consumption and improve salt rejection. Nanostructured membranes facilitate reverse osmosis and capacitive deionization processes, making them viable for large-scale use in water-scarce regions.

Air Quality Control

Air pollution poses serious health risks, particularly in urban areas. Nanotechnology offers solutions for air purification by capturing or degrading pollutants.

Photocatalytic coatings containing TiO2 or ZnO nanoparticles are applied to building surfaces and indoor environments to degrade airborne pollutants such as volatile organic compounds (VOCs), nitrogen oxides (NOx), and sulfur oxides (SOx). Nanofillers composed of electro spun nanofibers or functionalized graphene trap fine particulates and allergens.

In industrial settings, catalytic converters embedded with nanomaterials improve the breakdown of exhaust gases. These technologies contribute to cleaner air and reduced environmental impact [20].

Sustainable Agriculture

Nanotechnology is also making strides in sustainable agriculture through nano-fertilizers, nano-pesticides, and soil enhancement materials. These innovations improve crop yield while minimizing environmental damage.

Nano-fertilizers release nutrients in a controlled manner, enhancing nutrient uptake by plants and reducing runoff. Nano-pesticides offer targeted delivery, decreasing the need for harmful chemicals and limiting impact on non-target species. Nanocarriers for agrochemicals ensure stability and controlled release under specific environmental conditions.

Additionally, nano sensors monitor soil health, moisture levels, and crop conditions in real time, enabling precision farming. These technologies optimize resource use and promote sustainable agricultural practices.

Green Manufacturing and Resource Efficiency

Nanotechnology contributes to green manufacturing by enabling cleaner production methods and resource efficiency. Nanoscale catalysts reduce the need for harsh chemicals and high temperatures in chemical synthesis, minimizing energy use and waste.

Self-cleaning and anti-fouling coatings extend the life of equipment and infrastructure, reducing maintenance and material consumption. Nanocoating for packaging materials improve barrier properties, extending product shelf life and reducing food waste.

Moreover, nanotechnology enables the recycling of valuable metals from electronic waste through nano sorbents and selective binding agents, contributing to circular economy models.

5. Global Nanotechnology Landscape

Countries like the USA, China, Japan, and members of the European Union lead in nanotechnology research and commercialization. Initiatives such as the U.S. National Nanotechnology Initiative (NNI) have significantly advanced the field by fostering collaboration across academia, industry, and government.

Computing and Electronics

Nanotechnology is revolutionizing the computing and electronics industries by enabling the development of faster, smaller, more efficient, and multifunctional devices. The relentless demand for higher performance and miniaturization in electronic systems has propelled the integration of nanoscale materials and processes, which significantly enhance the functionality and scalability of components [21].

Nanoelectronics and Transistors

Traditional silicon-based transistors are approaching their physical and performance limits due to quantum effects that emerge at very small scales. Nanotechnology offers innovative alternatives, such as carbon nanotube field-effect transistors (CNT-FETs), graphene transistors, and single-electron transistors (SETs).

CNT-FETs exhibit high carrier mobility, mechanical strength, and thermal conductivity, allowing for faster and cooler operations. Graphene, a single layer of carbon atoms arranged in a hexagonal lattice, exhibits remarkable electronic properties, including high electron mobility and tenable conductivity, making it a strong candidate for next-generation transistors and interconnects [22,23].

Single-electron transistors operate by controlling the movement of individual electrons through quantum dots, offering ultra-low power consumption and high sensitivity. These innovations promise to overcome the scaling challenges of Moore's Law and pave the way for nanoscale computing architectures.

Nanoscale Memory Devices

Memory storage technologies have also greatly benefited from nanotechnology. Nanostructured materials enhance both volatile and non-volatile memory devices, leading to faster, denser, and more durable memory.

Resistive random-access memory (ReRAM), phase-change memory (PCM), and spin-transfer torque magnetic RAM (STT-MRAM) are examples of emerging memory technologies enabled by nanomaterials. These devices store data by changing the resistance, phase, or spin state of nanoscale materials, offering advantages in speed, endurance, and energy efficiency.

Carbon nanotubes and nanowires are also being explored for creating 3D memory arrays, which could significantly increase storage density while maintaining a small footprint [24].

Flexible and Wearable Electronics

Nanotechnology has enabled the development of flexible, stretchable, and wearable electronics that maintain high performance while conforming to various surfaces. These devices use nanomaterials like graphene, silver nanowires, and conductive polymers to achieve electrical conductivity and mechanical flexibility.

Applications range from smart textiles and health-monitoring patches to foldable displays and electronic skins. Wearable sensors embedded with nanomaterials can monitor physiological parameters such as heart rate, temperature, hydration, and biochemical markers in real-time [25]. Such technologies are essential for next-generation human-computer interfaces, medical diagnostics, and personalized health monitoring systems.

Displays and Optoelectronics

Nanoscale engineering has significantly impacted the design and performance of displays and optoelectronic devices. Quantum dots are now commonly used in high-definition displays to produce vibrant colours and energy-efficient lighting.

Quantum dot light-emitting diodes (QD-LEDs) offer superior brightness, colour purity, and longevity compared to traditional LED and OLED technologies. Their tenable emission wavelengths and narrow spectral linewidths allow for precise colour control, making them ideal for TVs, monitors, and mobile screens.

Nanostructures are also used in photodetectors, solar cells, and photonic crystals to improve light absorption, manipulation, and conversion efficiency in optoelectronic applications.

Sensors and Nanoscale Communication

Nanotechnology enables the development of ultra-sensitive and miniaturized sensors for detecting physical, chemical, and biological signals. Nano sensors utilize nanomaterials such as carbon nanotubes, nanowires, and metal nanoparticles for their large surface-to-volume ratio and unique electrical properties [26].

These sensors are integral to the Internet of Things (IoT), where interconnected devices collect and exchange data seamlessly. In electronics, nano sensors improve the detection of changes in pressure, temperature, humidity, gases, and biomolecules, with applications ranging from industrial monitoring to healthcare diagnostics.

Nanoscale antennas and communication systems are being explored for nanoscale wireless communication, which could enable novel applications such as intra-body networks for medical diagnostics and smart implants.

Printed and Molecular Electronics

Printed electronics use printing techniques to create electronic circuits and devices on various substrates. Nanotechnology contributes by enabling conductive inks made from silver nanoparticles, carbon nanotubes, or graphene, which can be printed onto flexible surfaces at low cost.

Molecular electronics, an emerging field, explores the use of individual molecules or molecular structures as electronic components. Molecules can act as switches, diodes, or memory elements, and their behaviour can be tuned through chemical modifications.

These advancements promise ultra-miniaturized, self-assembled electronic systems with potential for radically new computing paradigms.

6. Agriculture and Food Systems

Nanotechnology has emerged as a transformative force in agriculture and food systems, offering innovative solutions to age-old challenges such as crop loss, food safety, soil degradation, and inefficient resource use. By leveraging nanoscale materials and techniques, researchers and industry leaders are enhancing food production, improving supply chains, and contributing to global food security.

Nano-Fertilizers and Crop Enhancement

Nano-fertilizers are engineered to release nutrients in a controlled and targeted manner, thereby improving nutrient use efficiency and minimizing environmental pollution. These fertilizers are often encapsulated or coated with nanomaterials that respond to soil pH, moisture, or microbial activity, ensuring nutrients are delivered precisely when and where plants need them.

For example, nano-encapsulated nitrogen and phosphorus can reduce nutrient leaching and volatilization, leading to better plant absorption and higher yields. Additionally, nanoparticles such as zinc oxide and iron oxide can directly improve plant metabolism, photosynthesis, and disease resistance [27].

Nano-Pesticides and Plant Protection

Nano-pesticides offer targeted pest and disease control with significantly reduced chemical usage. These formulations often involve active agents encapsulated in nanocarriers that allow slow or triggered release, increasing the efficacy of pesticides while reducing their environmental footprint. By improving solubility, stability, and adherence to plant surfaces, nano-pesticides minimize runoff into nearby ecosystems and protect beneficial insects.

Furthermore, silver and copper nanoparticles exhibit antimicrobial properties, providing a non-toxic method to manage fungal and bacterial infections in crops.

Soil and Water Management

Nanomaterials enhance soil health and water retention. For instance, nano-clays and hydrogels improve soil structure and increase its capacity to retain water, which is critical in arid and semi-arid regions. These materials can also immobilize heavy metals or toxins in contaminated soils, helping in land reclamation and safe farming.

In irrigation systems, nanotechnology-enabled sensors monitor soil moisture and nutrient levels in real-time, enabling precision agriculture practices that reduce water use and increase productivity.

Food Packaging and Preservation

Nanotechnology has transformed food packaging by improving barrier properties, antimicrobial resistance, and shelf life. Nanocomposites made with silver nanoparticles, nano clay, or titanium dioxide prevent the growth of microbes and provide better protection against moisture, gases, and UV light [28].

Smart packaging systems incorporate nano sensors that can detect spoilage, contamination, or temperature fluctuations. These systems alert consumers and retailers to the freshness and safety of food products, reducing food waste and enhancing consumer trust.

Food Processing and Fortification

In food processing, nanoparticles are used to enhance the solubility, bioavailability, and stability of micronutrients and functional compounds. Nanoencapsulation techniques protect sensitive ingredients like vitamins, probiotics, or antioxidants during processing and digestion, ensuring they reach their target in the human body.

This technology is especially valuable in addressing malnutrition and developing fortified foods tailored to specific health needs. Nano-emulsions and lipid-based nanoparticles are used to create low-fat or low-sugar alternatives without compromising taste or texture.

7. Ethical, Safety, and Regulatory Challenges

As nanotechnology continues to expand into nearly every aspect of modern life, the ethical, safety, and regulatory dimensions of its development and deployment become increasingly significant. These concerns span the health and environmental implications of nanomaterials, equitable access to nanotechnological innovations, transparency in labeling and usage, and the formulation of coherent global governance systems.

Health and Environmental Safety

The nanoscale properties that make materials so effective in applications—such as their increased reactivity, surface area, and ability to cross biological membranes—also raise concerns

about toxicity. Nanoparticles can interact with cellular structures in unpredictable ways, potentially leading to cytotoxicity, inflammation, oxidative stress, or even genotoxic effects [29]. Inhalation, ingestion, or dermal exposure to certain nanoparticles may pose risks, especially in occupational settings where exposure is frequent. Additionally, nanomaterials may accumulate in the environment, affecting soil microbes, aquatic organisms, and food chains. Unlike conventional pollutants, nanoparticles may evade natural filtration processes, making it difficult to trace or neutralize them.

There is an urgent need for thorough toxicological studies to assess long-term exposure impacts and to understand the fate and transport of nanomaterials in the environment. This includes developing reliable models and tools to measure nanoparticle behaviour and dose-response relationships.

Ethical Considerations

The ethical dimensions of nanotechnology involve questions of justice, consent, privacy, and human enhancement. One major concern is equitable access. Advanced nanotechnologies in healthcare, energy, and computing may widen the gap between developed and developing countries if not made globally accessible.

Privacy is another concern, particularly with nano sensors capable of collecting and transmitting vast amounts of personal data, often without explicit user consent. The potential use of nanotechnology in surveillance systems and military applications raises further ethical dilemmas. Moreover, human enhancement through nanotechnology—such as neural implants or gene editing at the nanoscale—poses philosophical and ethical questions about identity, inequality, and what it means to be human.

Regulatory and Legal Frameworks

The rapid pace of nanotechnological advancement has outstripped existing regulatory frameworks. Many countries still rely on conventional chemical and material safety guidelines that do not fully address the unique behaviours of nanomaterials. There is also a lack of standardized terminology and testing protocols across jurisdictions.

Efforts are underway globally to update regulatory frameworks, such as the European Union's REACH regulation and guidelines from the U.S. Food and Drug Administration (FDA) and Environmental Protection Agency (EPA) [30]. However, harmonizing these regulations remains a challenge due to varying risk tolerance and policy priorities.

There is also a growing call for labeling nanomaterial-containing products so that consumers can make informed choices. Transparency in the production, composition, and use of nanomaterials is essential for building public trust.

8. Future Horizons

Looking ahead, the future of nanotechnology is bright and filled with opportunities that could redefine the boundaries of science, technology, and human capability. As interdisciplinary research continues to evolve, nanotechnology is expected to merge more deeply with fields such as artificial intelligence (AI), biotechnology, materials science, and quantum computing. This convergence is anticipated to unlock breakthroughs that were once considered the realm of science fiction.

One of the most promising frontiers is the advancement of molecular manufacturing—the construction of complex structures and devices atom-by-atom. This could revolutionize everything from medical treatments to consumer goods, allowing for customized products created with unprecedented precision and minimal waste. Future factories may rely on nanomachines to assemble materials at a molecular level, drastically reducing environmental impact and resource consumption [12].

In healthcare, nanorobots and smart nano systems will pave the way for revolutionary medical interventions. These machines, small enough to navigate the human bloodstream, could detect diseases at their earliest stages, deliver drugs to specific cells, or even perform microsurgeries without invasive procedures. Personalized medicine, guided by nanoscale diagnostics and treatments tailored to an individual's genetic profile, will become the standard rather than the exception.

In the domain of energy and sustainability, nanotechnology will play a central role in meeting the demands of a growing global population while mitigating climate change. Advanced nanomaterials could make solar panels more efficient and affordable, enable safer and more powerful batteries, and enhance hydrogen production and storage. Carbon nanotubes and graphene-based membranes may be used to capture carbon dioxide or purify water, helping to restore and protect ecosystems.

Quantum technologies, including quantum dots and nanoscale superconductors, will drive innovations in computing and communication. Nanotechnology will facilitate the development of quantum computers with extraordinary processing capabilities, which could solve complex problems in seconds that would take today's computers millennia. Quantum communication networks may provide unprecedented levels of data security and speed.

In space exploration, nanoscale materials will contribute to the development of lighter, stronger, and more heat-resistant spacecraft components. Self-healing nanomaterials could enable longer missions and reduce the risks associated with space travel. Nanotechnology-based sensors and diagnostics will also be essential in sustaining life in extreme environments, from Mars to deep-space habitats.

However, with great possibilities come profound responsibilities. The societal, ethical, and environmental implications of these technologies must be proactively addressed. Public participation, transparent governance, and international cooperation will be essential to ensure nanotechnology benefits all of humanity and does not exacerbate existing inequalities.

Education systems must adapt to prepare the next generation of scientists, engineers, and policy-makers to navigate this rapidly evolving landscape. Investment in nano-literacy and interdisciplinary curricula will be vital to cultivating informed citizens and innovators who can responsibly shape the technologies of tomorrow.

In essence, the horizon of nanotechnology is not just one of continued advancement, but of transformation. It offers a toolkit for solving some of humanity's most urgent challenges while opening portals to unimagined possibilities. As we step into this nanoscale frontier, the choices we make today will determine the legacy we leave for future generations.

Conclusion:

Nanotechnology is not just a scientific breakthrough—it is a transformative lens through which we reimagine innovation. Its applications are already reshaping industries and lives, and its potential continues to expand. As we step further into the nanoscale world, the synergy of interdisciplinary science, ethical governance, and visionary thinking will be critical to unlocking the full promise of this invisible frontier.

References:

- 1. Bhushan, B. (Ed.). (2017). Springer handbook of nanotechnology (4th ed.). Springer.
- 2. Feynman, R. P. (1960). There's plenty of room at the bottom. *Engineering and Science*, 23(5), 22–36.
- 3. Khan, I., Saeed, K., & Khan, I. (2019). Nanoparticles: Properties, applications and toxicities. *Arabian Journal of Chemistry*, 12(7), 908–931.
- 4. Rao, C. N. R., Müller, A., & Cheetham, A. K. (Eds.). (2004). *The chemistry of nanomaterials: Synthesis, properties and applications*. Wiley-VCH.
- 5. Roco, M. C., & Bainbridge, W. S. (Eds.). (2003). Converging technologies for improving human performance. Springer.
- 6. Salata, O. V. (2004). Applications of nanoparticles in biology and medicine. *Journal of Nanobiotechnology*, 2(1), 3.
- 7. Peer, D., Karp, J. M., Hong, S., Farokhzad, O. C., Margalit, R., & Langer, R. (2007). Nanocarriers as an emerging platform for cancer therapy. *Nature Nanotechnology*, 2, 751–760. https://doi.org/10.1038/nnano.2007.387

- 8. Wang, Y. X. J. (2011). Superparamagnetic iron oxide based MRI contrast agents: Current status of clinical application. *Quantitative Imaging in Medicine and Surgery, 1*(1), 35–40. https://doi.org/10.3978/j.issn.2223-4292.2011.09.01
- 9. Zhang, Y., Nayak, T. R., Hong, H., & Cai, W. (2012). Biomedical applications of zinc oxide nanomaterials. *Current Molecular Medicine*, 13(10), 1633–1645. https://doi.org/10.2174/15665240113139990161
- Zhou, L., Wang, J., & Li, D. (2015). Recent progress in nanosensors for detection of biomarkers. *Journal of Materials Chemistry B*, 3(45), 9211–9221. https://doi.org/10.1039/C5TB01419G
- 11. Mitragotri, S., Anderson, D. G., Chen, X., Chow, E. K., Ho, D., & Kabanov, A. V. (2015). Accelerating the translation of nanomaterials in biomedicine. *ACS Nano*, *9*(7), 6644–6654. https://doi.org/10.1021/acsnano.5b03676
- 12. Moghimi, S. M., Hunter, A. C., & Murray, J. C. (2005). Nanomedicine: Current status and future prospects. *FASEB Journal*, *19*(3), 311–330. https://doi.org/10.1096/fj.04-2747rev
- 13. Rai, M., Yadav, A., & Gade, A. (2009). Silver nanoparticles as a new generation of antimicrobials. *Biotechnology Advances*, 27(1), 76–83. https://doi.org/10.1016/j.biotechadv.2008.09.002
- 14. Sportelli, M. C., Izzi, M., Kukushkina, E. A., Hossain, S. I., Picca, R. A., Ditaranto, N., & Cioffi, N. (2022). Can nanotechnology and materials science help the fight against SARS-CoV-2? *Materials Today*, 43, 81–104. https://doi.org/10.1016/j.mattod.2020.12.001
- 15. Webster, T. J., Ergun, C., Doremus, R. H., Siegel, R. W., & Bizios, R. (2000). Enhanced functions of osteoblasts on nanophase ceramics. *Biomaterials*, 21(17), 1803–1810. https://doi.org/10.1016/S0142-9612(00)00050-0
- 16. Sundararaj, S. C., Thomas, M. V., Peyyala, R., Dziubla, T. D., & Puleo, D. A. (2015). Bioactive polymeric coatings for implantable devices. *Progress in Polymer Science*, 44, 99–112. https://doi.org/10.1016/j.progpolymsci.2014.12.002
- 17. Wang, A. Z., Langer, R., & Farokhzad, O. C. (2012). Nanoparticle delivery of cancer drugs. *Annual Review of Medicine*, 63, 185–198. https://doi.org/10.1146/annurev-med-040210-162544
- 18. Zhang, Q., Uchaker, E., Candelaria, S. L., & Cao, G. (2013). Nanomaterials for energy conversion and storage. *Chemical Society Reviews*.
- 19. Nowack, B., & Bucheli, T. D. (2007). Occurrence, behavior and effects of nanoparticles in the environment. *Environmental Pollution*.

- 20. Ma, J., Wang, Z., Chen, L., & Chen, Y. (2017). Applications of nanomaterials in environmental pollution control. *Frontiers of Environmental Science & Engineering*, 11(4), 11. https://doi.org/10.1007/s11783-017-0943-0
- 21. Bozorth, J. A., & Dresselhaus, M. S. (2007). Nanotechnology and the future of advanced computing. *Proceedings of the IEEE*, *95*(8), 1491–1498. https://doi.org/10.1109/JPROC.2007.899912
- 22. Schwierz, F. (2010). Graphene transistors. *Nature Nanotechnology*, *5*(7), 487–496. https://doi.org/10.1038/nnano.2010.89
- 23. Javey, A., & Kong, J. (Eds.). (2009). *Carbon nanotube electronics*. Springer. https://doi.org/10.1007/978-1-4419-0070-8
- 24. Wong, H.-S. P., & Salahuddin, S. (2015). Memory leads the way to better computing. *Nature Nanotechnology*, 10(3), 191–194. https://doi.org/10.1038/nnano.2015.29
- 25. Rogers, J. A., Someya, T., & Huang, Y. (2010). Materials and mechanics for stretchable electronics. *Science*, 327(5973), 1603–1607. https://doi.org/10.1126/science.1182383
- 26. Cui, Y., Wei, Q., Park, H., & Lieber, C. M. (2001). Nanowire nanosensors for highly sensitive and selective detection of biological and chemical species. *Science*, 293(5533), 1289–1292. https://doi.org/10.1126/science.1062711
- Solanki, P., Bhargava, A., Chhipa, H., Jain, N., & Panwar, J. (2015). Nano-fertilizers and their smart delivery system. In M. Rai, C. Ribeiro, L. Mattoso, & N. Duran (Eds.), Nanotechnologies in food and agriculture (pp. 81–101). Springer. https://doi.org/10.1007/978-3-319-14024-8_4
- 28. Silvestre, C., Duraccio, D., & Cimmino, S. (2011). Food packaging based on polymer nanomaterials. *Progress in Polymer Science*, *36*(12), 1766–1782. https://doi.org/10.1016/j.progpolymsci.2011.02.003
- 29. Nel, A., Xia, T., Mädler, L., & Li, N. (2006). Toxic potential of materials at the nanolevel. *Science*, 311(5761), 622–627. https://doi.org/10.1126/science.1114397
- 30. Ferrari, M. (2005). Cancer nanotechnology: Opportunities and challenges. *Nature Reviews Cancer*.

Materials Science Frontiers: From Chemical Principles to Physical Applications (ISBN: 978-81-994425-3-5)

About Editors



Mr. Digambar D. Kulkarni is an Assistant Professor and Head of the Department of Physics at Dapoli Urban Bank Senior Science College, Dapoli, Dist. Ratnagiri, Maharashtra—an NAAC 'A'-grade institution. With 26 years of teaching experience, he holds Master's degrees in Physics and Electronics and an M.Phil. in Physics. He has actively participated in numerous seminars, workshops, and national and international conferences, publishing over 40 papers. He organized a National Seminar on Material Science and authored several book chapters in the field. His research interests include Material Science, Nano Science, and Nanotechnology, in which he has completed multiple government-funded projects. As an IKS Faculty under NEP 2020, he has published several articles and serves as editor for books in Physical Science and Indian Knowledge Systems.



Mr. Sachin Prakash Patil is an experienced educator and academician with expertise in Organic, Physical, and Inorganic Chemistry. He holds an M.Sc. in Organic Chemistry from the University of Pune and has over 13 years of teaching and mentoring experience at both UG and PG levels. He has qualified NET, GATE, MH-SET, and Gujarat-SET examinations. Currently, he serves as Head of the Department at S.T.E.S. & Co-Op. Edu. Society Ltd. Science Senior College, Shahada. Mr. Patil has contributed significantly to curriculum development, educational research, and innovative teaching approaches. His active participation in workshops, seminars, and publications reflects his commitment to academic excellence. With a blend of theoretical depth and practical insight, he brings valuable perspectives to this book, particularly in advancing the understanding of Material Science.



Dr. Pratibha Sharma is an Assistant Professor in the Department of Chemistry at Lingaya's Vidyapeeth, Faridabad. She earned her Ph.D. in 2021 from IIS (Deemed to be University), Jaipur, focusing on the stereoselective aza-Michael addition of amines, which provided valuable insights into organic reaction mechanisms and synthetic methodologies. Her research interests include organic synthesis, stereochemistry, reaction dynamics, and green chemistry, with an emerging focus on computational approaches. At Lingaya's Vidyapeeth, she is actively engaged in teaching and mentoring, promoting conceptual understanding and research-based learning among students. Dr. Sharma has published research papers in reputed international and national journals. She continues to explore sustainable synthetic routes, integrating innovation with environmental responsibility in advancing modern organic chemistry.



Dr. Kailash Anandrao Gedekar is an Assistant Professor in the Department of Physics at KDK College of Engineering, Nagpur. He obtained his M.Sc. and Ph.D. degrees from Rashtrasant Tukadoji Maharaj Nagpur University, Nagpur, and has over 15 years of teaching experience. Dr. Gedekar has published more than 20 research papers in reputed national and international journals and conference proceedings indexed in Scopus. He has also served as a reviewer for several national and international conferences. Additionally, he has worked as Co-Convener for international conferences, FDPs, and STTPs, and has delivered expert talks at various reputed institutions. His primary research interests lie in Material Science and Photoluminescence, where he continues to contribute to the advancement of knowledge through research, collaboration, and academic engagement.





